FABRICATION AND APPLICATIONS OF DOPAMINE SENSITIVE ELECTRODES

Andre Hermans

A dissertation submitted to the faculty of the University of North Carolina at Chapel Hill in partial fulfillment for the degree of Doctor of Philosophy in the Department of Chemistry

Chapel Hill

2007

Approved by:

Advisor: R. Mark Wightman

Reader: Mark H. Schoenfish

Reader: Royce W. Murray

© 2007

Andre Hermans

ALL RIGHT RESERVED

ABSTRACT

ANDRE HERMANS: Fabrication and Applications of Dopamine Sensitive Electrodes (Under the direction of Dr. R. Mark Wightman)

The neurotransmitter dopamine has shown to be of central importance to difference brain functions, such as movement, reward, and addiction. A biosensor for the detection of dopamine in the brain should have a fast time response to monitor concentration changes which happen on a subsecond time scale. Furthermore, the sensor should have a high sensitivity to dopamine, because the physiological concentrations of dopamine were found to be in the range form nanomolar to lower micromolar. High selectivity is also necessary to distinguish the desired signal from electrochemical interferences in the brain such as ascorbic acid. Fast scan cyclic voltammetry at glass-encased carbon fiber microelectrodes has been shown to fulfill these requirements and is therefore often used for measurements of easily oxidizable neurotransmitters like dopamine. In this dissertation, some drawbacks of the technique and the sensor are addressed and improved.

Chapter 1 contains an overview of electrochemical methods that have been used to detect various neurotransmitters in the brain. Chapter 2 explains a method to increase the sensitivity and selectivity for dopamine of carbon fiber microelectrodes by covalent attachment of a cation-exchange layer to the

electrode surface. A method utilizing tungsten microwires as substrate for the construction of flexible gold, platinum, and carbon microelectrodes is described in Chapter 3 and 4. Carbon-coated tungsten microwires have then been examined for use as in vivo dopamine sensor. The microwires showed the same electrochemical properties as conventional glass-encased carbon fiber microelectrodes. In chapters 5 and 6 a novel instrumental method to subtract of the large background current, which occurs during application of fast scan rates, is presented. This method has then been used to examine the changes in this background current and account for these changes. This enabled us to expand the time course for fast scan voltammetric measurements 20-fold. Furthermore, the origin of these background changes was examined. In the last chapter tungsten based microelectrodes were used to evaluate changes in dopamine concentrations and pH of the extracellular fluid in a primate brain during reward delivery.

ACKNOWLEDEGMENTS

First, I would like to thank my academic advisor Dr. R. Mark Wightman for his support throughout the last 5 years. He has been a great mentor who gave me the opportunity to gain a lot of experience in the field of academic research and science.

I would like to thank my family and friends, especially Cherie Lanyi, for support and help outside the lab environment.

Furthermore, I would like to acknowledge everyone who worked with me over the last five years and help me pursuing my research goals. I thank Andrew Seipel, Justin Kita and Dr. Leslie Sombers for help with *in vivo* applications, Charlie Miller for slice experiments, Richard Keithley for his help with data analysis, the UNC electronics facility, and Dr. Michael Heien.

The experiments presented in chapter 7 were performed in the laboratories of Wolfram Schultz in Cambridge, England. I would like to thank Dr. Schultz and Dr. Istvan Hernardi for this wonderful collaboration.

This work was funded by NIH.

TABLE OF CONTENTS

LIST OF TABLES

Table

LIST OF FIGURES

Figure

LIST OF ABBREVIATIONS

3-MT	3–Methoxytyramine
4-SB	4-Sulfobenzene
4-SBD	4-Sulbebenzene diazonuim
AC	Alternating current
AChE	Acetylcholine esterase
ADP	Adenosine diphosphate
AP	Anterior / posterior
ChO	Choline oxidase
CLS	Classical least squares
CNS	Central nervous system
COMT	catechol-o-methyltransferase
DC	Direct current
DOPA	3,4 dihydroxyphenylalanine
DOPAC	3,4 dihydroxyphenylacetic acid
DPV	Differential pulse voltammetry
DV	Dorsal / ventral
$E_{1/2}$	Half-wave potential
F	Faraday’s constant
FAD	Flavine adenine dinucleotide
fMRI	Functional magnetic resonance imaging
FSCV	Fast-scan cyclic voltammetry

GABA	Gamma-aminobutyric acid
GluOx	Glucose oxidase
H	Aspect ratio of a cone
HPLC	High performance liquid chromatography
HRP	Horseradish peroxidase
HVA	Homovanilic acid
L-Dopa	Levo-dihydroxyphenylalanine
LOx	Lactate oxidase
MAO	Monoamine oxidase
MHPG	3-Methoxy-4-Hydroxy-phenylethyleneglycol
ML	Medial / lateral
n	Number of electrons
NADH	Nicotinamide adenine dinucleotide
PAN	Polyacrylonitrile
PCA	Principal component analysis
PPF	Pyrolyzed photoresist film
Q	Charge
RMS	Root-mean-square
SEM	Standard error of the mean, scanning electron microscopy
SSDH	Succinic semialdehyde dehydrogenase
UA	Uric acid
VMA	vanilylmandeleic acid
VTA	ventral tegmental area

CHAPTER 1

ELECTROCHEMICAL DETECTION IN THE BRAIN

Introduction

With respect to electrochemical detection, neurotransmitters can be separated into three different categories. The first group of neurotransmitters is the electrochemically active compounds such as the tyrosine derivatives dopamine, norepinephrine, and epinephrine. Many of their metabolites are also electroactive such as 3,4 dihydroxyphenylacetic acid (DOPAC), homovanilic acid (HVA), 3-methoxytyramine, or l-dopa. The neuroactive tryptophan derivatives are also electroactive and include 5-hydroxytryptamine (serotonin) precursors or metabolites like 5-hydroxyindolacetic acid, 5-hydroxyindoletryptophan or melatonin. Other electroactive neurotransmitters are histamine and adenosine. All of these compounds can be directly detected by electrochemical oxidation of the molecule. Furthermore, other electroactive substances in the brain like ascorbic acid, uric acid, nitric oxide, oxygen or hydrogen peroxide are also readily detectable by electrochemical methods.

The second group of neurotransmitters is not inherently electroactive, and thus these compounds cannot be detected by traditional electroanalytical methods. However, those that can be oxidized by an enzymatic reaction can be measured electrochemically by coupling the enzyme reaction with an electrochemical reaction.

Some of the neurotransmitters in this category are amino acid transmitters like glutamate and γ-aminobutyric acid (GABA), but also acetylcholine and its precursor choline have been detected with this approach. Glucose and lactate, compounds important in energy production in the brain, can also be detected with such indirect electrochemical approach.

Neuroactive peptides cannot be detected directly in the brain with electrochemical biosensors. However, neuropeptides with inherently electrochemically active group can be detected off-line electrochemically. Inate redox-active functionalities include tyrosine, tryptophan, methionine and cysteine residues. Neuropetides and some amino acid neurotransmitters form the third group of neurotransmitters.

Direct electrochemical detection of neurotransmitters in group 1

Catecholamine neurotransmitters are well suited for electrochemical detection because the potential required for their oxidation is well within normal scan ranges for carbon and metal electrodes in physiological buffer (Adams and Marsden, 1982). Catecholamines are derived in the biosynthetic pathway from tyrosine (Cooper et al., 2003). The rate limiting step in the synthesis is the hydroxylation of tyrosine to 3,4-dihydroxyphenylalanine (DOPA) with tyrosine hydroxylase. Dopamine is formed by the decarboxylation of l-DOPA. Norepinephrine is formed after transfer of a hydroxyl group onto the β-position of the side chain via dopamine-β-hydroxylase. The amine of norepinephrine can be methylated by phenylethanolamine-N-methyltransferase to form epinephrine. The major metabolites of dopamine are produced by reaction with

Molecule	Redox-Reaction	Approximate oxidation potential in vivo(Adams and Marsden, 1982) (vs Ag/AgCl)
Tyrosine derivatives	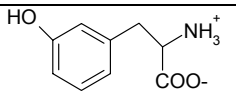	+0.7 V
L-DOPA	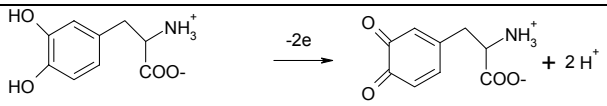	+0.4 V
Dopamine	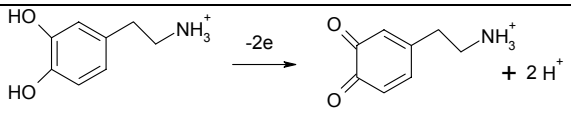	+0.2 V
Norepinephrine	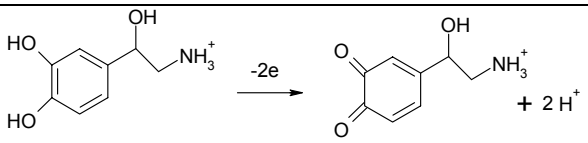	+0.2 V
Epinephrine	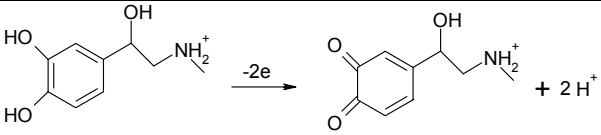	+0.2 V
DOPAC	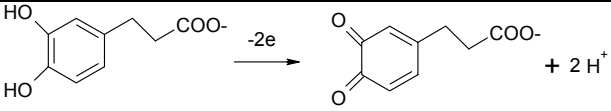	+0.2 V
Homovanilic Acid	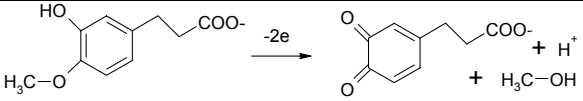	+0.5 V
3-Methoxytyramine	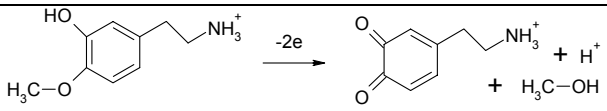	+0.5 V
Tryptophan derivatives	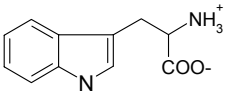	+0.8 V
Serotonin	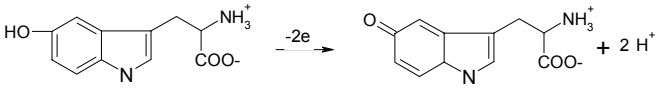	+0.35 V
5-Hydroxyindolacetic acid	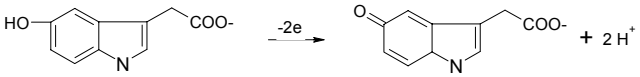	+0.35 V

Table 1.1. Electrochemical Oxidation of Tryosine and Tryptophan derivatives

Adenosine(Swamy and Venton, 2007)	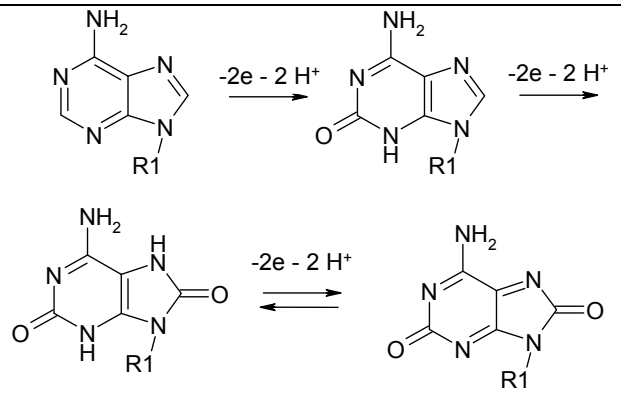	First step +1.2 V
Ascorbic Acid	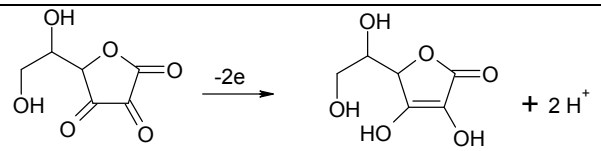	+0.2 V
Uric acid (Ramesh and Sampath, 2004)	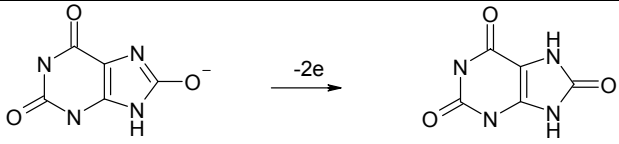	+0.3 V
H_2O_2	$H_2O_2 - 4e^- \rightarrow O_2 + 2\ H^+$	
Oxygen	$½\ O_2 + 2H^+ + 2e^- \rightarrow 2H_2O$	
NO (Ciszewski et al., 1998)	$NO - e^- \rightarrow NO^+$ $NO^+ + H_2O \rightarrow HNO_2$ $HNO_2 \rightarrow NO_2^- + H^+$ $NO_2^- + H_2O - 2e^- \rightarrow NO_3^- + 2\ H^+$	

Table 1.2. Electrochemical reactions of other detectable species in the brain

monoamine oxidase (MAO) and catechol-O-methyltransferase(COMT). These metabolites are dihydroxyphenylacetic acid (DOPAC), homovanilic acid and 3-methoxytyramine (3-MT). The action of MAO on norepinephrine mainly produces vanilylmandeleic acid (VMA) and 3-methoxy-4-hydroxy-phenlethyleneglycol (MHPG). As can be seen in table 1.1a all of these compounds show similar 2 electron oxidation reactions with similar oxidation potentials. For this reason it is difficult to distinguish different catecholamines and their metabolites with electrochemical methods. However, most of these compounds undergo secondary reactions. The methoxylated derivatives are oxidized at more positive potentials than the catecholamines, however, the oxidation product loses methanol and forms the o-quinone of the corresponding catecholamine. In the case of 3-MT oxidation, dopamine-o-quinone is formed while HVA leads to the formation of the oxidized form of DOPAC.

Another example for a secondary reaction intracyclization reaction of the oxidized hydroquinone form of catecholamines (Hawley et al., 1967; Blank et al., 1976; Zhang and Dryhurst, 1993).

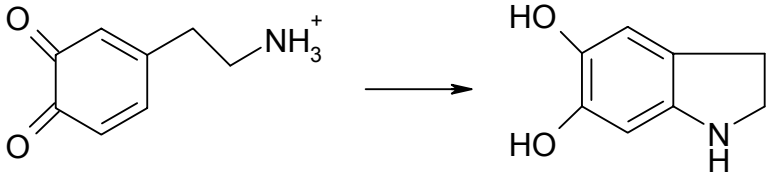

(1)

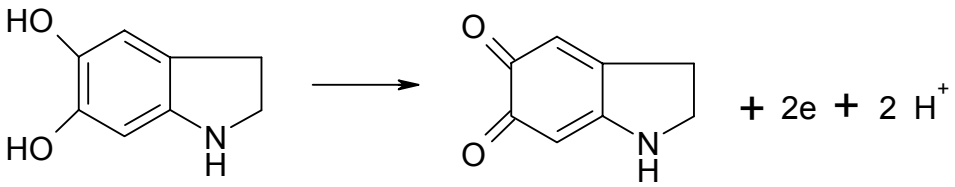

(2)

The 5-6 dihydroxyindoline product can undergo redox-reactions itself to an aminochrome (reaction (2)). However, In the case of dopamine the rate constant for the formation reaction is very slow, on the order of $k = 0.1\ s^{-1}$ at physiological pH. The rate of cyclization is faster for epinephrine than for norepinephrine. This has been used to distinguish these compounds electrochemically (Ciolkowski et al., 1992). By using fast scan methods or measuring quickly after a potential step the effect of these reactions can be diminished. The formation of the aminochrome product can be used to distinguish norepinephrine and epinephrine electrochemically since the rate of cyclization is faster for epinephrine (Ciolkowski et al., 1992). In addition to this, the secondary-amine side chain of epinephrine can be oxidized at very positive potentials whereas the primary-amine side chain of norepinephrine cannot (Pihel et al., 1994).

The other important group of electrochemically detectable neurotransmitter and metabolites are the tryptophan derivatives including serotonin. During biosynthesis tryptophan is converted by tryptophan hydroxylase to 5-hydroxytryptophan which then forms serotonin after decarboxylation. Metabolism of serotonin is primarily by MAO followed by an aldehyde dehydrogenase that leads to 5-hydroxyindole acetic acid. A more minor pathway is metabolism of serotonin to form 5-hydroxytryptophenol. Tryptophan derivatives can also be oxidized and electrochemically detected in a two electron process with similar oxidation potential as catecholamines. After oxidation many different secondary reactions have been observed (Wrona and Dryhurst, 1990). The reaction pathway is very complicated

and involves the dimerization of serotonin, as well as, after addition of water, formation of tryptamine 4-5 dione.

Histamine and adenosine are other oxidizable neurotransmitters but neither has been directly detected with electrochemical methods in the brain yet. Histamine secretion from isolated mast cells has been detected electrochemically(Pihel et al., 1995). Histamine is synthesized from histidine via decarboxylation and has multiple metabolic products such as imidazoleacetaldehyde and imidazolacetic acid. Recent research has shown that adenosine can be detected by fast scan cyclic voltammetry (Abou El-Nour and Brajter-Toth, 2000; Brajter-Toth et al., 2000; Abou El-Nour and Brajter-Toth, 2003; Swamy and Venton, 2007). Adenosine seems to undergo a 3 step oxidation of which the first two steps lead to a distinct voltammogram which can be differentiated from other interferences (see table 1.2).

The main electroactive interference for electrochemical measurements in the extracellular fluid of the brain is ascorbic acid. The ascorbic acid concentrations in the extracellular fluid of the brain are 0.5 mM which is 10^4-10^6 times higher than the concentrations of catecholamines (Mefford et al., 1981; Nagy et al., 1982). Early amperometric measurements showed that the oxidation of ascorbic acid was the main signal recorded in the brain (Kissinger et al., 1973; Mueller, 1986). However, the electron transfer kinetics for the oxidation of ascorbic acid at carbon are very sensitive to the surface conditions. Electrooxidation of carbon at very high potentials (~3.0 V) causes an acceleration of electron transfer rates so that the ascorbate oxidation peak occurs near its thermodynamically anticipated value. Using such treatments, Gonon and coworkers were able to show that ascorbate changed in

concentration following pharmacological treatments expected to affect cathecholamines (Gonon et al., 1980a; Gonon et al., 1981). This established that brain sensors for dopamine had to be able to distinguish the two molecules. This is accomplished in fast scan methods because the oxidation of ascorbate shifts to more positive potentials as a result of slow electron-transfer kinetics, distinguishing the ascorbate signal from other compounds (Marsden et al., 1988; Millar et al., 1992). Alternatively, electrode modification with selective membranes can reject ascorbate from the electrode surface (Nagy et al., 1982; Baur et al., 1988; Wiedemann et al., 1990).

Beside direct electrochemical interference ascorbic acid can contribute indirectly to the measured signal. Ascorbate functions as the major antioxidant in the body. Thus, even when it is rendered inactive at the electrode surface, it can play this role during the electrochemical detection. For example, after the oxidation of dopamine, dopamine-o-quinone is reduced by ascorbate, regenerating dopamine. This catalytic reaction by ascorbic acid provides more dopamine for electrooxidation with the net result that the electrochemical current is proportional to both dopamine and ascorbate (Sternson et al., 1973).

Recently it has been shown that hydrogen peroxide plays an important role in brain signaling and neurotransmitter regulation(Chen et al., 2001; Avshalumov et al., 2007). Hydrogen peroxide can be detected directly by electrochemical methods such as amperometry (Kulagina and Michael, 2003). Oxygen levels in the brain are also often determined with microelectrodes (Zimmerman and Wightman, 1991; Thompson et al., 2003; Venton et al., 2003b; Bolger and Lowry, 2005). For

determination of oxygenation of brain tissue, electrochemical methods are an alternative approach to BOLD-MRI measurements which monitors the oxygen dissociation from hemoglobin (Ogawa et al., 1990). Although electrochemical oxygen measurements have a much better spatial and temporal resolution than fMRI techniques for many studies use fMRI techniques because of the non-invasive nature. Furthermore, amperometric detection of hydrogen peroxide or oxygen is the basis for enzyme based electrodes that are discussed further later.

Nitric oxide (NO) has been shown to act in the central nervous system as secondary messenger and as mediator in cardiovascular system (Schuman and Madison, 1994; Dawson and Dawson, 1996; Cooper et al., 2003). Nitric oxide is synthesized from argenine. When measuring nitric oxide electrochemically, normally electrodes with coatings or membranes that are specific to NO are used. A description of these coating can be found later in this review.

Electrode materials

The developments of microelectrodes several decades ago formed the basis for *in vivo* applications of electrochemical detection of neurotransmitters. Early microelectrodes for voltammetric recordings in the CNS were constructed from carbon paste (Adams, 1958; Kissinger et al., 1973; O'Neill, 2005). The carbon paste was prepared by mixing carbon powder with either Nujol or silicone oil (O'Neill et al., 1982) and then packed into the end of Teflon insulated metal microwires resulting in disk electrodes with diameters between 100 and 300 μm. Glass capillaries can also be filled with carbon paste. Epoxy resin is often added to the carbon paste following

curing resulting in a more rigid electrode (Conti et al., 1978; Huff and Adams, 1980). Carbon paste electrodes have been reported to be stable over several months for *in vivo* applications. However, the relatively large size of carbon-paste electrodes limits the applications to larger brain regions. Because of the larger size more brain damage occurs in comparison to smaller sized electrodes.

Smaller carbon electrodes can be made from carbon fibers (Gonon et al., 1978; Ponchon et al., 1979). Carbon fibers range from a few micrometers in diameter to 40 μm but the majority of fibers range between 5-15 μm (McCreery, 1996). Carbon fibers are prepared from the pyrolysis of either petroleum pitch or polyacrylonitrile (PAN) and undergo thermal processing similar to glassy carbon. To make an electrode the carbon fiber is inserted into a glass capillary, pulled with a pipette puller, and cut to obtain a cylindrical electrode or polished for disk electrodes. To form a well insulated seal between the carbon fiber and the insulating glass sheath, epoxy resin is allowed to creep between the fiber and the glass and then cured (Kawagoe et al., 1993). Carbon-fiber microelectrodes constructed in this way cause minimal damage to the surrounding tissue (Peters et al., 2004) when inserted into the brain because the dimensions of the whole electrode including the surrounding insulation are in the lower micrometer range.

The electrochemical properties of carbon electrodes depend on the oxidation state of carbon-containing functional groups of the carbon surface. It has been proposed that surface carbonyl- and hydroxyl-groups can catalyze electron transfer for inner-sphere reactions at the electrode surface (Chen and McCreery, 1996). Furthermore, overoxidation of carbon electrode surfaces has been shown to

increase the sensitivity to positively charged analytes (Heien et al., 2003). This is probably due to increased adsorption of cations to the carbon surface. An increase in sensitivity of 5 to 7 has been observed in vitro for dopamine when using fast scan cyclic voltammetry at overoxidized carbon fibers. However, overoxidized electrodes show a slower time response and lower selectivity than electrode which have not been exposed to high oxidative potentials. In early studies overoxidation was accomplished by repetitive excursions + 3 V vs. Ag/AgCl at 70 Hz (Gonon et al., 1980b; Gonon et al., 1981). Electrodes treated this way showed higher sensitivity for catecholamines. However, in addition to increasing the amount of surface oxides, this surface treatment seems to drastically increase the surface area of the electrode (Swain and Kuwana, 1991).

Carbon microelectrodes are well suited for direct electrochemical detection of neurotransmitters of group 1 for various reasons. Beside the relatively easy and cost-effective construction, carbon electrodes show very little bio-fouling during in-vivo applications in contrast to metal electrodes which have to be further coated. Fouling of the electrode surface has a huge impact on electron transfer kinetics on which especially voltammetry techniques depend on. Furthermore, a larger potential range can be applied to carbon electrodes than to metal electrodes which readily undergo electro-oxidation.

Gold and platinum microelectrodes have been used to directly detect catecholamines *in vitro* (Matos et al., 2000; Vandaveer et al., 2003; Yan et al., 2003; Etienne et al., 2005). However, because of the relatively small potential window compared to carbon electrodes and problems with bio fouling, metal electrodes are

commonly not used for direct electrochemical detection of neurotransmitters of group one. However, platinum and gold electrodes are commonly used for enzyme electrodes to detect molecules of group two *in vivo*. Because of the possibility to micro pattern gold and platinum onto substrates metal microelectrodes are often fabricated in arrays with multiple electrode sites (Burmeister, 2000; Burmeister and Gerhardt, 2001, 2003).

Electrochemical techniques

Different electrochemical techniques are used to directly detect the molecules of group 1. The most common techniques are constant-potential amperometry, chonoamperometry, differential pulse voltammetry and fast-scan cyclic voltammetry.

In constant-potential amperometry the working electrode is held at a DC potential sufficient to oxidize or reduce the compound of interest at the electrode surface. The presence of an electroactive species that undergoes electron transfer at this potential will lead to a current. The integral of the current with respect to time (charge, Q) is directly proportional to the amount (m) of the species electrolyzed at the electrode surface by Faraday's law ($Q = nFm$ where n is the number of electrons in the redox step, and F is Faraday's constant). With constant-potential amperometry very high time resolution can be achieved. With a sampling rate in the kHz range constant-potential amperometry can resolve signals on the sub-millisecond time scale. Adsorption of reactants at electrodes is not a concern with constant-potential amperometry because species are electrolyzed immediately when they come in contact with the electrode. For this reason, adsorption processes do

not slow down the response to concentration changes of the analyte as occurs with voltammetric techniques. Collectively, these properties make constant-potential amperometry a useful technique to measure vesicular neurotransmitter release from single cells (Leszczyszyn et al., 1991; Wightman et al., 1991; Cahill and Wightman, 1995; Zhou and Misler, 1995). Studies using amperometry have allowed for the detection of attomole to zeptomole amounts secreted from single cells (Chen et al., 1994; Jaffe et al., 1998; Pothos et al., 1998; Hochstetler et al., 2000).

Although amperometry can be used to determine amounts secreted, it is not particularly useful for determining concentrations. This is because the dimensions and shape of the diffusion layer must be designed to be identical during calibration and at single cells. Despite this, amperometry has also been successfully used to study catecholamine concentrations in the brain and in brain slices (Falkenburger et al., 2001; Troyer et al., 2002). It has been shown that the addition of ascorbic acid provides a way to obtain accurate in calibrations for catecholamine detection (Venton et al., 2002). Recall that the catalytic reaction of ascorbate with dopamine-o-quinone regenerates dopamine. If the reaction occurs at a similar rate in the calibration solution and in the brain preparation, the diffusion layer dimensions will be the same in both environments, and the calibration factor obtained in vitroo will be valid in vivo. Despite these advantageous features, constant potential amperometry is inherently non-selective. All electroactive compounds that oxidize or reduce at the holding potential will produce a faradaic current detected at the electrode. Therefore it is important to use independent measures to identify the molecules responsible for the detected currents to confirm amperometric traces.

In chronoamperometry the applied potential is instantaneously stepped from an initial potential at which no electrochemical reaction is occurring to a potential sufficient to oxidize or reduce the molecule of interest. After that the potential is then stepped back to the initial holding potential in a rectangular fashion. The current observed during the initial potential step is proportional to the concentration of the electroactive species present, and it decays with the inverse of the square root of time if the current is governed by diffusion. Traditionally the current is measured at a fixed time into the potential step and this is used to calculate the concentration of the analyte. On the potential step back to the initial potential the species that were originally oxidized will be reduced. From the ratio of the currents measured on the reverse and forward potential step, information about the stability of the oxidized species can be made. This feature provides chronoamperometry with somewhat greater selectivity than constant-potential amperometry. Chronoamperometry has often been used to measure neurotransmitter concentrations especially serotonin (Daws et al., 2005; Perez and Andrews, 2005) and dopamine (Hoffman and Gerhardt, 1998; Miller et al., 2005; Unger et al., 2006) in the extracellular fluid of the brain in real time. However, because of its limited chemical selectivity, it is most often used to measure neurotransmitter dynamics following injection of the authentic substance or an agent that immediately causes release.

An electrochemical method used in many early reports of *in vivo* neurotransmitter measurements is differential-pulse voltammetry (DPV). DPV is a combination of linear sweep voltammetry with square wave techniques. The applied signal is a small amplitude square wave (~25mV) at a constant frequency

superimposed on a slow linear potential ramp. The current is measured both shortly before each square wave is applied and again shortly before each pulse ends. The difference between these currents is potted versus the potential of the linear sweep. The differential currents give a symmetrical voltammetric peak whose amplitude is proportional to the concentration of the analyte. In contrast to amperometric methods, it is possible with DPV to measure simultaneously different analytes as long as the oxidation potentials of these compounds are separated by more than 100 mV(Adams and Marsden, 1982). DPV has been used in the past for in-vivo neurotransmitter detection of catecholamines (Gonon et al., 1980b; Gonon et al., 1984) and serotonin (Crespi et al., 1984) as well as oxygen (Bolger and Lowry, 2005) measurements. However, DPV shows a relatively poor time resolution since one scan takes longer than 30s while neurotransmitter fluctuations occur on a subsecond time scale.

Fast-scan cyclic voltammetry (FSCV) is an electrochemical technique that provides a much higher temporal resolution than DPV but still shows high selectivity (Millar et al., 1985). In an FSCV experiment the potential applied to the electrode is ramped at scan rates larger than 100 V/s in a triangular fashion. The voltage limits are chosen so that the reduction and oxidation of the analyte of interest lies within this potential window.. At high scan rates the majority of the current detected at the working electrode is a background current due to charging of the double layer and, depending on the material of the electrode used, redox processes at the electrode surface (Chen and McCreery, 1996; Hsueh et al., 1997). Typically this large background current is subtracted (Howell et al., 1986) so that the smaller changes in

faradaic currents due to redox processes of electroactive species can be monitored. Because the background current is only stable for a brief time, FSCV is typically only used to observe concentration changes over the time course of a minute. Furthermore, because of the differential nature of the technique it is not possible to measure basal level concentrations of electroactive species. FSCV has been shown to be very useful for the detection of catecholamines in vivo because of the high sensitivity and selectivity (Cahill et al., 1996). Typically with FSCV a time resolution of 100 ms is achieved by applying the waveform for 10 ms and repeating it at 100 ms intervals. Because it involves a potential sweep, FSCV provides the possibility to distinguish analytes with different oxidation potentials by their peak positions for the oxidation and the reduction as well as by their peak shape (Heien et al., 2004).

In the intervals between each scan, where the electrode is typically held at a negative potential the catecholamines have been shown to adsorb to the electrode surface (Bath et al., 2000). This adsorption causes a preconcentration of the catecholamine at the surface before each voltammetric scan. Anionic compounds do not show this preconcentration process, which increases selectivity for the cations. A further increase in selectivity is achieved by the application of high scan rates itself. Compounds with slower electron transfer rates like ascorbate can be distinguished very easily form biogenic amines at high scan rates because the oxidation is drawn out to higher potentials (Marsden et al., 1988; Millar et al., 1992).

Modified electrodes

Different surface coatings have been applied to electrode surfaces to overcome some of the limitations of the electrochemical detection schemes. Surface coatings are widely employed to increase sensitivity and selectivity for certain analytes as well as way to prevent surface fouling. Nafion, a perfluorinated cation-exchange polymer, is a commonly used electrode coating(Baur et al., 1988) for catecholamine detection because the biogenic amines are positively charged at physiological pH. Nafion can be applied by dip coating the electrode in a suspension of 2.5% Nafion in isopropanol and allowing the solvent to evaporate leaving a Nafion film. The considerable hydrophobicity of the Nafion layer minimizes surface fouling while sulfonate groups within the Nafion network promote accumulation of cations while rejecting anions. An alternate approach is the deposition of an overoxidized polypyrrole-film on the electrode surface (Witkowski and Brajtertoth, 1992; Hsueh and Brajtertoth, 1994; Pihel et al., 1996; Wang et al., 1997). These films exhibit similar properties to those described for Nafion films. However, both coatings are noncovalently attached layers that have finite thickness. The thickness means that there is a finite time required for molecules to diffuse through the coating. This increases the response time of the electrode. To remove this component, deconvolution methods have to be used to extract real time response curve at electrodes modified with this way(Kawagoe and Wightman, 1994). Carbon paste electrodes have been modified by mixing stearic acid into the carbon paste (Lyne and Oneill, 1989; Lane and Blaha, 1990; Blaha and Phillips, 1996). These electrodes have been reported to have a high sensitivity and selectivity to

dopamine over other electrochemical interferences present in the brain like ascorbic acid and DOPAC. More recently carbon-fiber microelectrodes have been modified by covalent attachment of molecules via diazonuim salt reduction. Most commonly the electrodes are modified with anionic functional groups like carboxyphenyl (Bath et al., 2001), phenylacetate (Downard et al., 1995), or sulfobenzene (Hermans et al., 2006). Electrodes modified this way show a higher sensitivity and selectivity to cationic analytes such as catecolamines over anionic analytes like ascorbic acid without slowing down the time response of the detection.

To create an electrode that is sensitive to nitric oxide different surface coatings have been used to minimize interferences from oxygen and other derivates of nitric oxide such as the main interference NO_2^-. Elimination of these interferences is the biggest challenge in creating a nitric oxide sensor. Early nitric oxide sensing electrodes used a Clark-type electrode with chloroprene rubber as NO selective membrane (Shibuki, 1990). Carbon fiber microelectrodes coated with o-phenylenediamine and Nafion (Friedemann et al., 1996) showed also a very high selectivity for nitric oxide. Platinum-iridium electrodes coated with a nitrocellulose/pyroxylin layer were used to measure NO concentrations in various biological applications (Ichimori et al., 1994). Recently NO concentrations have been electrochemically detected in tumor-bearing mice with a a Nafion/o-phenyldiamine coating on a platinum-iridium microelectrode (Griveau et al., 2007). Other approaches include electrodes modified with layers of Nafion and Ni tetrasulfonate phthalocyanine tetrasodium salt (Isik et al., 2007) or electrodes coated

with silicone based xerogels which are doped with methoxysilanes (Shin et al., 2005). However, these approaches have not been tested in vivo yet.

Reference and auxiliary electrodes

When using a 3-electrode setup for in-vivo electrochemical measurements the auxiliary electrode is most commonly a stainless steel electrode which is brought in contact with the cortex at a convenient location. When using microelectrodes often a 2-electrode setup is used consisting just of a working electrode and a reference electrode. Two electrode systems are preferred because the currents are sufficiently small that the reference electrode does not get polarized during the course of the experiment. Also, with an extracellular NaCl concentration of ~ 150mM the electrolyte concentration is high enough to minimize the solution resistance. Reference electrodes are normally a small-diameter silver wire, which has been anodized in hydrochloric acid to form a silver chloride layer on the surface of the wire (Phillips et al., 2003). The wire is directly implanted into the brain tissue.

Detection of changes in pH in vivo

pH changes have been shown to follow electrical stimulation of dopamine neurons and seem to be an indirect measure of blood vessel dilation and oxygenation of the tissue (Venton et al., 2003a). Microelectrodes to measure pH in the brain have been developed with different approaches. One approach for electrodes for in vivo pH-measurements have been construction from double barreled thin wall capillary glass (Chesler and Chan, 1988; Chen and Chesler, 1992;

Chesler et al., 1994). The pH sensitive barrel is filled with a hydrogen ionophore cocktail to provide a liquid pH sensitive junction. The second barrel is traditionally the reference barrel that is filled with a buffer solution at physiological pH. The electrodes are used in a potentiometric mode with the voltage difference between the two electrodes measured. Electrodes produced in this fashion have shown to be able to resolve at least 0.001 pH units in a millisecond time scale (Chesler and Chan, 1988). A different approach uses metal microelectrodes as micro-pH sensors. Most commonly iridium-oxide has been used electrode as electrode material. Iridium oxide electrodes show a linear sensitivity over a pH range of pH 2 - pH 10 and have low susceptibility to other cationic interferences and seem to function under in-vivo conditions (Marzouk et al., 1998; Bezbaruah and Zhang, 2002). Recent research showed that iridium-oxide pH sensors can be patterned in a microelectrode array to allow simultaneous recording at multiple sites (Johnson et al., 2007). Anhydrous iridium oxides have Nernstian responses to pH changes that originate from the reactions between the +III and the +IV states of iridium:

$$IrO \cdot OH \rightarrow IrO_2 + H^+ + e^- \quad (3)$$

$$Ir_2O_3 + H_2O \rightarrow 2\ IrO_2 + 2H^+ + e^- \quad (4)$$

Commonly the measurement is done in a potentiometric measurement versus a silver-silver chloride reference electrode. In-vivo pH changes can also be measured with background subtracted fast-scan cyclic voltammetry at carbon electrodes (Runnels et al., 1999; Venton et al., 2003a; Cheer et al., 2006). Carbon-fiber electrodes respond to pH changes because one of the contributions to the background current is electrolysis of oxide groups on the electrode surface. The

electrolysis is pH dependent, and a differential signal is formed when the background is subtracted. The amplitude of this change is directly proportional to the amplitude of the pH change.

Enzyme electrodes for detection of molecules in group 2

Considerable research has been conducted over the last couple of decades to design electrochemical sensors for molecules that are not electroactive. These sensors rely on the principle that during the oxidation of an analyte by an enzymatic reaction an electroactive species is formed that can be detected at the electrode surface. With this technique electrochemical sensors that measure glucose and lactate concentrations in the brain have been constructed to study brain metabolism. The design features of those electrodes have been adapted to detect glutamate, choline, acetylcholine, GABA and adenosine (Dale et al., 2000; Llaudet et al., 2003a). Detection with enzyme electrodes is normally used with amperometric detection. This means that is of great importance to construct electrodes with selective membranes to minimize interfering signals (Wilson and Gifford, 2005).

An important driving force for the development of enzyme electrodes was the need for a reliable glucose sensor for blood measurements for diabetic patients. The first enzyme-based glucose sensing electrodes have been developed in the 60's (Clark and Lyons, 1962; Updike and Hicks, 1967) by immobilizing glucose oxidase embedded in a gel-matrix on Clark-type oxygen electrode. The enzymatic reaction turns glucose into gluconic acid with consumption of oxygen.

$$\text{glucose} + O_2 \xrightarrow{GOx} \text{gluconic acid} + H_2O_2 \quad (6)$$

The configuration of the sensor depends on whether reaction (6) is monitored by measuring H_2O_2 or oxygen. When oxygen is measured a low reducing potential is required for amperometric detection which eliminates interferences because only a few endogenous electroactive species undergo electron transfer in this potential region. However, often hydrogen peroxide detection is preferred because of easier construction although the relatively high potential (0.6 V vs. Ag/AgCl) that is applied to the electrode significantly increases the number of interfering species. An alternative approach uses redox mediators which enable the use of lower potentials applied (0V vs Ag/AgCl). These mediators are commonly horseradish peroxidase coupled to an osmium complex or polypyrrole (Gregg and Heller, 1990, 1991; Georganopoulou et al., 2000). An example of a redox-mediated enzyme reaction is shown the reaction schemes 10a to 12a.

Miniaturized glucose sensors based on hydrogen peroxide sensing have been developed for subcutaneous monitoring (Bindra et al., 1991) as well as direct measurements in the brain (Silver and Erecinska, 1994; Hu and Wilson, 1997b) to study brain metabolism (Hu and Wilson, 1997a). Lactate oxidase (Wang and Heller, 1993; Shram et al., 1998; Shram et al., 2002) can also be used as reactive enzyme to obtain further information about brain metabolism

$$\text{lactate} + O_2 \xrightarrow{\text{LOx}} \text{pyruvate } H_2O_2 \qquad (7)$$

Often electrochemical glucose and lactate detectors have also been used with micro dialysis probes that allow removal of extracellular fluid for on-line detection outside of the brain (Jones et al., 2000; Parkin et al., 2005).

The developments in the field of glucose sensors were exploited to develop electrochemical detectors for other neurotransmitters in the brain. Glutamic acid, or glutamate, is the major excitatory neurotransmitter in the central nervous system. It is synthesized from glutamine in glial cells and then converted by glutaminase into glutamate or synthesized from glucose via the Krebs cycle. Most electrochemical glutamate sensors have been constructed from metal electrodes, most commonly platinum, coated with a thin layer of electropolymerized o-phenylenediamine (Alvarez-Crespo et al., 1997) or Nafion. These surface coated polymers minimize interferences, especially anionic compounds. Glutamate oxidase can be embedded in a cross-linked redox polymer with horseradish peroxidase (Kulagina et al., 1999), or, more commonly in a layer of BSA and glutaraldehyde on top of the Nafion layer (Pan and Arnold, 1996; Burmeister and Gerhardt, 2001; Huettl et al., 2002; Burmeister and Gerhardt, 2003). In a recent research study glucose oxidase was embedded in a hydrogel matrix (Oldenziel et al., 2006). Horseradish peroxidase, and ascorbate oxidase were wired via poly(ethylene glycol) diglycidyl ether to an osmium-containing redox polymer and integrated into the hydrogel to provide high selectivity to glutamate.

All these electrodes follow the basic electrochemical detection scheme for glutamate (8 to 10) as described by Kusakabe (Kusakabe et al., 1983):

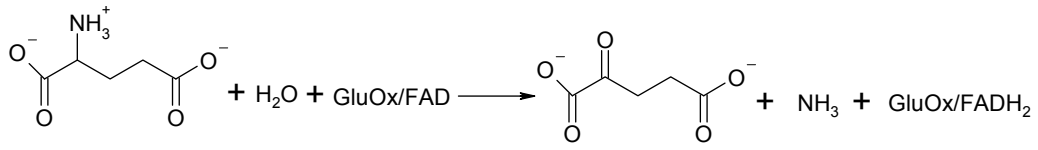

(8)

$$GluOx/FADH_2 + O_2 \rightarrow GluOx/FAD + H_2O_2 \qquad (9)$$

$$H_2O_2 - 2e^- \rightarrow O_2 + 2\,H^+ \qquad (10)$$

$$H_2O_2 + HRPred \rightarrow O_2 + 2\ H^+ + HRPox \quad (10a)$$

$$HRPox + Os(II) \rightarrow HRPred + Os\ (III) \quad (11a)$$

$$Os\ (III) + 1\ e^- \rightarrow Os\ (II) \quad (12a)$$

The first 2 steps of this reaction scheme occur in the outer enzyme containing layer. The hydrogen peroxide that is generated in reaction (0) diffuses then through the selective membrane to the electrode surface where it gets oxidized in a 2 electron process (reaction (9)). An alternative detection with an osmium-containing redox-layer is shown in the reaction (10a to 12a). In this case the hydrogen peroxide will be reduced by horseradish peroxidase (HRP) which then will be oxidized itself by Osmium (II) to Osmium (III). At the electrode the reduction of Osmium (III) will then be detected. Glutamate electrodes currently show a limit of detection of around 1 µM and a linear range up to 200 µM for calibrations in vitro (Burmeister and Gerhardt, 2001).

The neurotransmitter acetylcholine is synthesized in vivo from choline by choline acetyltransferase. Electrodes designed for the detection of choline are similar to those described for glutamate detection(Garguilo and Michael, 1993, 1994). Instead of immobilization of glutamate oxidase, choline oxidase is used. The first reaction step is shown in the following reaction scheme:

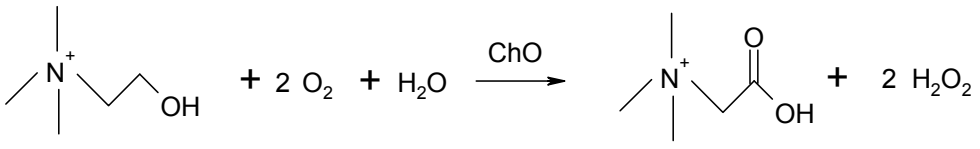

(13)

Hydrogen peroxide can then either be detected directly at the electrode(Guerrieri et al., 2006) as shown in reaction (10) or via a redox-polymer as shown in reactions

(10a) to (12a). To monitor acetylcholine concentrations acetylcholine esterase is added to the electrode surface to convert acetylcholine to choline:

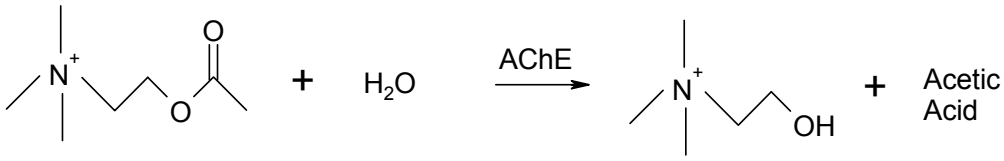

(14)

Choline is then oxidized according to reaction (13) which then will lead to the reaction (10) or (10a) to (12a). Because choline is present in the brain as well as being one of the products in the reaction cascade, it is important to have an independent measure of choline. This can be done in a differential manner to subtract out the signal from a choline sensor from the overall signal recorded at the actetylcholine sensitive electrode (Garguilo and Michael, 1996; Guerrieri et al., 2006).

Another neurotransmitter that can be detected electrochemically after an enzymatic reaction is the inhibitory amino acid transmitter γ-aminobutyric acid (GABA). Glutamate is the biochemical precursor for GABA. GABA is formed after α-decarboxylation of glutamate. The bioenzymatic system used for GABA detection is comprised of the enzymes GABA-α-oxoglutarate transaminase (GABA-T) and succinic semialdehyde dehydrogenase (SSDH)(Mazzei et al., 1996):

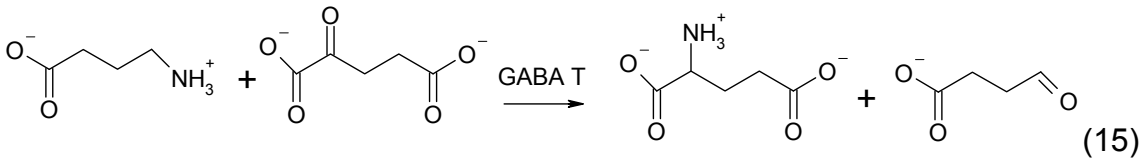

(15)

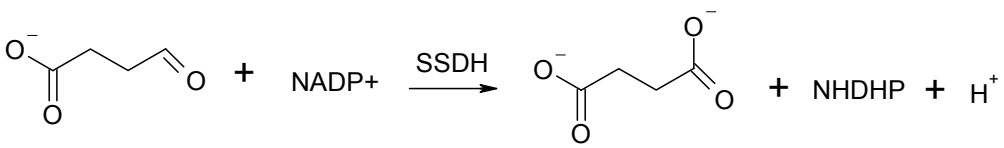

(16)

$$2NADPH + O_2 + 2H^+ \xrightarrow{HRP} 2NADP^+ + 2H_2O \quad (17)$$

The reaction steps for the electrochemical detection of GABA three step process. The product of the first two enzymatic reactions (15+16) is NADHP, which is formed from $NADH^+$ embedded in the enzyme layer. NADHP is then re-oxidized to $NADP^+$ after reacting with horseradish peroxidase. The amperometric detection is based on oxygen consumption in reaction (17). However, GABA electrodes are not commonly used today for direct in-vivo applications. Mostly GABA detection is conducted with HPLC detection after microdialysis.

Beside direct electrochemical detection(Swamy and Venton, 2007) purines such as ATP (Llaudet et al., 2005), ADP, and adenosine (Llaudet et al., 2003b) have been detected in vivo with enzyme electrodes (Dale et al., 2005). ATP sensors have been constructed by combining glucose oxidase and hexokinase. The signal recorded for changes in ATP is due to the reduction in the glucose signal via phosphorylation of glucose to glucose 6-phosphate (Compagnone and Guilbault, 1997; Kueng et al., 2004). A different detection scheme relies on the phosphorylation of glycerol (Murphy and Galley, 1994; Llaudet et al., 2005).

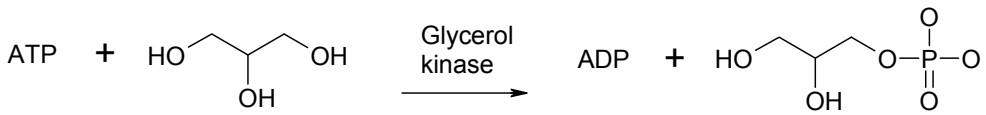

(18)

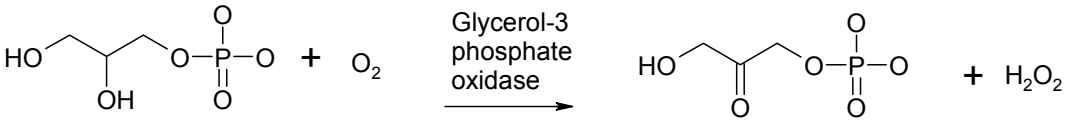

(19)

This detection scheme enables again the amperometric detection of hydrogen peroxide at the electrode.

To further eliminate interferences in the amperometric signal self-referencing electrodes have been developed (Burmeister and Gerhardt, 2001, 2003). With this electrode setup two electrodes are placed within a very close proximity of each other. This can be achieved by the construction of microelectrode via photolithographic etching. Only one of the electrodes sites will be coated with the enzyme containing coating, while the other site will be coated in the same manner just without addition of the enzyme. The non-enzyme containing electrode serves as a reference electrode that can sense all electrochemical signals originating from interfering species. This signal is then subtracted from the signal measured at the enzyme-containing electrode to obtain a signal that is purely due to the analyte of interest. This method can be applied to all enzyme electrode-types described here. However, the prerequisite for this technique is that the chemical environment is identical at each of the two electrode sites.

Detection of molecules in group 3

Some neurotranmitters and neuromodulators cannot be detected directly in the brain with electrochemical biosensors at this time. The most prominent members of this group are some of the amino acid transmitters like gycine as well as the large group of neuroactive peptides. For the detection of these molecules typically microdialysis probes are used. In microdialysis a small probe containing a dialysis membrane is inserted into the target region. A perfusion fluid, the dialysate, is pumped through the probe and the molecules of interest can diffuse though the membrane into the dialysate. The dialysate can then be removed and analyzed by

different independent analytical methods (Watson et al., 2006). Typically HPLC is used to analyze the composition and concentrations of the dialysate. For analysis of neuropeptides, commonly isolated or cultured neurons or whole neuronal tissue is homogenized and then separated with chromatographic techniques. Detection can be done with variety of methods such as UV absorbance, florescence, electrochemical detection or radioactive detection (Sandberg and Weber, 2003). Soft ionization techniques in mass spectrometry are also employed in discovering and analyzing neuropedtides (Hummon et al., 2003; Hummon et al., 2006).

REFERENCES

Abou El-Nour K, Brajter-Toth A (2000) Sensitivity of electrochemically nanostructured carbon fiber ultramicroelectrodes in the determination of adenosine. Electroanalysis 12:805-810.

Abou El-Nour K, Brajter-Toth A (2003) Development of adenosine sensor: effect of physiological buffers on activity and sensitivity in adenosine determinations by fast scan voltammetry. Analyst 128:1056-1061.

Adams RN (1958) Carbon Paste Electrodes. Analytical Chemistry 30:1576-1576.

Adams RN, Marsden CA (1982) Electrochemical detection methods for monoamine measurements in vitro and in vivo. Handb Psychopharmacol 15:1-74.

Alvarez-Crespo SL, Lobo-Castanon MJ, Miranda-Ordieres AJ, Tunon-Blanco P (1997) Amperometric glutamate biosensor based on poly(o-phenylenediamine) film electrogenerated onto modified carbon paste electrodes. Biosensors & Bioelectronics 12:739-747.

Avshalumov MV, Bao L, Patel JC, Rice ME (2007) H2O2 signaling in the nigrostriatal dopamine pathway via ATP-sensitive potassium channels: Issues and answers. Antioxidants & Redox Signaling 9:219-231.

Bath BD, Martin HB, Wightman RM, Anderson MR (2001) Dopamine adsorption at surface modified carbon-fiber electrodes. Langmuir 17:7032-7039.

Bath BD, Michael DJ, Trafton BJ, Joseph JD, Runnels PL, Wightman RM (2000) Subsecond adsorption and desorption of dopamine at carbon-fiber microelectrodes. Anal Chem 72:5994-6002.

Baur JE, Kristensen EW, May LJ, Wiedemann DJ, Wightman RM (1988) Fast-scan voltammetry of biogenic amines. Analytical Chemistry 60:1268-1272.

Bezbaruah AN, Zhang TC (2002) Fabrication of anodically electrodeposited iridium oxide film pH microelectrodes for microenvironmental studies. Analytical Chemistry 74:5726-5733.

Bindra DS, Zhang YN, Wilson GS, Sternberg R, Thevenot DR, Moatti D, Reach G (1991) Design and Invitro Studies of a Needle-Type Glucose Sensor for Subcutaneous Monitoring. Analytical Chemistry 63:1692-1696.

Blaha CD, Phillips AG (1996) A critical assessment of electrochemical procedures applied to the measurement of dopamine and its metabolites during drug-induced and species-typical behaviours. Behavioural Pharmacology 7:675-708.

Blank CL, Mccreery RL, Wightman RM, Chey W, Adams RN, Reid JR, Smissman EE (1976) Intracyclization Rates of 6-Hydroxydopamine and 6-Aminodopamine Analogs under Physiological Conditions. Journal of Medicinal Chemistry 19:178-180.

Bolger FB, Lowry JP (2005) Brain tissue oxygen: In vivo monitoring with carbon paste electrodes. Sensors 5:473-487.

Brajter-Toth A, Abou El-Nour K, Cavalheiro ET, Bravo R (2000) Nanostructured carbon fiber disk electrodes for sensitive determinations of adenosine and uric acid. Analytical Chemistry 72:1576-1584.

Burmeister JJ, Gerhardt GA (2001) Self referencing ceramic based multisite microelectrodes for the detection and elimination of interferences from the measurement of L-glutamate and other analytes. Analytical Chemistry 73:1037-1042.

Burmeister JJ, Gerhardt GA (2003) Ceramic-based multisite microelectrode arrays for in vivo electrochemical recordings of glutamate and other neurochemicals. Trac-Trends in Analytical Chemistry 22:498-502.

Burmeister JJ, Moxon, Karen, Gerhardt, Greg A. (2000) Ceramic-Based Multisite Microelectrodes for Electrochemical Recordings. Anal Chem 72:187-192.

Cahill PS, Wightman RM (1995) Simultaneous Amperometric Measurement of Ascorbate and Catecholamine Secretion from Individual Bovine Adrenal-Medullary Cells. Analytical Chemistry 67:2599-2605.

Cahill PS, Walker QD, Finnegan JM, Mickelson GE, Travis ER, Wightman RM (1996) Microelectrodes for the measurement of catecholamines in biological systems. Analytical Chemistry 68:3180-3186.

Cheer JF, Wassum KM, Wightman RM (2006) Cannabinoid modulation of electrically evoked pH and oxygen transients in the nucleus accumbens of awake rats. Journal of Neurochemistry 97:1145-1154.

Chen BT, Avshalumov MV, Rice ME (2001) H2O2 is a novel, endogenous modulator of synaptic dopamine release. Journal of Neurophysiology 85:2468-2476.

Chen JCT, Chesler M (1992) Ph Transients Evoked by Excitatory Synaptic Transmission Are Increased by Inhibition of Extracellular Carbonic-Anhydrase. Proceedings of the National Academy of Sciences of the United States of America 89:7786-7790.

Chen P, McCreery RL (1996) Control of electron transfer kinetics at glassy carbon electrodes by specific surface modification. Analytical Chemistry 68:3958-3965.

Chen TK, Luo G, Ewing AG (1994) Amperometric monitoring of stimulated catecholamine release from rat pheochromocytoma (PC12) cells at the zeptomole level. Anal Chem 66:3031-3035.

Chesler M, Chan CY (1988) Stimulus-Induced Extracellular Ph Transients in the Invitro Turtle Cerebellum. Neuroscience 27:941-948.

Chesler M, Chen JCT, Kraig RP (1994) Determination of Extracellular Bicarbonate and Carbon-Dioxide Concentrations in Brain-Slices Using Carbonate and Ph-Selective Microelectrodes. Journal of Neuroscience Methods 53:129-136.

Ciolkowski EL, Cooper BR, Jankowski JA, Jorgenson JW, Wightman RM (1992) Direct Observation of Epinephrine and Norepinephrine Cosecretion from Individual Adrenal-Medullary Chromaffin Cells. Journal of the American Chemical Society 114:2815-2821.

Ciszewski A, Milczarek G, Kubaszewski E, Lozynski M (1998) Oxidation of nitric oxide at a porphyrinic-based sensor new results from rotating disk experiments. Electroanalysis 10:628-632.

Clark LC, Lyons C (1962) Electrode Systems for Continuous Monitoring in Cardiovascular Surgery. Annals of the New York Academy of Sciences 102:29-&.

Compagnone D, Guilbault GG (1997) Glucose oxidase/hexokinase electrode for the determination of ATP. Analytica Chimica Acta 340:109-113.

Conti JC, Strope E, Adams RN, Marsden CA (1978) Voltammetry in Brain-Tissue - Chronic Recording of Stimulated Dopamine and 5-Hydroxytryptamine Release. Life Sciences 23:2705-2715.

Cooper JR, Bloom FE, Roth RH, Editors (2003) The Biochemical Basis of Neuropharmacology, Eighth Edition.

Crespi F, Paret J, Keane PE, Morre M (1984) An Improved Differential Pulse Voltammetry Technique Allows the Simultaneous Analysis of Dopaminergic and Serotonergic Activities Invivo with a Single Carbon-Fiber Electrode. Neuroscience Letters 52:159-164.

Dale N, Pearson T, Frenguelli BG (2000) Direct measurement of adenosine release during hypoxia in the CA1 region of the rat hippocampal slice. Journal of Physiology-London 526:143-155.

Dale N, Hatz S, Tian F, Llaudet E (2005) Listening to the brain: microelectrode biosensors for neurochemicals. Trends Biotechnol 23:420-428.

Daws LC, Montanez S, Owens WA, Gould GG, Frazer A, Toney GM, Gerhardt GA (2005) Transport mechanisms governing serotonin clearance in vivo revealed by high-speed chronoamperometry. J Neurosci Methods 143:49-62.

Dawson VL, Dawson TM (1996) Nitric oxide actions in neurochemistry. Neurochemistry International 29:97-110.

Downard AJ, Roddick AD, Bond AM (1995) Covalent modification of carbon electrodes for voltammetric differentiation of dopamine and ascorbic acid. Analytica Chimica Acta 317:303-310.

Etienne M, Oni J, Schulte A, Hartwich G, Schuhmann W (2005) Solvent-free electrodeposition of polypyrrole as a base for the preparation of carbonised platinum microelectrodes. Electrochimica Acta 50:5001-5008.

Falkenburger BH, Barstow KL, Mintz IM (2001) Dendrodendritic inhibition through reversal of dopamine transport. Science 293:2465-2470.

Friedemann MN, Robinson SW, Gerhardt GA (1996) o-phenylenediamine-modified carbon fiber electrodes for the detection of nitric oxide. Analytical Chemistry 68:2621-2628.

Garguilo MG, Michael AC (1993) An Enzyme-Modified Microelectrode That Detects Choline Injected Locally into Brain-Tissue. Journal of the American Chemical Society 115:12218-12219.

Garguilo MG, Michael AC (1994) Quantitation of Choline in the Extracellular Fluid of Brain-Tissue with Amperometric Microsensors. Analytical Chemistry 66:2621-2629.

Garguilo MG, Michael AC (1996) Amperometric microsensors for monitoring choline in the extracellular fluid of brain. Journal of Neuroscience Methods 70:73-82.

Georganopoulou DG, Carley R, Jones DA, Boutelle MG (2000) Development and comparison of biosensors for in-vivo applications. Faraday Discussions:291-303.

Gonon F, Buda M, Cespuglio R, Jouvet M, Pujol JF (1980a) In vivo electrochemical detection of catechols in the neostriatum of anesthetized rats: Dopamine or DOPAC? Nature 286:902-904.

Gonon F, Buda M, Cespuglio R, Jouvet M, Pujol JF (1980b) Invivo Electrochemical Detection of Catechols in the Neostriatum of Anesthetized Rats - Dopamine or Dopac. Nature 286:902-904.

Gonon F, Cespuglio R, Ponchon JL, Buda M, Jouvet M, Adams RN, Pujol JF (1978) [In vivo continuous electrochemical determination of dopamine release in rat neostriatum]. C R Acad Sci Hebd Seances Acad Sci D 286:1203-1206.

Gonon FG, Navarre F, Buda MJ (1984) Invivo Monitoring of Dopamine Release in the Rat-Brain with Differential Normal Pulse Voltammetry. Analytical Chemistry 56:573-575.

Gonon FG, Fombarlet CM, Buda MJ, Pujol JF (1981) Electrochemical Treatment of Pyrolytic Carbon-Fiber Electrodes. Analytical Chemistry 53:1386-1389.

Gregg BA, Heller A (1990) Cross-Linked Redox Gels Containing Glucose-Oxidase for Amperometric Biosensor Applications. Analytical Chemistry 62:258-263.

Gregg BA, Heller A (1991) Redox Polymer-Films Containing Enzymes .2. Glucose-Oxidase Containing Enzyme Electrodes. Journal of Physical Chemistry 95:5976-5980.

Griveau S, Dumezy C, Seguin J, Chabot GG, Scherman D, Bedioui F (2007) In vivo electrochemical detection of nitric oxide in tumor-bearing mice. Analytical Chemistry 79:1030-1033.

Guerrieri A, Lattanzio V, Palmisano F, Zambonin PG (2006) Electrosynthesized poly(pyrrole)/poly(2-naphthol) bilayer membrane as an effective anti-interference layer for simultaneous determination of acethylcholine and choline by a dual electrode amperometric biosensor. Biosensors & Bioelectronics 21:1710-1718.

Hawley MD, Tatawawa.Sv, Piekarsk.S, Adams RN (1967) Electrochemical Studies of Oxidation Pathways of Catecholamines. Journal of the American Chemical Society 89:447-&.

Heien ML, Phillips PE, Stuber GD, Seipel AT, Wightman RM (2003) Overoxidation of carbon-fiber microelectrodes enhances dopamine adsorption and increases sensitivity. Analyst 128:1413-1419.

Heien MLAV, Johnson MA, Wightman RM (2004) Resolving neurotransmitters detected by fast-scan cyclic voltammetry. Analytical Chemistry 76:5697-5704.

Hermans A, Seipel AT, Miller CE, Wightman RM (2006) Carbon-fiber microelectrodes modified with 4-sulfobenzene have increased sensitivity and selectivity for catecholamines. Langmuir 22:1964-1969.

Hochstetler SE, Puopolo M, Gustincich S, Raviola E, Wightman RM (2000) Real-time amperometric measurements of zeptomole quantities of dopamine released from neurons. Analytical Chemistry 72:489-496.

Hoffman AF, Gerhardt GA (1998) In vivo electrochemical studies of dopamine clearance in the rat substantia nigra: Effects of locally applied uptake inhibitors and unilateral 6-hydroxydopamine lesions. Journal of Neurochemistry 70:179-189.

Howell JO, Kuhr WG, Ensman RE, Wightman RM (1986) Background Subtraction for Rapid Scan Voltammetry. Journal of Electroanalytical Chemistry 209:77-90.

Hsueh C, Bravo R, Jaramillo AJ, BrajterToth A (1997) Surface and kinetic enhancement of selectivity and sensitivity in analysis with fast scan voltammetry at scan rates above 1000 V/s. Analytica Chimica Acta 349:67-76.

Hsueh CC, Brajtertoth A (1994) Electrochemical Preparation and Analytical Applications of Ultrathin Overoxidized Polypyrrole Films. Analytical Chemistry 66:2458-2464.

Hu YB, Wilson GS (1997a) A temporary local energy pool coupled to neuronal activity: Fluctuations of extracellular lactate levels in rat brain monitored with rapid-response enzyme-based sensor. Journal of Neurochemistry 69:1484-1490.

Hu YB, Wilson GS (1997b) Rapid changes in local extracellular rat brain glucose observed with an in vivo glucose sensor. Journal of Neurochemistry 68:1745-1752.

Huettl P, French K, Pomerleau FP, Palmer MR, Burmeister JJ, Granholm AC, Gerhardt GA (2002) Dynamics of glutamate release and uptake in the rat CNS. Experimental Neurology 175:439-439.

Huff RM, Adams RN (1980) Dopamine Release in N Accumbens and Striatum by Clozapine - Simultaneous Monitoring by Invivo Electrochemistry. Neuropharmacology 19:587-590.

Hummon AB, Sweedler JV, Corbin RW (2003) Discovering new neuropeptides using single-cell mass spectrometry. Trac-Trends in Analytical Chemistry 22:515-521.

Hummon AB, Amare A, Sweedler JV (2006) Discovering new invertebrate neuropeptides using mass spectrometry. Mass Spectrometry Reviews 25:77-98.

Ichimori K, Ishida H, Fukahori M, Nakazawa H, Murakami E (1994) Practical Nitric-Oxide Measurement Employing a Nitric Oxide-Selective Electrode. Review of Scientific Instruments 65:2714-2718.

Isik S, Castillo J, Blochl A, Csoregi E, Schuhmann W (2007) Simultaneous detection of L-glutamate and nitric oxide from adherently growing cells at known distance using disk shaped dual electrodes. Bioelectrochemistry 70:173-179.

Jaffe EH, Marty A, Schulte A, Chow RH (1998) Extrasynaptic vesicular transmitter release from the somata of substantia nigra neurons in rat midbrain slices. Journal of Neuroscience 18:3548-3553.

Johnson MD, Kao OE, Kipke DR (2007) Spatiotemporal pH dynamics following insertion of neural microelectrode arrays. Journal of Neuroscience Methods 160:276-287.

Jones DA, Ros J, Landolt H, Fillenz M, Boutelle MG (2000) Dynamic changes in glucose and lactate in the cortex of the freely moving rat monitored using microdialysis. Journal of Neurochemistry 75:1703-1708.

Kawagoe KT, Wightman RM (1994) Characterization of Amperometry for in-Vivo Measurement of Dopamine Dynamics in the Rat-Brain. Talanta 41:865-874.

Kawagoe KT, Zimmerman JB, Wightman RM (1993) Principles of voltammetry and microelectrode surface states. Journal of neuroscience methods 48:225-240.

Kissinger PT, Hart JB, Adams RN (1973) Voltammetry in Brain-Tissue - New Neurophysiological Measurement. Brain Research 55:209-213.

Kueng A, Kranz C, Mizaikoff B (2004) Amperometric ATP biosensor based on polymer entrapped enzymes. Biosens Bioelectron 19:1301-1307.

Kulagina NV, Michael AC (2003) Monitoring hydrogen peroxide in the extracellular space of the brain with amperometric microsensors. Analytical Chemistry 75:4875-4881.

Kulagina NV, Shankar L, Michael AC (1999) Monitoring glutamate and ascorbate in the extracellular space of grain tissue with electrochemical microsensors. Analytical Chemistry 71:5093-5100.

Kusakabe H, Midorikawa Y, Fujishima T, Kuninaka A, Yoshino H (1983) Purification and Properties of a New Enzyme, L-Glutamate Oxidase, from Streptomyces Sp X-119-6 Grown on Wheat Bran. Agricultural and Biological Chemistry 47:1323-1328.

Lane RF, Blaha CD (1990) Detection of Catecholamines in Brain-Tissue - Surface-Modified Electrodes Enabling Invivo Investigations of Dopamine Function. Langmuir 6:56-65.

Leszczyszyn DJ, Jankowski JA, Viveros OH, Diliberto EJ, Near JA, Wightman RM (1991) Secretion of Catecholamines from Individual Adrenal-Medullary Chromaffin Cells. Journal of Neurochemistry 56:1855-1863.

Llaudet E, Botting NP, Crayston JA, Dale N (2003a) A three-enzyme microelectrode sensor for detecting purine release from central nervous system. Biosensors & Bioelectronics 18:43-52.

Llaudet E, Botting NP, Crayston JA, Dale N (2003b) A three-enzyme microelectrode sensor for detecting purine release from central nervous system. Biosens Bioelectron 18:43-52.

Llaudet E, Hatz S, Droniou M, Dale N (2005) Microelectrode biosensor for real-time measurement of ATP in biological tissue. Anal Chem 77:3267-3273.

Lyne PD, Oneill RD (1989) Selectivity of Stearate-Modified Carbon Paste Electrodes for Dopamine and Ascorbic-Acid. Analytical Chemistry 61:2323-2324.

Marsden CA, Joseph MH, Kruk ZL, Maidment NT, Oneill RD, Schenk JO, Stamford JA (1988) Invivo Voltammetry - Present Electrodes and Methods. Neuroscience 25:389-400.

Marzouk SAM, Ufer S, Buck RP, Johnson TA, Dunlap LA, Cascio WE (1998) Electrodeposited iridium oxide pH electrode for measurement of extracellular myocardial acidosis during acute ischemia. Analytical Chemistry 70:5054-5061.

Matos RC, Angnes L, Araujo MCU, Saldanha TCB (2000) Modified microelectrodes and multivariate calibration for flow injection amperometric simultaneous determination of ascorbic acid, dopamine, epinephrine and dipyrone. Analyst 125:2011-2015.

Mazzei F, Botre F, Lorenti G, Porcelli F (1996) Peroxidase based amperometric biosensors for the determination of gamma-aminobutyric acid. Analytica Chimica Acta 328:41-46.

McCreery RL (1996) Laboratory Techniques in Electroanalytical Chemistry, Dekker, New York Chapter 10.

Mefford IN, Oke AF, Adams RN (1981) Regional Distribution of Ascorbate in Human-Brain. Brain Research 212:223-226.

Millar J, Stamford JA, Kruk ZL, Wightman RM (1985) Electrochemical, Pharmacological and Electrophysiological Evidence of Rapid Dopamine Release and Removal in the Rat Caudate-Nucleus Following Electrical-Stimulation of the Median Forebrain-Bundle. European Journal of Pharmacology 109:341-348.

Millar J, Oconnor JJ, Trout SJ, Kruk ZL (1992) Continuous Scan Cyclic Voltammetry (Cscv) - a New High-Speed Electrochemical Method for Monitoring Neuronal Dopamine Release. Journal of Neuroscience Methods 43:109-118.

Miller AD, Forster GL, Yeomans JS, Blaha CD (2005) Midbrain muscarinic receptors modulate morphine-induced accumbal and striatal dopamine efflux in the rat. Neuroscience 136:531-538.

Mueller K (1986) Invivo Voltammetric Recording with Nafion-Coated Carbon Paste Electrodes - Additional Evidence That Ascorbic-Acid Release Is Monitored. Pharmacology Biochemistry and Behavior 25:325-328.

Murphy LJ, Galley PT (1994) Measurement in-Vitro of Human Plasma Glycerol with a Hydrogen-Peroxide Detecting Microdialysis Enzyme Electrode. Analytical Chemistry 66:4345-4353.

Nagy G, Rice ME, Adams RN (1982) A New Type of Enzyme Electrode - the Ascorbic-Acid Eliminator Electrode. Life Sciences 31:2611-2616.

O'Neill RD (2005) Long-term monitoring of brain dopamine metabolism in vivo with carbon paste electrodes. Sensors 5:317-342.

O'Neill RD, Grunewald RA, Fillenz M, Albery WJ (1982) Linear sweep voltammetry with carbon paste electrodes in the rat striatum. Neuroscience 7:1945-1954.

Ogawa S, Lee TM, Kay AR, Tank DW (1990) Brain magnetic resonance imaging with contrast dependent on blood oxygenation. Proc Natl Acad Sci U S A 87:9868-9872.

Oldenziel WH, Dijkstra G, Cremers TIFH, Westerink BHC (2006) Evaluation of hydrogel-coated glutamate microsensors. Analytical Chemistry 78:3366-3378.

Pan ST, Arnold MA (1996) Selectivity enhancement for glutamate with a Nafion/glutamate oxidase biosensor. Talanta 43:1157-1162.

Parkin MC, Hopwood SE, Jones DA, Hashemi P, Landolt H, Fabricius M, Lauritzen M, Boutelle MG, Strong AJ (2005) Dynamic changes in brain glucose and lactate in pericontusional areas of the human cerebral cortex, monitored with rapid sampling on-line microdialysis: relationship with depolarisation-like events. Journal of Cerebral Blood Flow and Metabolism 25:402-413.

Perez XA, Andrews AM (2005) Chronoamperometry to determine differential reductions in uptake in brain synaptosomes from serotonin transporter knockout mice. Anal Chem 77:818-826.

Peters JL, Miner LH, Michael AC, Sesack SR (2004) Ultrastructure at carbon fiber microelectrode implantation sites after acute voltammetric measurements in the striatum of anesthetized rats. Journal of Neuroscience Methods 137:9-23.

Phillips PEM, Robinson DL, Stuber GD, Carelli RM, Wightman RM (2003) Real-time measurements of phasic changes in extracellular dopamine concentration in freely moving rats by fast-scan cyclic voltammetry. Methods in Molecular Medicine 79:443-464.

Pihel K, Schroeder TJ, Wightman RM (1994) Rapid and Selective Cyclic Voltammetric Measurements of Epinephrine and Norepinephrine as a Method

to Measure Secretion from Single Bovine Adrenal-Medullary Cells. Analytical Chemistry 66:4532-4537.

Pihel K, Walker QD, Wightman RM (1996) Overoxidized polypyrrole-coated carbon fiber microelectrodes for dopamine measurements with fast-scan cyclic voltammetry. Analytical chemistry 68:2084-2089.

Pihel K, Hsieh S, Jorgenson JW, Wightman RM (1995) Electrochemical Detection of Histamine and 5-Hydroxytryptamine at Isolated Mast-Cells. Analytical Chemistry 67:4514-4521.

Ponchon JL, Cespuglio R, Gonon F, Jouvet M, Pujol JF (1979) Normal pulse polarography with carbon fiber electrodes for in vitro and in vivo determination of catecholamines. Anal Chem 51:1483-1486.

Pothos EN, Davila V, Sulzer D (1998) Presynaptic recording of quanta from midbrain dopamine neurons and modulation of the quantal size. Journal of Neuroscience 18:4106-4118.

Ramesh P, Sampath S (2004) Selective determination of uric acid in presence of ascorbic acid and dopamine at neutral pH using exfoliated graphite electrodes. Electroanalysis 16:866-869.

Runnels PL, Joseph JD, Logman MJ, Wightman RM (1999) Effect of pH and Surface Functionalities on the Cyclic Voltammetric Responses of Carbon-Fiber Microelectrodes. Analytical Chemistry 71:2782-2789.

Sandberg M, Weber SG (2003) Techniques for neuropeptide determination. Trac-Trends in Analytical Chemistry 22:522-527.

Schuman EM, Madison DV (1994) Nitric-Oxide and Synaptic Function. Annual Review of Neuroscience 17:153-183.

Shibuki K (1990) An Electrochemical Microprobe for Detecting Nitric-Oxide Release in Brain-Tissue. Neuroscience Research 9:69-76.

Shin JH, Weinman SW, Schoenfisch MH (2005) Sol-gel derived amperometric nitric oxide microsensor. Analytical Chemistry 77:3494-3501.

Shram N, Netchiporouk L, Cespuglio R (2002) Lactate in the brain of the freely moving rat: voltammetric monitoring of the changes related to the sleep-wake states. European Journal of Neuroscience 16:461-466.

Shram NF, Netchiporouk LI, Martelet C, Jaffrezic-Renault N, Bonnet C, Cespuglio R (1998) In vivo voltammetric detection of rat brain lactate with carbon fiber microelectrodes coated with lactate oxidase. Analytical Chemistry 70:2618-2622.

Silver IA, Erecinska M (1994) Extracellular Glucose-Concentration in Mammalian Brain - Continuous Monitoring of Changes during Increased Neuronal-Activity and Upon Limitation in Oxygen-Supply in Normoglycemic, Hypoglycemic, and Hyperglycemic Animals. Journal of Neuroscience 14:5068-5076.

Sternson AW, Mccreery R, Feinberg B, Adams RN (1973) Electrochemical Studies of Adrenergic Neurotransmitters and Related Compounds. Journal of Electroanalytical Chemistry 46:313-321.

Swain GM, Kuwana T (1991) Electrochemical Formation of High Surface-Area Carbon-Fibers. Analytical Chemistry 63:517-519.

Swamy BEK, Venton BJ (2007) Subsecond detection of physiological adenosine concentrations using fast-scan cyclic voltammetry. Analytical Chemistry 79:744-750.

Thompson JK, Peterson MR, Freeman RD (2003) Single-neuron activity and tissue oxygenation in the cerebral cortex. Science 299:1070-1072.

Troyer KP, Heien MLAV, Venton BJ, Wightman RM (2002) Neurochemistry and electroanalytical probes. Current Opinion in Chemical Biology 6:696-703.

Unger EL, Eve DJ, Perez XA, Reichenbach DK, Xu YQ, Lee MK, Andrews AM (2006) Locomotor hyperactivity and alterations in dopamine neurotransmission are associated with overexpression of A53T mutant human alpha-synuclein in mice. Neurobiology of Disease 21:431-443.

Updike SJ, Hicks GP (1967) Enzyme Electrode. Nature 214:986-&.

Vandaveer WR, Woodward DJ, Fritsch I (2003) Redox cycling measurements of a model compound and dopamine in ultrasmall volumes with a self-contained microcavity device. Electrochimica Acta 48:3341-3348.

Venton BJ, Troyer KP, Wightman RM (2002) Response Times of Carbon Fiber Microelectrodes to Dynamic Changes in Catecholamine Concentration. Analytical Chemistry 74:539-546.

Venton BJ, Michael DJ, Wightman RM (2003a) Correlation of local changes in extracellular oxygen and pH that accompany dopaminergic terminal activity in the rat caudate-putamen. Journal of Neurochemistry 84:373-381.

Venton BJ, Michael DJ, Wightman RM (2003b) Correlation of local changes in extracellular oxygen and pH that accompany dopaminergic terminal activity in the rat caudate-putamen. J Neurochem 84:373-381.

Wang DL, Heller A (1993) Miniaturized Flexible Amperometric Lactate Probe. Analytical Chemistry 65:1069-1073.

Wang J, Pamidi PVA, Cepria G, Basak S, Rajeshwar K (1997) Overoxidized poly{pyrrole-co-[3-(pyrrol-1-yl)propanesulfonate]}-coated platinum electrodes for selective detection of catecholamine neurotransmitters. Analyst 122:981-984.

Watson CJ, Venton BJ, Kennedy RT (2006) In vivo measurements of neurotransmitters by microdialysis sampling. Analytical Chemistry 78:1391-1399.

Wiedemann DJ, Bassetomusk A, Wilson RL, Rebec GV, Wightman RM (1990) Interference by Dopac and Ascorbate during Attempts to Measure Drug-Induced Changes in Neostriatal Dopamine with Nafion-Coated, Carbon-Fiber Electrodes. Journal of Neuroscience Methods 35:9-18.

Wightman RM, Jankowski JA, Kennedy RT, Kawagoe KT, Schroeder TJ, Leszczyszyn DJ, Near JA, Diliberto EJ, Jr., Viveros OH (1991) Temporally resolved catecholamine spikes correspond to single vesicle release from individual chromaffin cells. Proc Natl Acad Sci U S A 88:10754-10758.

Wilson GS, Gifford R (2005) Biosensors for real-time in vivo measurements. Biosens Bioelectron 20:2388-2403.

Witkowski A, Brajtertoth A (1992) Overoxidized Polypyrrole Films - a Model for the Design of Permselective Electrodes. Analytical Chemistry 64:635-641.

Wrona MZ, Dryhurst G (1990) Electrochemical Oxidation of 5-Hydroxytryptamine in Aqueous-Solution at Physiological Ph. Bioorganic Chemistry 18:291-317.

Yan JL, Du Y, Liu JF, Cao WD, Sun SH, Zhou WH, Yang XR, Wang EK (2003) Fabrication of integrated microelectrodes for electrochemical detection on electrophoresis microchip by electroless deposition and micromolding in capillary technique. Analytical Chemistry 75:5406-5412.

Zhang F, Dryhurst G (1993) Oxidation Chemistry of Dopamine - Possible Insights into the Age-Dependent Loss of Dopaminergic Nigrostriatal Neurons. Bioorganic Chemistry 21:392-410.

Zhou Z, Misler S (1995) Action Potential-Induced Quantal Secretion of Catecholamines from Rat Adrenal Chromaffin Cells. Journal of Biological Chemistry 270:3498-3505.

Zimmerman JB, Wightman RM (1991) Simultaneous Electrochemical Measurements of Oxygen and Dopamine Invivo. Analytical Chemistry 63:24-28.

CHAPTER 2

CARBON-FIBER MICROELECRODES MODIFIED WITH 4-SULFOBENZENE HAVE INCREASED SENSETIVITY AND SELECTIVITY FOR CATECHOLAMINES

Introduction

Voltammetric microelectrodes provide a platform for the construction of sensors of the concentration fluctuations of easily oxidized neurotransmitters in the extracellular fluid of the brain (Kawagoe et al., 1993). The neurotransmitter dopamine can be detected in this way. Dopamine has shown to be of central importance to normal behavior. For example, depletion of dopamine in the striatum is a consequence of Parkinson's disease, (Cooper et al., 1996) and the symptoms can be alleviated by administration of its biosynthetic precursor, L-DOPA. In addition, dopaminergic neurons are involved in brain circuitry that is important in reward and addiction (Schultz et al., 1993; Waelti et al., 2001).

Several sensor properties are desirable for the detection of dopamine. The sensor should have a fast response time because concentration changes *in vivo* occur on a sub-second time scale (Pothos et al., 1998). High sensitivity is required because the physiological actions of dopamine at its receptors occur at concentrations in the range from nanomolar to low micromolar(Richfield et al., 1989; Berke and Hyman, 2000). High selectivity is required because other electroactive species are present

in the extracellular fluid of the brain at much higher concentrations than dopamine. Background subtracted, fast-scan cyclic voltammetry at carbon-fiber microelectrodes has been shown to have many of these characteristics so that it is a useful technique for detection of dopamine and other oxidizable neurotransmitters at single biological cells and within intact tissue (Garris and Wightman, 1995; Travis and Wightman, 1998). Recent improvement in instrumentation and computer control allowed this technique to achieve very high sensitivities (Cahill et al., 1996; Michael et al., 1998; Michael et al., 1999). The basis for the high sensitivity of fast-scan cyclic voltammetry for dopamine depends is its accumulation by adsorption at the carbon surface in the time between collection of each cyclic voltammogram. An alternate approach to increase sensitivity and selectivity with carbon-fiber electrodes is to use surface coatings such as Nafion®, a perfluorinated cation-exchange polymer, or overoxidized polypyrrole (Baur et al., 1988; Pihel et al., 1996). These coatings promote dopamine accumulation at the electrode surface while rejecting anions. However, both coatings are noncovalently attached layers that have finite thickness. The time required for molecules to diffuse through the coating increases the response time of the electrode. An alternate approach to achieve high sensitivity is electrochemical overoxidation of the carbon surface (Heien et al., 2003). This appears to increase anionic sites on the surface because it promotes increased adsorption of amines that are protonated at physiological pH such as dopamine. However, overoxidation decreases selectivity and also increases the response time of the electrode to dopamine.

Savéant and coworkers introduced a procedure for covalent attachment to carbon surfaces by grafting aryl radicals produced by electrochemical reduction of diazonium salts (Delamar et al., 1992). Subsequently diazonium salt reduction has been demonstrated to be a versatile method to functionalize carbon-electrode surfaces (Downard and Roddick, 1995; Downard et al., 1995; Liu and McCreery, 1995; Allongue et al., 1997; Delamar et al., 1997; Pinson and Podvorica, 2005). While strong bonding and dense packing of monolayers produced by diazonium reduction were initially established, later studies demonstrated that some aryl diazonium salts tend to form multilayer structures on the electrode surfaces.(Kariuki and McDermott, 1999, 2001; Anariba et al., 2003; D'Amours and Belanger, 2003) Recent research has shown that reduction of diazonuim salts at metal electrodes also forms surface layers at non-carbon electrodes (Dequaire et al., 1999; Adenier et al., 2001; Chausse et al., 2002; Boukerma et al., 2003; Laforgue et al., 2005).

To create a dopamine sensitive and selective electrode we have modified carbon microelectrodes via reduction of 4-sulfobenzenediazonium tetrafluoroborate (4-SBD). The sulfonate group can provide a cation exchange site similar to Nafion® but with a thinner grafted layer that is covalently attached to the electrode surface. In this study we compare the fast-scan cyclic voltammetric response at modified electrodes and untreated electrodes to several neurochemicals as well as examine the adsorption behavior of dopamine. In addition, the functionality of these electrodes was tested in mouse brain slices.

EXPERIMENTAL SECTION

Chemicals

All chemicals for flow injection analysis were purchased from Sigma-Aldrich (St. Louis, MO) and used as received. Solutions were prepared using doubly distilled water (Megapure system, Corning, New York). Solutions for flow injection analysis were prepared in a TRIS buffer solution, pH 7.4 containing 15 mM TRIS, 140 mM NaCl, 3.25 mM KCl, 1.2 $CaCl_2$, 1.25 mM NaH_2PO_4, 1.2 mM $MgCl_2$ and 2.0 mM Na_2SO_4. This buffer mimics the ionic environment present in cerebral spinal fluid. Stock solutions of analyte were prepared in 0.1 M $HClO_4$, and were diluted to the desired concentration with TRIS buffer on the day of use.

Synthesis and characterization of 4-sulfobenzenediazonium tetrafluoroborate (4-SBD)

0.1 mol (17.3 g) of 4-aminobenzenesulphonic acid (Sigma-Aldrich, St. Louis, MO) was dissolved in 0.2 mol (37 g) of tetrafluoroboric acid (48 %) (Fischer Chemicals, Fair lawn, NJ). This solution was cooled in an ice-salt bath to -5°C. Water was added to 0.1 mol (6.9 g) sodium nitrite (Aldrich, Milwaukee, WI) until dissolution was complete and the nitrite solution was added dropwise to 4-aminobenzenesulphonic acid over 30 min while mechanically stirring. The resulting suspension was vacuum filtered and the white salt was washed with an ice cold ether-methanol mixture (4:1), purified by washing with small amounts of ice cold ethanol, and dried over calcium chloride. The compound was stored at 4°C. The

purified compound was characterized by 400 MHz- NMR measurements. (DMSO) δ 7.80 (1H,d), 7.68 (1H,d), 7.29 (1H,d) , 7.27 (1H,d) with no proton signal for the amine group. IR analysis showed a strong band at 2300 cm^{-1} that indicated the presence of the diazonium group. Melting point determination showed decomposition at 127°C – 130°C consistent with the range determined by Kolar(Kolar, 1972) for 4-SBD.

Electrode preparation

The microelectrodes were fabricated as previously described(Kawagoe et al., 1993) with both P-55 and T650 carbon fibers (Thornel, Amoco Corp., Greenville, SC). A single fiber was aspirated into a glass capillary and pulled on a micropipette puller (Narashige, Tokyo, Japan). For elliptical electrodes the fiber was sealed into the capillary with epoxy resin (Epon 828 with 14% m-phenlylenediamine by weight, Miller Stephenson Chemical Co., Danbury,CT). After curing the epoxy, the electrodes were polished at a 45° angle on a diamond embedded polishing wheel (Sutter Instruments), resulting in an elliptical surface of approximately 10^{-6} cm^2 for P-55 disks and 4 x 10^{-7} cm^2 for T-650 disks.

The capillaries of the microelectrodes were backfilled with electrolyte solution (4M potassium acetate, 150 mM potassium chloride), and wires were inserted into the capillary for electrical contact. Macroelectrodes were constructed by attaching contact wires to the back of glassy carbon plates (Tokai, between 1 cm^2 and 2 cm^2 surface area) with silver epoxy (H2O-PFC, EPO-TEK, Billerica, MA). The epoxy was cured for 5 minutes at 150°C. The glassy carbon plate was sealed with

High Vacuum Torr Seal (Varian Vacuum Technologies) that was cured overnight at room temperature. The carbon surface was exposed by polishing with alumina slurries of 1μm, 0.3μm, and 0.05μm size subsequently.(McCreery, 1996) Before use all electrodes were soaked in isopropanol purified with Norit A activated carbon (ICN, Costa Mesa, CA) for at least 20 minutes.(Bath et al., 2000)

Chemical surface modification

4-sulfobenzene (4-SB) was attached to the carbon surface by electroreduction at a potential of -1.0 V vs Ag/AgCl for 5 minutes(Delamar et al., 1992; Allongue et al., 1997). Electrolysis was done in acetonitrile, dried over alumina before use, containing 1 mM 4-SBD and 0.1 M tetraflouroboric acid (48 %, Fischer Chemicals, Fair lawn, NJ). Dissolution of 4-SBD was aided by 5 minutes of sonication. Tetraflouroboric acid was used as electrolyte because it improved dissolution of the diazonium compound. It also provided better reproducibility of the surface layers than with tetrabutylammonium tertrafluoroborate as electrolyte. The small amount of water added with the tetraflouroboric acid did not adversely effect the formation of the grafted layer because the covalent attachment also occurs following diazonium reduction in aqueous solutions (Delamar et al., 1997). Before electrolysis the solution was deaerated with nitrogen for 10 minutes. For experiments examining formation of the layer cyclic voltammetry was used. The potential was cycled in 4-SBD solutions at a scan rate of 0.2 V/s from 0.5 V to -1 V vs. Ag/AgCl for 30 cycles.

XPS analysis

A Perkin Elmer PHI 5400 ESCA instrument with an Mg X-ray source was used. For survey scans, three scans were averaged: 0.5 eV/step, 50 msec/step with a pass energy of 89.45 eV, and a work function of 4.75 eV. Multiplex scans to determine the percentage composition of the sample surface were done with 0.1 eV/step, 50 msec/step, pass energy 35.75 eV, and a work function of 4.75 eV. For all multiplex scans, nine scans were taken and averaged.

Electrochemical measurements

Cyclic voltammograms were acquired and analyzed using locally constructed hardware and software written in LabVIEW (National Instruments, Austin, TX) that has been described previously(Michael et al., 1999; Heien et al., 2003). The electrochemical cell was placed inside a grounded Faraday cage to minimize electrical noise. For flow–injection analysis the electrode was positioned at the outlet of a 6-port rotary valve. A loop injector was mounted on an actuator (Rheodyne model 5041 valve and 5701 actuator) that was controlled by a 12-V DC solenoid valve kit (Rheodyne, Rohnert Park, CA) and introduced the analyte to the surface of the electrode. Solution was driven with a syringe infusion pump (2 cm/s, Harvard Apparatus Model 22, Holliston, MA) through the valve and the electrochemical cell.

For fast-scan cyclic voltammetry, the rest potential was normally -0.4 V vs. Ag/AgCl. Triangular excursions were to 1.0 V at a scan rate of 300 V/s. The waveform was repeated at a frequency of 10 Hz.

Measurements in brain slices

Coronal brain slices, 300 μm thick, from C57 black mice were prepared using a Lancer Vibratome (Technical Products International Inc., St.Louis, MO, USA)(Alger et al., 1984; Kennedy et al., 1992). The slices were placed in a recording chamber and superfused for 45 min with a preheated (34ºC) Krebs buffer before recordings were made. The buffer consisted of 126 mM NaCl, 2.5 mM KCl, 1.2 mM NaH_2PO_4, 2.4 mM $CaCl_2$, 25 mM $NaHCO_3$, 11 mM dextrose and 20 mM HEPES. The buffer was adjusted to pH 7.4 and saturated with 95% O_2 and 5% CO_2. Stimulating and working electrodes were inserted 75 μm below the surface in the dorsal lateral caudate-putamen. The placement was made with the aid of a stereomicroscope and a stereotaxic atlas(Paxinos and Watson, 1998). Local electrical stimulation was accomplished with a bipolar tungsten electrode and consisted of a single bipolar (2 ms each phase), constant current pulse with an amplitude of 350 μA. Data was acquired and collected with the same equipment as for flow injection analysis except that an Axopatch 200B served as the potentiostat (Axon Instruments, Molecular Devices Cooperation, Chicago, Illinois). The cyclic voltammetry parameters were the same as used for flow-injection analysis.

RESULTS AND DISCUSSION

Growth of sulfobenzene layers

Figure 2.1 shows a cyclic voltammogram at 200 mV/s for the reduction of 4-SBD at P-55 elliptical electrodes. During the first cycle the reduction current

approached the expected limiting current and then declined, peaking at ~ -0.65V vs Ag/AgCl. This wave was absent in subsequent cycles, a behavior observed at all types of electrodes. The peaked shape of the initial cyclic voltammogram and the diminished current on the second scan both indicate surface passivation following 4-SB attachment. The amount of the diazonium reduced was calculated by integrating the current under the voltammetric wave during the first cycle. The amounts obtained for different geometries of microelectrodes and a normal sized glassy carbon electrode are shown in figure 2.1b. P-55 elliptical electrodes showed the highest surface coverage of 57.5 nmol/cm^2 whereas P-55 cylindrical microelectrodes fabricated from the same fiber only showed 9 nmol/cm^2. Cylinders and ellipses fabricated from T-650 carbon fibers, on the other hand, showed no significant difference in amount reduced (21.5 ± 5.3 and 23.7 ± 4.0 for T-650 disks and cylinders respectively), with an amount reduced that is about 2.5 times smaller than observed at P-55 disks. T-650 carbon fibers have a polyacrylonitrile (PAN) precursor, and the structure is thought to consist of mostly disordered regions of basal and edge planes(McCreery, 1996). Thus, the surfaces at T-650 disks and T-650 cylinders are expected to have similar reactivities. In contrast, P-55 carbon fibers are produced from a pitch precursor with the basal planes ordered in concentric layers around the core. This should give a higher fraction of edge sites at the fiber end than on the cylindrical surface. Thus, the elliptical area should be more reactive than the shaft of the P-55 cylinder, consistent with the higher amounts of 4-SBD reduced.

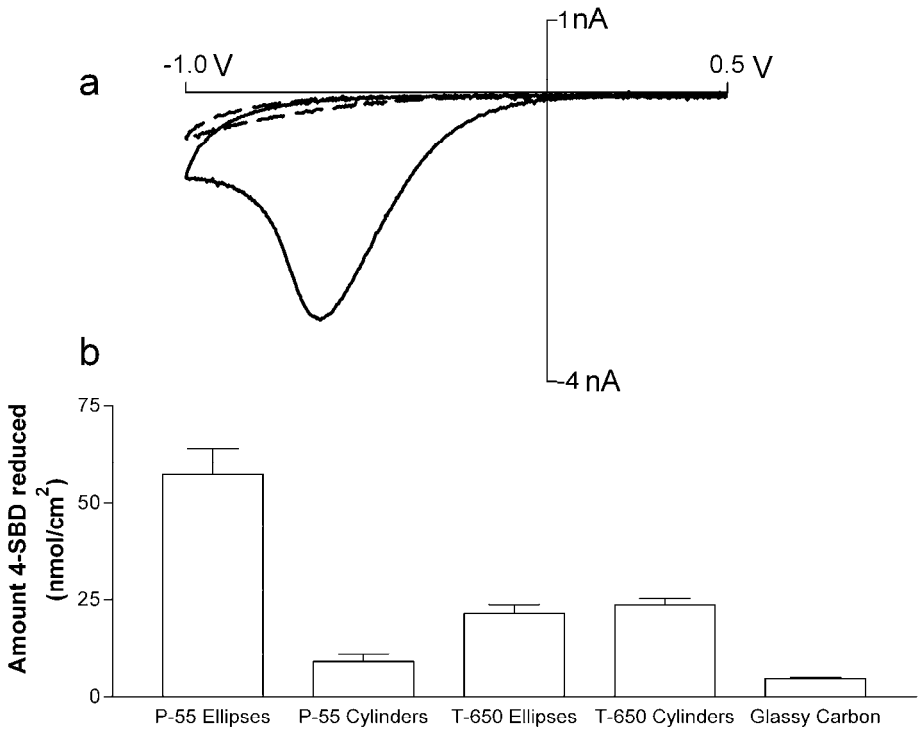

Figure 2.1. Modification of carbon electrodes with 4-SBD. (a) Cyclic voltammograms for the reduction of 1 mM 4-SBD at P-55 disk electrode in acetonitrile containing 0.1M HBF4. Solid line: first cycle; Dashed line: second cycle. (Peak potential for reduction -0.65V vs Ag/AgCl) (b) Surface coverage at different geometries after one cycle (n=6 electrodes each) Error bars represent standard error of the mean.

With dense packing a monolayer coverage would equal about 1 nmol/cm². Thus, during the first cycle a multilayer is formed at all geometries and types of electrodes examined, assuming that all the reduced 4-SBD grafts to the electrode. Multilayer formation with diazonium modification has been frequently observed. The proposed mechanism involves the intermediate radical species reacting not only with the electrode surface, but, following diffusion, reaction with molecules already attached to the electrode.(Kariuki and McDermott, 1999, 2001) This mechanism is favored for 4-SB grafting because, after depositing the initial monolayer on the surface, a negative charge originating in the sulfo group accumulates on the electrode. This layer can attract and orient the positively charged diazonium group.

The surface coverage determined from the reduction of 4-SDB likely overestimates the surface coverage because radical recombinations compete with surface attachment. Furthermore, oligomeric structures may also be formed, which do not graft to the surface. However, the amount of 4-SBD reduced can be taken as relative measurement of the surface concentration of 4-SB assuming a similar yield of the side reactions at each type of electrode. The attachment of sulfobenzene was confirmed with XPS measurements at glassy carbon electrodes treated with the same cathodic potential. Survey scans showed a sulfur S2p peak at 169 eV which was absent in blank samples. The sulfur to carbon ratio was increased 1.8-fold in a sample electrolyzed for 5 minutes compared to a one cycle reduction suggesting further layer growth after the first cycle as described previously.(Solak et al., 2002) In subsequent experiments, all electrodes were therefore electrolyzed for 5 minutes at -1.0 V vs Ag/AgCl in 4-SDB solution. Modified in this way, electrodes can be

stored in air at room temperature for up to a month without alteration of their electrochemical properties.

Fast-scan cyclic voltammetry at electrodes with grafted 4-sulfobenzene

Figure 2.2 compares the fast-scan cyclic voltammetric results at bare electrodes and electrodes with grafted 4-SB. The background current, arising from double layer charging and oxidation of surface functional groups is larger after modification. This is attributed to an increased electrode capacitance due to the grafted layer. The current for the oxidation of 5 μM dopamine at P-55 elliptical electrodes grafted with 4-SB have a peak current which is 5.3 ± 2 greater than at an unmodified surface. The covalently attached multilayer on the electrode surface serves as cation exchange membrane thus providing an opportunity for positively charged analytes to accumulate. However, the response time of 0.6 s, measured as the time required to increase from 10 to 90% of the maximum response in the flow-injection apparatus, did not change with surface modification. This indicates that diffusional transport through the layer is not significantly retarded.

The peak current for dopamine oxidation is linear with concentration from 500 nM to 5 μM. However, as shown in figure 2.2 d, the increase in peak current for dopamine at T-650 cylindrical electrodes with grafted 4-SB is 2.5 ± 0.5, only half of the increase seen at P-55 ellipses. This reduced sensitivity correlates well with the lower amounts of 4-SBD reduced seen at cylindrical T-650 electrodes (**figure 1**). The increased sensitivity was stable even after cycling the potential at 50 Hz repetition rates for several hours.

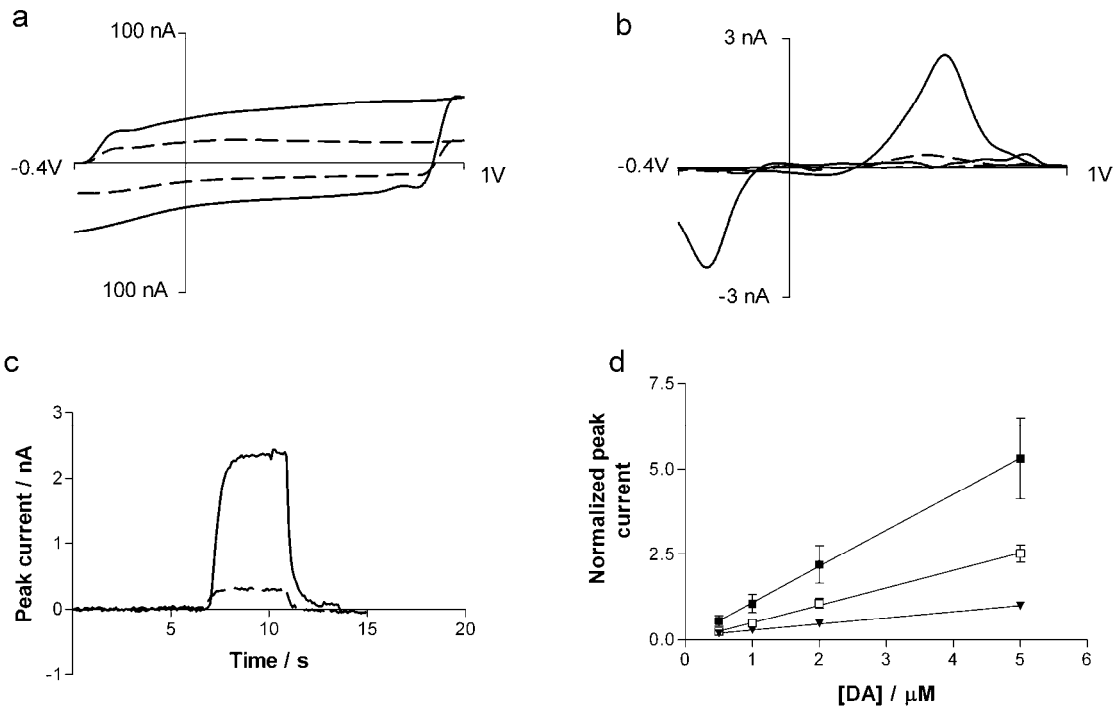

Figure 2.2. Characterization of 4SBD modified electrodes in pH 7.4 Tris buffer. (a-c): The response at bare electrodes is shown in dashes lines, while the response at modified electrodes is shown in solid lines. (a): Background cyclic voltammogram at 300 V/s form -0.4 V to 1.0V at a repletion rate of 10 Hz. (b): Background-subtracted cyclic voltammogram for 5 μM dopamine (c) Peak oxidation current for dopamine measured following a bolus injection of dopamine. (d) Calibration curve for dopamine at untreated electrodes (▼) and at 4SBD modified P-55 ellipses (■) and modified T-650 cylinders (□) (n=5 electrodes each). Due to variations between electrodes the peak oxidation current for dopamine was normalized to the current obtained at bare electrodes for 5 μM dopamine injection. Error bars represent SEM.

Dopamine adsorption at electrodes grafted with 4-sulfobenzene

The high sensitivity for dopamine at untreated carbon fiber electrodes is the result of adsorption of dopamine to the electrode in between each scan. To compare adsorption at untreated and modified P-55 elliptical electrodes, adsorption isotherms for dopamine were constructed. The peak current at various concentrations of dopamine from 0.5 μM to 500 μM were measured at each type of electrode. The peak current measured has two essential contributors: adsorption and diffusion. The expected current due to diffusion control was computed with DigiSim® and subtracted from the total peak current to obtain the current due to adsorbed dopamine. By integration of this current over time it is possible to calculate the surface coverage. At unmodified electrodes, dopamine adsorption to carbon-fiber electrodes follows the equation for a Langmuir isotherm(Bath et al., 2000):

$$\frac{\Gamma_{DA}}{\Gamma_S - \Gamma_{DA}} = \beta[DA] \qquad (1)$$

where Γ_{DA} is the surface concentration of dopamine, Γ_s is the saturation coverage, and β is the equilibrium constant for adsorption. Consistent with prior work, the isotherm for bare P-55 elliptical electrodes fits well to equation 1 with a limiting coverage of $\Gamma_s = 10^{-10}$ mol/cm^2 and $\beta = 2.8 \times 10^{-5}$ cm^3/pmol (Bath et al., 2000; Solak et al., 2002; Heien et al., 2003). The adsorption isotherm for 4-SBD modified electrodes shown in figure 2.3a does not follow equation (1). A more complex model is needed to describe the adsorption. With the arbitrary addition of a linear component with a slope of 3.5×10^{-3} cm to equation 1 an isotherm with Γ_s of

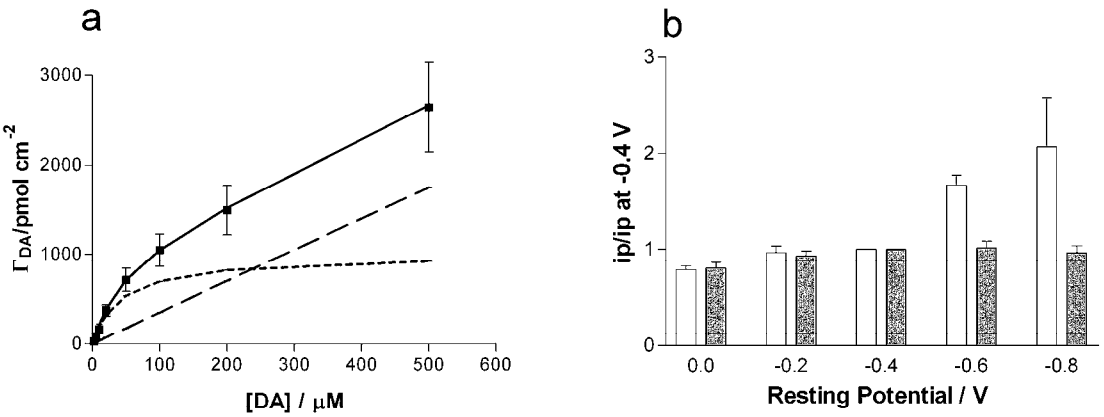

Figure 2.3. Adsorption characteristics of dopamine at P-55 elliptical electrodes. (a) Fit of the experimentally obtained surface coverage (■) to an adsorption isotherm (solid line). The isotherm is a summation of a regular Langmuir-isotherm (dotted line) and a linear component (dashed line). (b) The effect of rest potential on the peak current for dopamine. Values are normalized to the current obtained with a holding potential of -0.4V. Open bars show the response for bare P-55 disk electrodes and filled bars for 4SBD modified P-55 ellipses (n=5 electrodes). Error bars represent SEM

10^{-9} mol/cm^2 and an equilibrium constant of 2.3 x 10^{-5} cm^3/pmol does fit to the data. Thus the data indicates a 10-fold increase in saturation coverage at the modified electrode lead to the higher sensitivity.

Dopamine adsorption at untreated electrodes increases with more negative rest potentials at which the electrode is held between scans.(Heien et al., 2003) This effect is attributed to the greater negative charge on the surface at more negative potentials. At 4-SBD electrodes this effect is removed (Figure 3.3 b). This further indicates that the increased dopamine adsorption at 4-SB electrodes is due to the added sulfo group that predominates over the effect of the applied potential.

Voltammetric response to other compounds

The selectivity for dopamine detection with modified electrodes was examined by comparing its background-subtracted cyclic voltammogram to those for a variety of other neurochemical species. The analytes studied included the metabolites of dopamine (dihydroxy phenyl acid (DOPAC), homovanilic acid (HVA) and 3-methoxytyramine (3-MT)), other neurotransmitters like norepinephrine (NE) and serotonin (5-HT) and its metabolite 5-hydroxyindole acetic acid (5-HIAA), as well as other easily oxidized substances such as uric acid (UA) and ascorbic acid (AA). The response to pH was also examined. Untreated carbon-fiber electrodes respond to pH changes because one of the contributors to the background is electrolysis of oxide groups on the carbon surface.(Runnels et al., 1999) A pH change therefore causes a background shift that is enhanced by the background subtraction process. In vivo, pH changes have been measured following electrical stimulation of

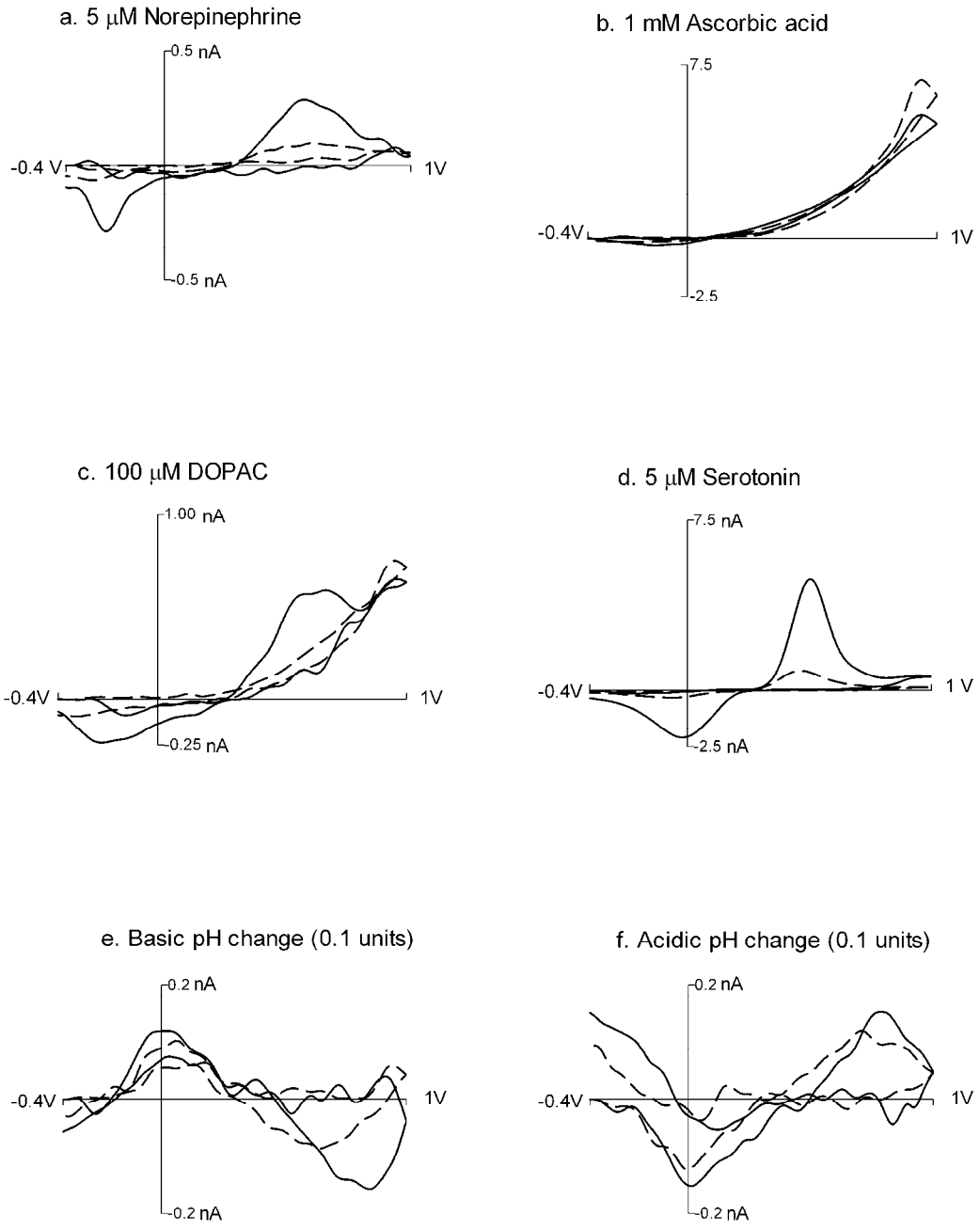

Figure 2.4. Background-subtracted cyclic voltammograms for various compounds. Response at bare P-55 elliptical electrodes is shown with dashed lines while the response at 4-SBD modified electrode is shown with solid lines. The cyclic voltammograms were recorded in a flow injection cell 300 ms following injection of the analyte.

	DOPAC	3-MT	HVA	5-HT	5-HIAA	NE	AA	UA	Acidic pH	Basic pH
Increase in signal	0.78 ± 0.36	5.83 ± 2.53	0.91 ± 0.63	4.27 ± 1.70	1.28 ± 0.43	2.14 ± 1.00	1.08 ± 0.34	0.83 ± 0.28	2.73 ± 1.24	2.45 ± 1.28
R bare electrode	0.57 ± 0.10	0.66 ± 0.06	0.47 ± 0.09	0.81 ± 0.05	0.68 ± 0.07	0.87 ± 0.03	0.42 ± 0.10	0.45 ± 0.08	0.59 ± 0.11	-0.61 ± 0.11
R modified electrode	0.51 ± 0.06	0.79 ± 0.09	0.40 ± 0.08	0.73 ± 0.02	0.62 ± 0.05	0.91 ± 0.06	0.31 ± 0.10	0.32 ± 0.13	0.37 ± 0.10	-0.49 ± 0.11

Table 2.1. Sensitivity and selectivity of 4-SBD modified electrodes; First row: Maximal amplitude of the peak current at modified electrodes relative to that at unmodified electrodes for various analytes. Second/Third row: Correlation coefficient r between the cyclic voltammogram for dopamine and for the various other neurochemical for bare P-55 elliptical electrodes and for 4SBD modified P-55 disk electrodes (n= 7 electrodes). Values are given with standard deviations

dopamine neurons and have been shown to be an indirect measure of dilation of blood vessels.(Venton et al., 2003)

Representative cyclic voltammograms at polished disks and modified electrodes for several of the substances tested are shown in figure 2.4. At pH 7.4 the protonated amines, dopamine, norepinephrine, serotonin, and 3-MT, all show increased amplitudes at modified electrodes indicating accumulation in the grafted layer. The amplitudes of the cyclic voltammograms for the compounds that are anions at physiological pH are not significantly different from the responses at polished elliptical electrodes indicating that they are unaffected by the layer. This observation, coupled with the unaltered response time of the modified electrodes, indicates that the grafted layer is quite permeable. Given the branch-like structure that evolves from multilayer formation, this result is not surprising but in contrast to blocking effects that have been observed at electrodes after reduction of other aryl-diazonium compounds that lead to monolayer formation(Saby et al., 1997). It is likely that 4-SBD under the conditions presented in this study forms a different structured layer than the 4-nitro analogue. The modification seems to increase the sensitivity for pH changes by a factor of about 2.

The shapes of the cyclic voltammograms are used to identify substances detected in vivo. To evaluate quantitatively the similarities in the shapes of the voltammograms, a correlation coefficient (Table 2.1) was computed for each cyclic voltammogram with that for dopamine.(Troyer et al., 2002; Venton and Wightman, 2003) The correlation coefficients are computed by recording a template cyclic voltammogram for dopamine at each electrode and comparing the set of other

analytes to it. To do this the oxidation peak is normalized to the amplitude of the oxidation peak in the dopamine template. Then the mean square error is calculated for each cyclic voltammogram versus the template. The more similar the cyclic voltammogram is to that of dopamine, the closer to unity the correlation coefficient will be. Before modification, the cyclic voltammograms for all of the analytes except NE show a correlation coefficient of less than 0.85 when compared to dopamine, and the correlation coefficient decreases for the majority of compounds after modification. The structure of norepinephrine is very similar to that of dopamine, differing only by a hydroxyl group on the side chain. Thus, 4-SB modified electrodes not only show higher sensitivity but also have higher selectivity for dopamine then polished carbon fiber electrodes.

Use in brain slices

To evaluate the performance of 4-SB modified electrodes in a neurochemical application, they were used in a mouse brain slices containing the caudate-putamen, a region with multiple dopamine terminals. Dopamine release was evoked by local depolarization of the nerve terminals with a bipolar stimulating electrode. The carbon-fiber microelectrode was placed adjacent to the stimulating electrode to monitor the release. Fast-scan cyclic voltammetry responses at bare and modified P-55 ellipses were compared (n =4 for each electrode type, example responses in Figure 2.5). In all cases, the 4-SB modified electrode showed larger signals. Based on the signal-to-noise ratios in brain slices, a detection limit of 30 nM dopamine was

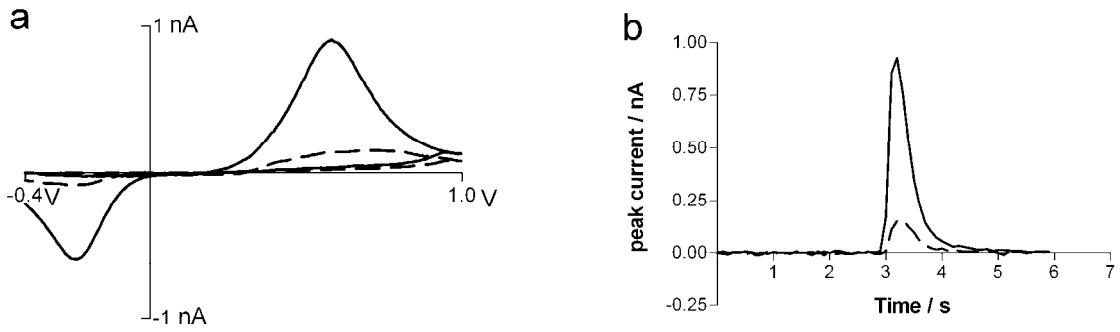

Figure 2.5. Dopamine detection in mouse brain slices with carbon fiber electrodes. Response at bare P-55 elliptical electrodes is shown with dashed lines while the response at 4-SBD modified electrode is shown with solid lines. a) Background subtracted cyclic voltammograms measured following a single pulse, 350 μA stimulation. b) Temporal response to the same stimulations shown in figure 5a) obtained for the oxidation current of dopamine.

calculated. This is a factor of 5 more sensitive than the detection limit at bare elliptical electrodes. As shown in figure 2.5b the time response is the same at 4-SB modified electrode compared to bare electrodes. The modified electrode maintained its sensitivity for dopamine over the time course of the experiment.

Summary

The results show that electrochemical reduction of 4-SBD forms a covalently attached cation-exchange multilayer on carbon-electrode surfaces. 4-SB modified electrodes are an alternative to Nafion-coated(Baur et al., 1988) and to overoxidized(Heien et al., 2003) electrodes to achieve improved detection of dopamine. With this layer attached, adsorption of dopamine to carbon fibers is increased in a manner that is potential independent. The highest reactivity to 4-SBD was found for P-55 elliptical electrodes, and they showed the greatest increase in dopamine signal. Increased adsorption led to an increase in sensitivity for dopamine by a factor of 5 with a concomitant increase in selectivity. This increase is in the same range of what can be achieved with overoxidation and much higher than the current increase seen at Nafion-coatings which is reported to be 1.5(Baur et al., 1988). However, in contrast to Nafion, the 4-SB layer does not exclude negatively charged compounds. Furthermore the time response of the electrode is unaffected by 4-SBD modification which makes it advantageous over the other two method which both slow down response time. This indicates that the grafted layer has a very open structure as expected for a multilayer graft following diazonium salt reduction.

REFERENCES

Adenier A, Bernard M-C, Chehimi MM, Cabet-Deliry E, Desbat B, Fagebaume O, Pinson J, Podvorica F (2001) Covalent Modification of Iron Surfaces by Electrochemical Reduction of Aryldiazonium Salts. Journal of the American Chemical Society 123:4541-4549.

Alger BE, Dhanjal SS, Dingledine R, Garthwaite J, Henderson G, King GL, Lipton P, North A, Schwartzkroin PA, Sears TA, Seagal M, Whittington TS, Williams J (1984) Appendix. Brain Slices, Plenum Press, New York:381-438.

Allongue P, Delamar M, Desbat B, Fagebaume O, Hitmi R, Pinson J, Saveant J-M (1997) Covalent Modification of Carbon Surfaces by Aryl Radicals Generated from the Electrochemical Reduction of Diazonium Salts. Journal of the American Chemical Society 119:201-207.

Anariba F, DuVall SH, McCreery RL (2003) Mono- and Multilayer Formation by Diazonium Reduction on Carbon Surfaces Monitored with Atomic Force Microscopy \"Scratching\". Analytical Chemistry 75:3837-3844.

Bath BD, Michael DJ, Trafton BJ, Joseph JD, Runnels PL, Wightman RM (2000) Subsecond adsorption and desorption of dopamine at carbon-fiber microelectrodes. Anal Chem 72:5994-6002.

Baur JE, Kristensen EW, May LJ, Wiedemann DJ, Wightman RM (1988) Fast-scan voltammetry of biogenic amines. Analytical Chemistry 60:1268-1272.

Berke JD, Hyman SE (2000) Addiction, dopamine, and the molecular mechanisms of memory. Neuron 25:515-532.

Boukerma K, Chehimi MM, Pinson J, Blomfield C (2003) X-ray Photoelectron Spectroscopy Evidence for the Covalent Bond between an Iron Surface and Aryl Groups Attached by the Electrochemical Reduction of Diazonium Salts. Langmuir 19:6333-6335.

Cahill PS, Walker QD, Finnegan JM, Mickelson GE, Travis ER, Wightman RM (1996) Microelectrodes for the measurement of catecholamines in biological systems. Analytical Chemistry 68:3180-3186.

Chausse A, Chehimi MM, Karsi N, Pinson J, Podvorica F, Vautrin-Ul C (2002) The Electrochemical Reduction of Diazonium Salts on Iron Electrodes. The Formation of Covalently Bonded Organic Layers and Their Effect on Corrosion. Chemistry of Materials 14:392-400.

Cooper JS, Bloom FE, Roth RH (1996) The biochemical basis of Neuropharmacology, Oxford University Press, Oxford 7th edition.

D'Amours M, Belanger D (2003) Stability of substituted phenyl groups electrochemically grafted at carbon electrode surface. Journal of Physical Chemistry B 107:4811-4817.

Delamar M, Hitmi R, Pinson J, Saveant JM (1992) Covalent modification of carbon surfaces by grafting of functionalized aryl radicals produced from electrochemical reduction of diazonium salts. Journal of the American Chemical Society 114:5883-5884.

Delamar M, Desarmot G, Fagebaume O, Hitmi R, Pinson J, Saveant JM (1997) Modification of carbon fiber surfaces by electrochemical reduction of aryl diazonium salts: application to carbon-epoxy composites. Carbon 35:801-807.

Dequaire M, Degrand C, Limoges B (1999) Biotinylation of screen-printed carbon electrodes through the electrochemical reduction of the diazonium salt of p-aminobenzoyl biocytin. Journal of the American Chemical Society 121:6946-6947.

Downard AJ, Roddick AD (1995) Protein Adsorption at Glassy-Carbon Electrodes - the Effect of Covalently Bound Surface Groups. Electroanalysis 7:376-378.

Downard AJ, Roddick AD, Bond AM (1995) Covalent modification of carbon electrodes for voltammetric differentiation of dopamine and ascorbic acid. Analytica Chimica Acta 317:303-310.

Garris PA, Wightman RM (1995) Neuromethods: Voltammetric Methods in Brain Systems, Humana Press, Totowa, NJ Chapter 6.

Heien ML, Phillips PE, Stuber GD, Seipel AT, Wightman RM (2003) Overoxidation of carbon-fiber microelectrodes enhances dopamine adsorption and increases sensitivity. Analyst 128:1413-1419.

Kariuki JK, McDermott MT (1999) Nucleation and Growth of Functionalized Aryl Films on Graphite Electrodes. Langmuir 15:6534-6540.

Kariuki JK, McDermott MT (2001) Formation of Multilayers on Glassy Carbon Electrodes via the Reduction of Diazonium Salts. Langmuir 17:5947-5951.

Kawagoe KT, Zimmerman JB, Wightman RM (1993) Principles of voltammetry and microelectrode surface states. Journal of neuroscience methods 48:225-240.

Kennedy RT, Jones SR, Wightman RM (1992) Dynamic observation of dopamine autoreceptor effects in rat striatal slices. J Neurochem 59:449-455.

Kolar GF (1972) Synthesis of biologically active triazenes from isolable diazonium salts. Zeitschrift fuer Naturforschung, Teil B: Anorganische Chemie, Organische Chemie, Biochemie, Biophysik, Biologie 27:1183-1185.

Laforgue A, Addou T, Belanger D (2005) Characterization of the deposition of organic molecules at the surface of gold by the electrochemical reduction of aryldiazonium cations. Langmuir 21:6855-6865.

Liu Y-C, McCreery RL (1995) Reactions of Organic Monolayers on Carbon Surfaces Observed with Unenhanced Raman Spectroscopy. Journal of the American Chemical Society 117:11254-11259.

McCreery RL (1996) Laboratory Techniques in Electroanalytical Chemistry, Dekker, New York Chapter 10.

Michael D, Travis ER, Wightman RM (1998) Color images for fast-scan CV. Analytical Chemistry 70:586a-592a.

Michael DJ, Joseph JD, Kilpatrick MR, Travis ER, Wightman RM (1999) Improving data acquisition for fast scan cyclic voltammetry. Analytical Chemistry 71:3941-3947.

Paxinos W, Watson C (1998) The Rat Brain in stereotaxic coordiantes. Academic Press, Orlando, Florida.

Pihel K, Walker QD, Wightman RM (1996) Overoxidized polypyrrole-coated carbon fiber microelectrodes for dopamine measurements with fast-scan cyclic voltammetry. Analytical chemistry 68:2084-2089.

Pinson J, Podvorica F (2005) Attachment of organic layers to conductive or semiconductive surfaces by reduction of diazonium salts. Chemical Society Reviews 34:429-439.

Pothos EN, Davila V, Sulzer D (1998) Presynaptic recording of quanta from midbrain dopamine neurons and modulation of the quantal size. J Neurosci 18:4106-4118.

Richfield EK, Penney JB, Young AB (1989) Anatomical and affinity state comparisons between dopamine D1 and D2 receptors in the rat central nervous system. Neuroscience 30:767-777.

Runnels PL, Joseph JD, Logman MJ, Wightman RM (1999) Effect of pH and Surface Functionalities on the Cyclic Voltammetric Responses of Carbon-Fiber Microelectrodes. Analytical Chemistry 71:2782-2789.

Saby C, Ortiz B, Champagne GY, Belanger D (1997) Electrochemical modification of glassy carbon electrode using aromatic diazonium salts .1. Blocking effect of 4-nitrophenyl and 4-carboxyphenyl groups. Langmuir 13:6805-6813.

Schultz W, Apicella P, Ljungberg T (1993) Responses of monkey dopamine neurons to reward and conditioned stimuli during successive steps of learning a delayed response task. J Neurosci 13:900-913.

Solak AO, Ranganathan S, Itoh T, McCreery RL (2002) A Mechanism for Conductance Switching in Carbon-Based Molecular Electronic Junctions. Electrochemical and Solid-State Letters 5:E43-E46.

Travis ER, Wightman RM (1998) Spatio-temporal resolution of exocytosis from individual cells. Annual Review of Biophysics and Biomolecular Structure 27:77-103.

Troyer KP, Heien ML, Venton BJ, Wightman RM (2002) Neurochemistry and electroanalytical probes. Curr Opin Chem Biol 6:696-703.

Venton BJ, Wightman RM (2003) Psychoanalytical electrochemistry: dopamine and behavior. Analytical Chemistry 75:414A-421A.

Venton BJ, Zhang H, Garris PA, Phillips PE, Sulzer D, Wightman RM (2003) Real-time decoding of dopamine concentration changes in the caudate-putamen during tonic and phasic firing. J Neurochem 87:1284-1295.

Waelti P, Dickinson A, Schultz W (2001) Dopamine responses comply with basic assumptions of formal learning theory. Nature 412:43-48.

CHAPTER 3

CONICAL TUNSGTEN TIPS AS SUBSTRATES FOR THE PREPARATION OF ULTRAMICROELECTRODES

Introduction

Ultramicroelectrodes have clearly demonstrated advantages in a variety of applications. They can be used to probe chemistry in small volumes, to examine chemistry that occurs on a submicrosecond time scale, and to examine electrochemical reactions in solutions of very high resistance(Wightman and Wipf, 1989). These properties have made microelectrodes particularly useful for applications in biological systems, (Wightman, 2006) but also in other applications such as chromatography scanning-probe microscopy (Holder et al., 2005; Walsh et al., 2005), and photoelectrochemical processes (Fan, 2004). The most common substrates for voltammetric ultramicroelectrodes are platinum, gold, and carbon. Microscopic platinum and gold wires and carbon fibers are all commercially available, and have been used to prepare ultramicroelectrodes. Typically, these materials are sealed into sealed soft glass capillaries (Zoski, 2002) leaving a disk or cylindrical section of the conductor exposed. Epoxy-resin can be used to seal any cracks between the fiber and the glass insulation(Zoski, 2002). Diamond microelectrodes have been constructed by growing the diamond layer on etched

stainless steel or tungsten microwires and insulating the shaft of the electrode (Cvacka et al., 2003; Park et al., 2005) to form a conical microelectrode.

Predating voltammetric microelectrodes are microelectrodes used by electrophysiologists for voltage sensing. For example, conical microelectrodes formed from tungsten wires with an etched tip and with lacquer (Hubel, 1957) or glass (Levivk, 1971) insulation can measure the electrical activity of a single neuron. They are commercially available as tungsten electrodes insulated with paralene (Loeb et al., 1977) or epoxy resin (Freeman, 1969; Ciancone and Rebec, 1989; Verhagen et al., 2003), with an exposed tip formed by removing the insulation with a laser. These electrodes are unsuitable for voltammetric measurement because of the corrosion properties (Lillard et al., 1998) of tungsten. The oxides produce large background currents that interfere with faradaic currents from species in solution. However, they have several useful physical attributes. Tungsten microelectrodes have a higher rigidity than glass insulated microelectrodes but can be bent without damaging the insulation. The rigidity of a material can be quantified by the tensile modulus, which is the quotient of the tensile stress over the tensile strain. With a tensile modulus of 411 GPa compared to 170 gPa for platinum and 78.5 GPa (Goodfellow-Cambridge-Limited) for gold, small tungsten wires are sufficiently stiff that they can be used without further support. Furthermore, tungsten wires are less brittle than carbon and glass rods of similar dimensions. Thus, in addition to small a sensing area, the overall diameter of tungsten-based electrodes coated with an insulator can be much smaller than microelectrodes that use glass tubes as the insulating material.

In this work we describe electrodes that have the physical properties of tungsten microwires and voltammetric properties of the commonly used electrode materials platinum, gold, and carbon. The electrodes were prepared by coating the conical tip of 125 μm-diameter tungsten microwires with the desired electrode material. To prepare gold and platinum electrodes, commercial electrophysiological electrodes, insulated tungsten wires with an exposed conical tip, were electroplated with the desired metal. For carbon tips, a technique developed by McCreery and coworkers was adapted which involves coating a substrate with photoresist followed by pyrolysis (Ranganathan et al., 2000; Ranganathan and McCreery, 2001). The pyrolyzed photoresist film (PPF) has similar electrochemical properties to glassy carbon. Electrodes produced this way open a new range of applications because of their simultaneous flexibility and rigidity. They are freely bendable and have micrometer dimensions (125 μm) over the whole length of the electrode.

EXPERIMENTAL SECTION

Preparation of conical tungsten tips

For the preparation of gold and platinum electrodes, the substrate was an epoxy-insulated tungsten microelectrode (AM-systems, 0.005'', 5 MΩ, 8 degree). The exposed tips were cleaned for 10 seconds in hydrofluoric acid (48%, Sigma-Aldrich, St. Louis, MO) then electrolyzed for 30 sec at 50 ^{o}C in electrocleaning solution (Electrocleaner, Shor Int., Mt. Vernon, NY) at -5 V vs. a platinum or gold counter electrode.

Because the carbon deposition employs pyrolysis, the substrate for these microelectrodes was an uninsulated tungsten wire (99.95 %, diameter 0.125mm, length 75mm, Advent Research Material, Eynsham, England). A conical tip was prepared by etching in a saturated sodium nitrite solution containing 1M NaOH at an AC potential of 10V (60Hz). The counter electrode was a stainless steel coil. The wires were lowered slowly into the etching solution until gas evolution was observed and raised again when the gas evolution stopped. After etching, the tungsten wires were cleaned with hydrofluoric acid and electrocleaning solution as described above.

Electrodeposition of platinum and gold

After the tungsten tip was cleaned, the electrode was rinsed with doubly distilled water (Megapure system, Corning, NY) and transferred into a plating solution. For platinum it was Platinum TP PTU, 240451GL (Technic Inc, Cranston, RI). Platinum was plated for 5 sec at -0.5 V vs a platinum counter electrode at 50 ^{o}C. After plating, the electrode was rinsed with double distilled water and then used or stored in ethanol.

Gold microelectrodes were formed similarly as described for platinum microelectrodes. For the cleaning and plating processes a gold counter electrode was used instead of platinum to minimize contamination. The plating was done at in gold plating solution (Gold plating solution 24k Royale, Shor Int., Mt. Vernon, NY) for 30 sec at -1V vs a gold counter electrode. The electrodes were also stored in ethanol.

Carbon deposition

Multiple (up to 15) cleaned and etched tungsten wires were dipped 3 times into photoresist (AZ P4330-RS, Clariant, Sommerville, NJ) in 5 min intervals with a Burleigh micromanipulator (Burleigh Inchworm, CE-1000, fishers, NY). The electrodes were pulled out of the photoresist at a speed of 2mm/min. The electrodes were then transferred into a furnace oven (Lindberg Blue, TF55035A-1) fitted with a quartz tube. Forming gas (95% nitrogen, 5% hydrogen, National Specialty Gases) flowed though the tube furnace at an approximate rate of 100 ml/min. The tube was purged for 20 min at room temperature and then the temperature was increased linearly for 100 min to 1000 ^{o}C, held at 1000 ^{o}C for 2 hours, and then cooled to room temperature. To insulate the electrodes, the tip was masked with paraffin wax (mp 53-57, Sigma-Aldrich). Paraffin wax was melted in a heating coil that was positioned under a stereoscope. The electrode was then carefully inserted into the wax with a micromanipulator to cover the desired surface area, and then the electrode was pulled back leaving a wax layer at the tip. The masked wires were then dipped 3 times into Epoxylite insulation (#6001, Altanta Varnish compounds, St. Louis, MO) in 5 min intervals with a Burleigh micromanipulator at a speed of 2mm/min. The electrodes were cured standing with the tip up at 200 ^{o}C for 30 min. Excess wax was removed with turpentine (Klean Strip, W.M. Barr & Co Inc, Memphis, TN). Before use the electrodes were soaked in 2-propanol purified with Norit A activated carbon (ICN, Costa Mesa, CA) for at least 20 min(Bath et al., 2000).

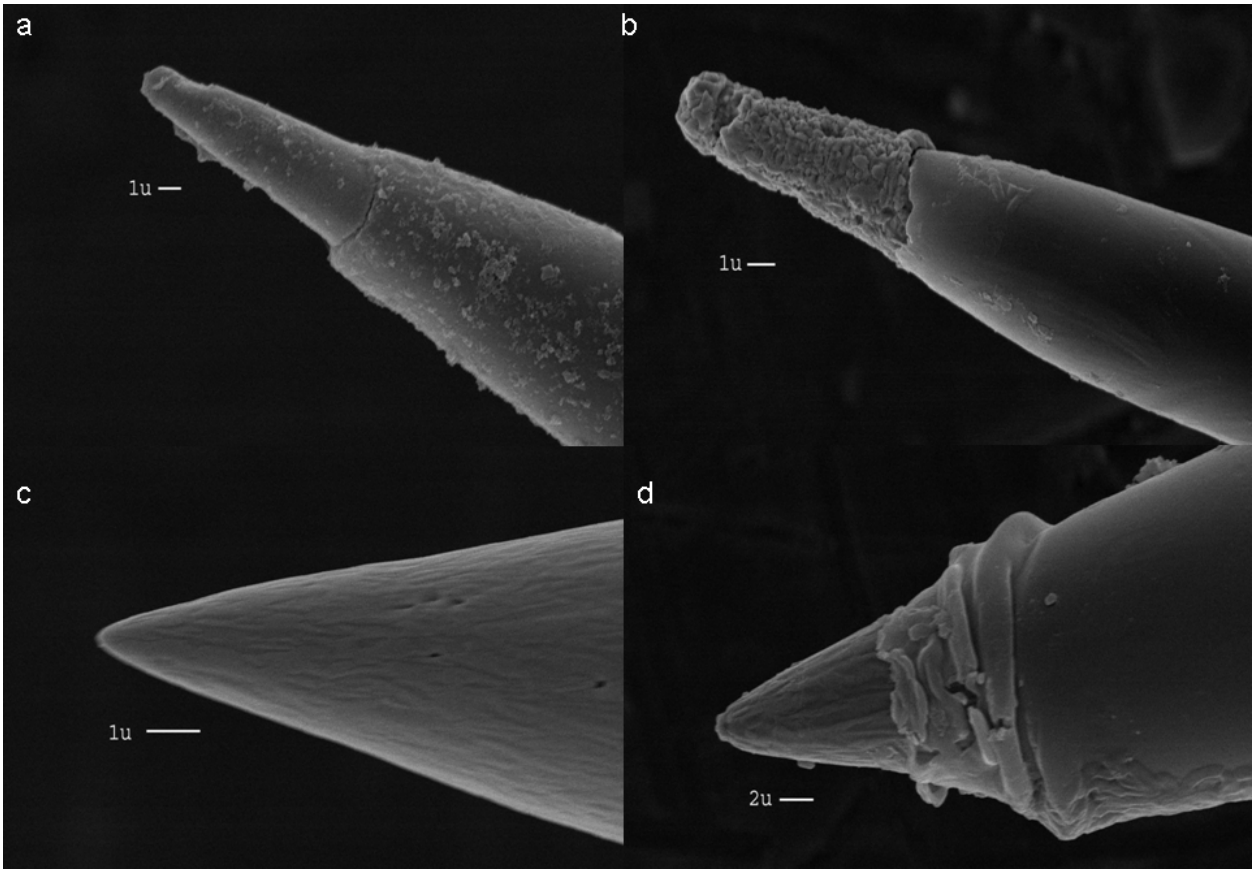

Figure 3.1. SEM images of conical microelectrodes: (a) Platinum plated electrode (b) Gold plated electrode (c) Etched tungsten wire coated with PPF (d) PPF electrode insulated with Epoxylite

Glass encased microelectrodes

For comparison, conventional microelectrodes were prepared. A short length (2 cm) platinum or gold wire (99.99%, 25 μm diameter, Goodfellow Cambridge Limited, England) was mounted on a wire with silver epoxy (H2O-PFC, EPO-TEK, Billerica, MA) and inserted into a soft glass capillary so that the tip of the microwire extended beyond the capillary. The hookup wire was attached to the back of the capillary with Torr Seal (Varian Vacuum Technologies). The tip of the electrode was then melted with a heating coil, which yielded a tight glass seal around the gold wire. The electrode was polished subsequently with alumina slurries of 1 μm, 0.3 μm and 0.05 μm size. Before each experiment the polishing step with 0.05 μm alumina slurry was repeated and the electrode was rinsed with doubly distilled water (Megapure system, Corning, NY).

Carbon-fiber microelectrodes were fabricated as previously described (Kawagoe et al., 1993) with P-55 carbon fibers (Thornel, Amoco Corp., Greenville, SC). A single fiber was aspirated into a glass capillary and pulled on a micropipette puller (Narashige, Tokyo, Japan). The fiber was sealed into the capillary with epoxy resin (Epon 828 with 14% m-phenlylenediamine by weight, Miller Stephenson Chemical Co., Danbury,CT). After curing the epoxy, the electrodes were polished at a 45° angle on a diamond embedded polishing wheel (Sutter Instruments), resulting in an elliptical surface of approximately 10^{-6} cm. The capillaries of the microelectrodes were backfilled with electrolyte solution (4 M potassium acetate, 150 mM potassium chloride), and wires were inserted into the capillary for electrical

contact. Before use electrodes were soaked in isopropanol purified with Norit A activated carbon (ICN, Costa Mesa, CA) for at least 20 minutes.

Voltammetric characterization

Cyclic voltammograms were acquired with the EI-400 potentiostat (Ensman Instrumentation, Bloomington, IN), locally constructed hardware, and software written in LabVIEW (National Instruments, Austin, TX) that has been described previously(Michael et al., 1999). The electrochemical cell was placed inside a grounded Faraday cage to minimize electrical noise. For background-subtracted cyclic voltammograms the electrode was positioned at the outlet of a 6-port rotary valve. The loop injector was mounted on an actuator (Rheodyne model 5041 valve and 5701 actuator) that was controlled by a 12-V DC solenoid valve kit (Rheodyne, Rohnert Park, CA). This introduced the analyte to the electrode surface. Solution was driven with a syringe infusion pump (2 cm/s, Harvard Apparatus Model 22, Holliston, MA) through the valve and the electrochemical cell. For all experiments a Ag-AgCl reference electrode (Bioanalytical Systems, West Lafayette, ID) was used. Fast-scan cyclic voltammograms were low-pass filtered in the software at 5 kHz, slow scan measurements were filtered with a built-in second order low-pass hardware filter at 1 Hz. Steady state currents obtained from slow scan measurements were used to calculate the electroactive area of the electrodes.

Chemicals

Aqueous solutions employed doubly distilled water (Megapure system, Corning, NY). Solutions were degassed for 15 min with nitrogen before use. All chemicals for electrochemical analysis were purchased form Sigma-Aldrich (St. Louis, MO) and used as received. Solutions of potassium hexacyanoferrate(III) were prepared in 1M potassium chloride. Solutions of ferrocenecarboxylic acid were prepared in 0.01M phosphate buffer (pH 7.0) with the addition of 1M potassium chloride. Background scans were performed in 0.5 M sulfuric acid, 0.1 M perchloric acid and in TRIS buffer solution which was adjusted to pH 7.4 containing 15 mM TRIS, 140 mM NaCl, 3.25 mM KCl, 1.2 $CaCl_2$, 1.25 mM NaH_2PO_4, 1.2 mM $MgCl_2$ and 2.0 mM Na_2SO_4.

RESULTS AND DISCUSSION

Fabrication Considerations

In the fabrication process, three aspects are central to obtain a functional microelectrode. The first issue is the resistance between the tungsten substrate and the deposited metal or carbon layer. Tungsten metal forms a passivated oxide layer when exposed to oxygen (Lillard et al., 1998), and tungsten oxide is formed during the electrochemical etching procedure. It has been shown that this oxide layer causes instabilities in the tunneling current when used as an STM tip (Hockett and Creager, 1993). In our case the oxide layer will add to the resistance between the tungsten and the deposited surface. However, concentrated hydrofluoric acid

dissolves surface tungsten oxides (Hockett and Creager, 1993; Paparazzo et al., 1999; Ottaviano et al., 2003) and thus minimizes the resistance.

Secondly it is important to achieve a relatively smooth, complete, and durable deposition of the electrode surface. The noble-metal plating solutions used in this study include complexing agents that buffer the free concentration of metal ions and promote formation of a smooth surface. However, plating variables such as temperature, plating time, and plating potential have to be carefully optimized. Otherwise dendritic growth or incomplete surface covering will occur. The conditions described here lead to a smooth platinum surface as can be seen in figure 1a. However, the gold layer is considerably rougher with the conditions employed (figure3.1b). The deposition conditions selected for gold were a compromise. At higher plating potentials even rougher surface were formed due to dendritic growth while at a lower potential plating was often incomplete. Dip-coating with photoresist, the carbon precursor, required removal at a constant but slow speed to achieve complete coverage. The pyrolyzed photoresist films have been reported to have very smooth surfaces on silicon wafers (Ranganathan and McCreery, 2001). SEM images of photoresist-coated tungsten wires indicate a similar morphology on the etched tungsten (Figure 3.1c).

The final requirement for a functional microelectrode is an intact insulation layer. Both types of electrode insulation (the commercially available electrodes and Epoxylite insulated electrodes) are stable when used in aqueous solution over the time course of several days. Exposure to alcohols or non oxidizing concentrated acids for several hours did not affect the insulation quality measured by AC

impedance of the electrode. According to the specifications (The PD George Company) the Epoxylite insulation is stable in alkali as well as many organic solvents, however, these conditions were not tested in this study. Both types of insulation were sufficiently flexible to remain intact during vibration of the tungsten wire. Direct physical impact, especially close to the exposed tip, or permanently bending the wire can damage the insulation. As can be seen in figure 1d the Epoxylite insulation forms a slight bulge on the shaft of the electrode. This originates from excess Epoxylite that accumulated around the wax mask. During curing the insulation flows back and hardens to function as a reinforcement of the insulation close to the electrode tip. The size of the exposed area at the PPF electrodes varies according to the size of the wax mask applied to the electrode tip.

Electrochemical behavior of platinum plated electrodes

To test the electrochemical performance of the conical ultramicroelectrodes we compared cyclic voltammetric responses of the plated electrodes with the responses at analogous glass encased electrodes. For the platinum, gold and carbon electrodes cyclic voltammograms in background solution were taken to compare oxidation and reduction of the electrode material as well to observe hydrogen and oxygen adsorption and evolution. To characterize faradaic reactions, the reduction of ferricyanide and the oxidation of the water soluble ferrocene compound, ferrocenecarboxylic acid, were used. For these analytes both background subtracted fast-scan cyclic voltammograms as well as slow scan voltammograms were recorded.

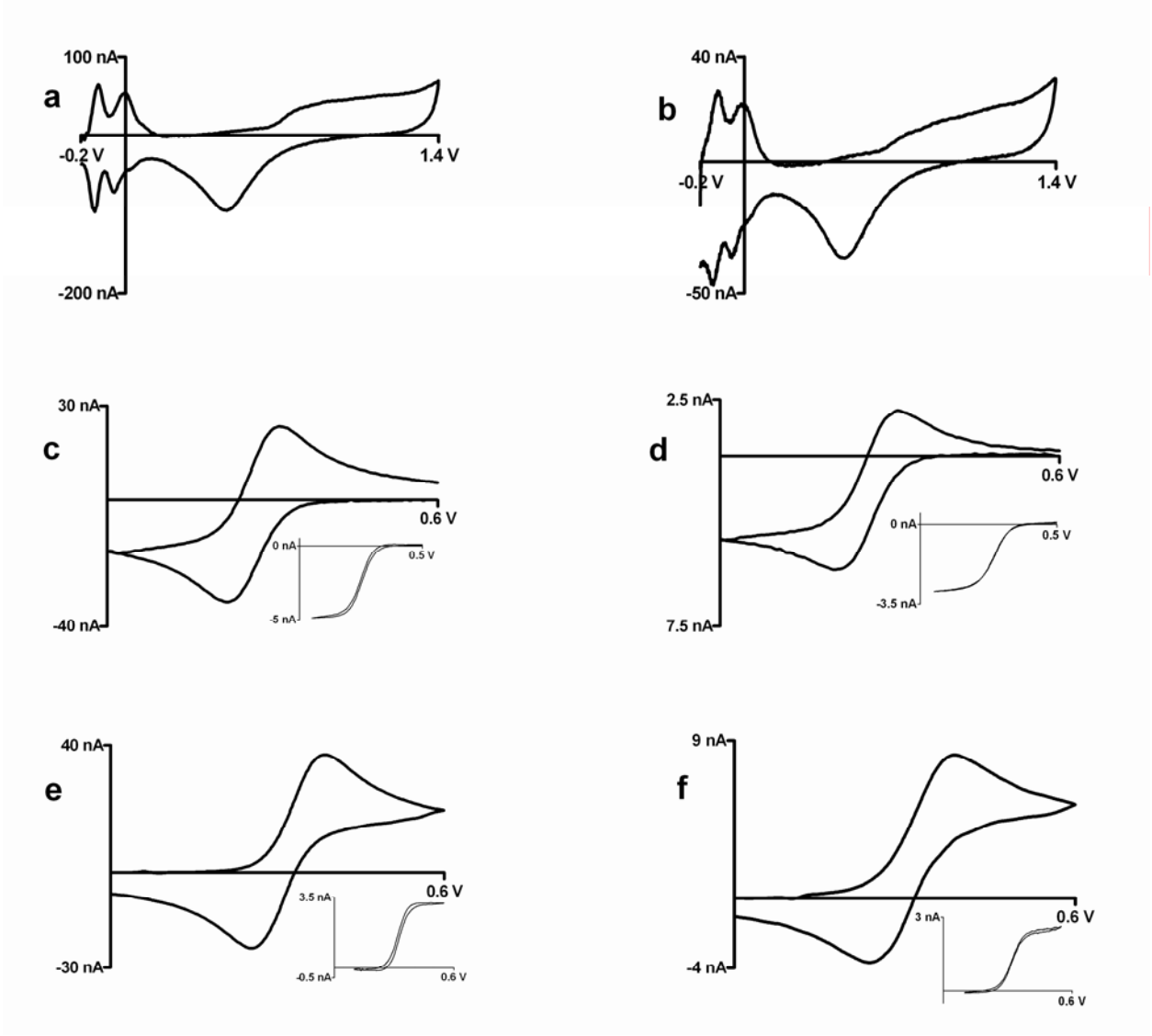

Figure 3.2. Cyclic voltammograms at platinum microelectrodes; left panel: Glass encased platinum disk electrodes, right panel: Platinum plated tungsten electrodes (a,b) 0.5 M sulfuric acid at 10 V/s (c,d) Background subtracted cyclic voltammogram at 100 V/s for injection of 1 mM ferricyanide in 1M KCl; insets: cyclic voltammogram for 1mM ferricyanide in 1M KCl at 10 mV/sec, c) ΔE_p= 73 mV, $E_{1/2}$ = 0.254 V vs. Ag/AgCl , d) ΔE_p= 83 mV, $E_{1/2}$ = 0.265 V vs. Ag/AgCl (e,f) Background subtracted cyclic voltammogram at 100 V/s for injection of 1 mM ferrocenedicarboxylic acid in 0.01 M phosphate buffer with 1M KCl; insets: cyclic voltammogram for 1mm ferrocenedicarboxylic acid in 0.01 M phosphate buffer with 1M KCl at 10 mV/sec, e) ΔE_p= 84 mV, $E_{1/2}$ = 0.317 V vs. Ag/AgCl, f) ΔE_p= 89 mV, $E_{1/2}$ = 0.323 V vs. Ag/AgCl

Figure 3.2b shows the cyclic voltammogram of a platinum-plated electrode in 0.5 M sulfuric acid recorded at 10 V/s. This background response is identical with a cyclic voltammogram recorded at a microelectrode prepared from a platinum wire (figure 3.2a) and those reported in the literature (Bard and Faulkner, 2001). The peaks in the hydrogen region are well developed (Tu et al., 1998). The presence of clearly distinct peaks for adsorption and desorption of hydrogen shows that the surface of the plated electrode is relatively clean and useful for electroanalysis (Suzuki et al., 1999). Both ferricyanide and ferrocenecarboxylic acid show similar voltammetric responses at slow and fast scan rates at the two platinum surfaces. The peak separation (ΔE_p) for both analytes indicates similar electron transfer kinetics. Slow scan cyclic voltammograms show the expected sigmoidal shape and have a similar half-wave potential, $E_{1/2}$. During this study, 30 electrodes were plated with platinum, and approximately 90 % showed well behaved electrochemistry similar to that shown in Figure 3.2. For the remaining 10% the slow scan voltammograms exhibited resistive effects characterized by a severely ramping current. This was attributed to incomplete metal coverage of the underlying tungsten or a defect in the insulation. In these cases, replating often led to improved performance. The electrodes were used in several experiments and were cleaned between experiments by cycling to positive potentials (Manica et al., 2003).

Electrochemical behavior of gold plated electrodes

The cyclic voltammogram obtained at gold plated electrodes in perchloric acid shows clearly defined oxidation and reduction peaks that are comparable to the

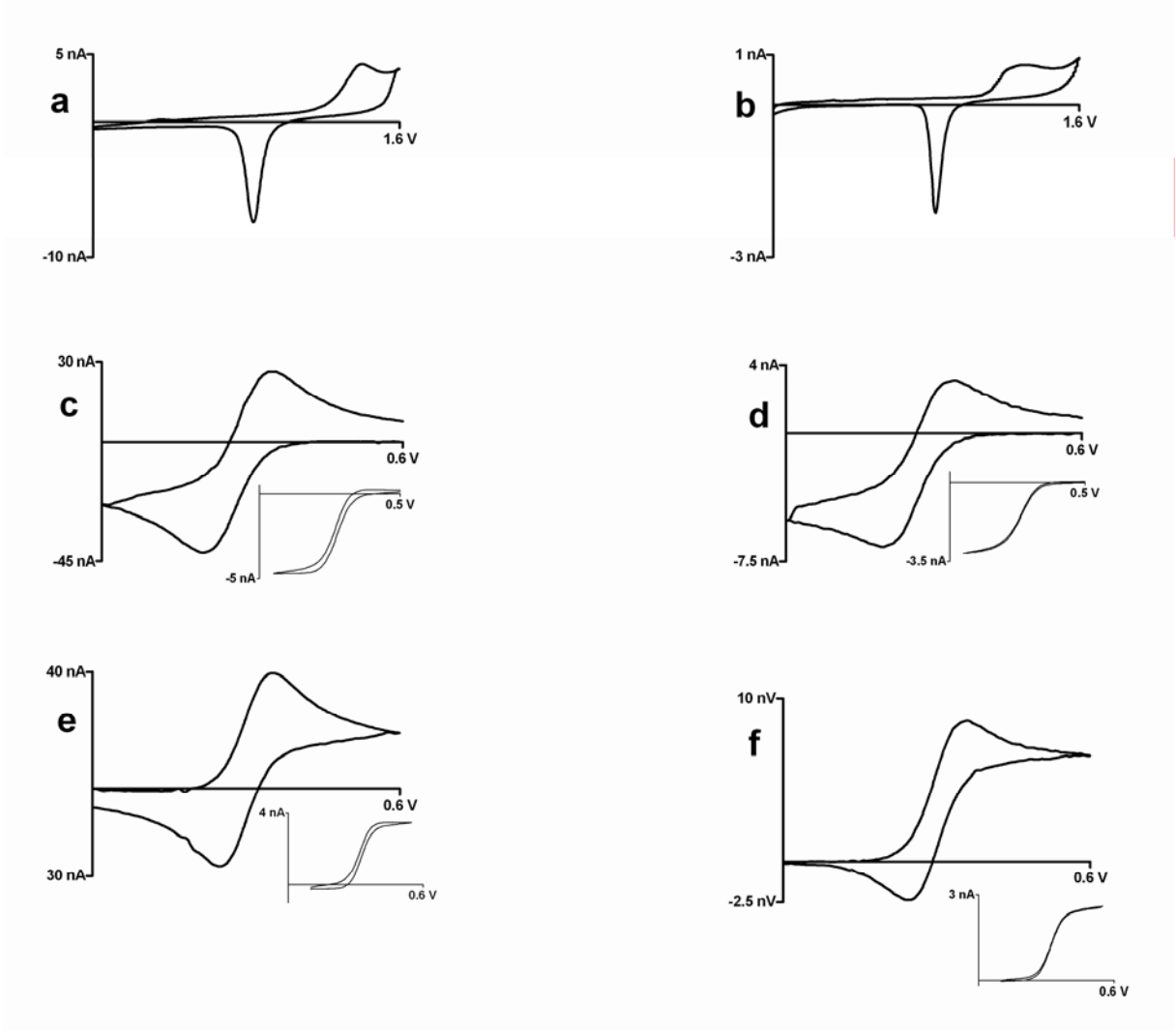

Figure 3.3. Cyclic voltammograms at gold microelectrodes; left panel: glass encased platinum disk electrodes, right panel: gold plated tungsten electrodes (a,b) 0.1 M perchloric acid at 0.1V/s (c,d) Background subtracted cyclic voltammogram at 100 V/s for injection of 1mM ferricyanide in 1M KCl; insets: cyclc voltammogram for 1mM ferricyanide in 1M KCl at 10 mV/sec, c) ΔE_p= 120 mV, $E_{1/2}$ = 0.277 V vs. Ag/AgCl, d) ΔE_p= 114 mV, $E_{1/2}$ = 0.259 V vs. Ag/AgCl (e,f) Background subtracted cyclic voltammogram at 100 V/s for injection of 1 mM ferrocenecarboxylic acid in 0.01 M phosphate buffer with 1M KCl; insets: cyclc voltammogram for 1 mM ferrocenecarboxylic acid in 0.01 M phosphate buffer with 1 M KCl at 10 mV/sec, e) ΔE_p= 80 mV, $E_{1/2}$ = 0.316 V vs. Ag/AgCl, f) ΔE_p= 89 mV, $E_{1/2}$ = 0.319 V vs. Ag/AgCl

cyclic voltammograms obtained at glass encased gold microelectrodes (figure 3.3a). The responses to the analytes shown in figure 3.3 c-f are similar to the observation made at platinum electrodes regarding electron transfer, diffusion, and surface coverage as can be seen in similar ΔE_p values for fast-scan measurements and similar $E_{1/2}$ values at for slow-scans. However, cleanliness and complete surface coverage is a harder to achieve by gold plating compared to platinum plating as indicated by the rougher coating in figure 3.1c. Alternative procedures like vacuum deposition or sputtering of gold layers may result in smoother surfaces, but the electroplating does not require expensive equipment or clean room facilities. Twenty electrodes were plated with gold layer in this study. The success rate for gold electrodes was around 70%, lower than for platinum plating. As with platinum, gold plated electrodes could be recycled by stripping of the gold layer followed by replating. Successfully plated electrodes can be used over the course of several experiments.

Electrochemical behavior of pyrolyzed photoresist film (PPF) electrodes

For large electrodes prepared from pyrolyzed photoresist films (PPF), the electrochemical properties are similar to glassy carbon. The electrochemical properties of PPF films have been described in the literature (Ranganathan et al., 2000; Ranganathan and McCreery, 2001). The first panel in figure 4 a,b shows fast scan background voltammograms in physiological TRIS Buffer (pH 7.4) as reported earlier (Hermans et al., 2006) and slow-scan cyclic voltammograms recorded in sulfuric acid. The slow-scan cyclic voltammograms show no significant oxidation or

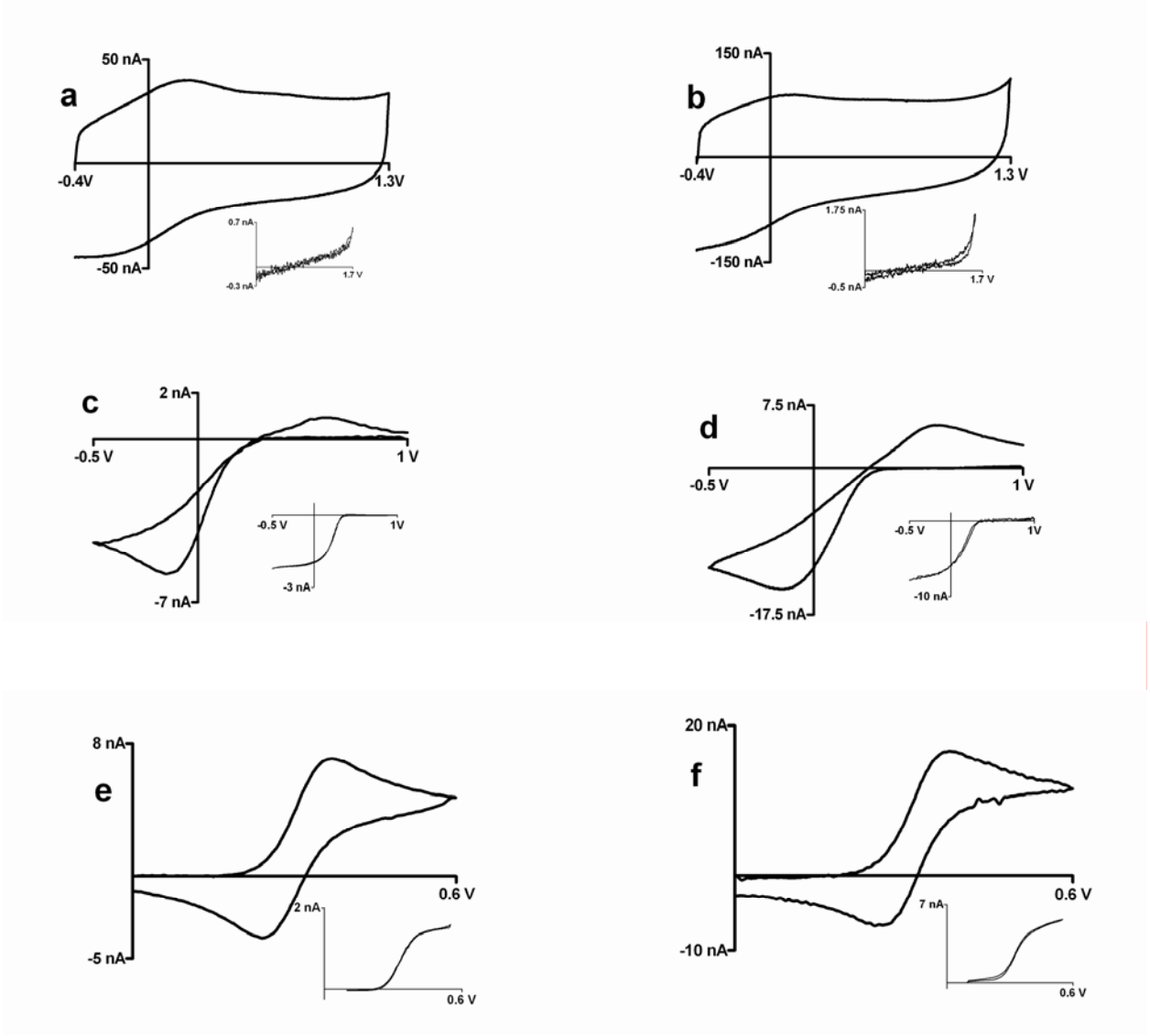

Figure 3.4. Cyclic voltammograms at carbon microelectrodes; left panel: glass encased carbon-fiber disk electrodes, right panel: PPF microelectrodes (a,b) TRIS buffer (pH 7.4); insets : sulfuric acid at 0.1 V/s (c,d), c) ΔE_p= 712 mV, $E_{1/2}$ = 0.219 V vs. Ag/AgCl, d) ΔE_p= 745 mV, $E_{1/2}$= 0.205 V vs. Ag/AgCl Background subtracted cyclic voltammogram at 100 V/s for injection of 1mM ferricyanide in 1 M KCl; insets: cyclc voltammogram for 1 mM ferricyanide in 1 M KCl at 40 mV/sec (e,f) Background subtracted cyclic voltammogram at 100 V/s for injection of 1 mM ferrocenecarboxylic acid in 0.01 M phosphate buffer with 1 M KCl; insets: cyclic voltammogram for 1mM ferrocenecarboxylic acid in 0.01 M phosphate buffer with 1 M KCl at 10 mV/sec, e) ΔE_p= 106 mV, $E_{1/2}$ = 0.334 V vs. Ag/AgCl, f) ΔE_p= 110 mV, $E_{1/2}$ = 0.327 V vs. Ag/AgCl

reduction features except for oxygen formation as expected. At neutral pH and fast-scan rates, carbon-fiber microelectrodes exhibit features in the cyclic voltammogram due to change in oxidation state of oxygen-containing functional groups on the surface. These can be observed on the anodic scan around 0.2V vs Ag/AgCl and on the cathodic scan at -0.2V vs Ag/AgCl. Both the glass encased carbon-fiber microelectrode as well as the PPF- microelectrode show these waves.

The shape of the voltammogram for ferricyanide at the PPF-electrode is similar to that obtained at carbon-fiber electrodes. Electron transfer at carbon electrodes for ferricyanide has been shown to be relatively slow(Deakin et al., 1985; Cline et al., 1994) at untreated carbon electrodes. Studies have shown that these slow kinetics might be due to surface contaminants (Kiema et al., 2003), the microstructure of carbon, or surface oxidation (Ji et al., 2006). Overall the responses for the analytes ferricyanide and ferrocenecarboxlylic acid at PPF electrodes and carbon fiber microelectrodes show similar peak separation and half-wave potentials indicating similar electron transfer kinetics. Twenty-five carbon-deposited electrodes were examined in this study. All electrodes with a full coverage of pyrolyzed photoresist as observed under a stereoscope resulted in functional electrodes. However, about 35% of the tungsten wires did not show complete coverage of the tungsten rod, especially at the tip, and these exhibited highly resistive behavior or were not functional.

Surface area of conical electrodes

The electrode area was determined from the limiting current obtained from the slow-scan cyclic voltammograms in figure 2.2 – 2.4 d and f. For a disk electrode the steady-state current can be calculated as(Bard and Faulkner, 2001):

$$i_{disk}^{ss} = 4nFDcr \qquad (1)$$

where n is the number of electron transferred, F is Faraday's constant, D is the diffusion coefficient of the analyte, c is the bulk concentration of the analyte, and r is the radius of the disk. The steady-state current at finite conical microelectrodes can be approximated by (Zoski and Mirkin, 2002) :

$$i_{cone}^{ss} = i_{disk}^{ss}\left[A + B(RG - C)^{D}\right] \qquad (2)$$

where i_{disk}^{ss} is the steady state current of a disk electrode of equivalent radius (r), RG is the ratio of the radius of the base of the insulating sheath over the radius of the cone, A, B, C, and D are numerical constants which depend on the aspect ratio, H, of the cone. H is defined as the height of the cone divided by the radius. Equation (2) can be rewritten to yield the radius of the cone.

$$r = \frac{i_{cone}^{ss}}{4nFDc\left[A + B(RG - C)^{D}\right]} \qquad (3)$$

The insulating sheath is very thin, so the value for RG was taken as 1.1.

The area for all the platinum- and gold-plated electrodes was quite similar because it was primarily determined by the amount of uninsulated tungsten on the commercially obtained electrode substrates. H for these electrodes was determined to be 4 (figure 3.1a), however values for A, B, C, and D for aspect ratios higher than 3 have not been reported. Therefore, for platinum and gold electrodes the base

radius was calculated with the term in brackets in equation (3) extrapolated from theoretical working curves (Zoski and Mirkin, 2002) to be equal to 3.25 for H = 4 and RG = 1.1. With the corresponding height calculated from the aspect ratio H, the surface area were calculated. For platinum conical electrodes the area was 1.2 ± 0.4 X 10^{-6} cm^2 and for gold the area was 1.4 ± 0.4 X 10^{-6} cm^2 (errors given as standard deviations). The geometrical area, estimated from figure 1a, is 1x10^{-6} cm^2 in reasonable agreement with the electrochemical data. The gold-surface area was also estimated by calculating the amount of charge consumed by reduction of the gold oxide layer in perchloric acid (figure 3.3b) using a reported value of 400μC/cm^2 (El-Deab et al., 2003). This method led to surface areas almost twice as large, presumably reflecting the surface roughness.

The current amplitudes from the PPF electrodes varied more than those of the platinum and gold electrodes, because the exposed area depends on the wax mask applied to the tip, an imprecise procedure. To calculate the electrochemical area, an H of 3 (figure 3.1c) was used and the values for the constants A, B, C, and D were taken from the literature (Zoski and Mirkin, 2002). Areas of these electrodes varied from 1x10^{-6} cm^2 to 10x10^{-6} cm^2, with the majority in the range of 4x10^{-6} cm^2 to 6x10^{-6} cm^2.

Summary

Intact films of platinum, gold and carbon were deposited onto tungsten mirowires to obtain microelectrodes that are functional for voltammetric studies. These microelectrodes show similar electrochemical responses for the reduction of

ferricyanide as well as for the oxidation of ferrocenecarboxylic acid as ultramicroelectrodes formed from pure metals. The formation and reduction of surface oxides for the deposited materials are also similar to the glass encased analogues. The microwires retain the flexibility and rigidity of tungsten microelectrodes with the electrochemical properties of platinum gold and carbon. The micrometer dimensions of the electroactive areas offer the possibility to arrange the electrodes in closely spaced arrays which is not possible with glass encased electrodes.

REFERENCES

Bard AJ, Faulkner LR (2001) In: Electrochemical Methods, 2nd Ed., p 18. New York: Wiley.

Bath BD, Michael DJ, Trafton BJ, Joseph JD, Runnels PL, Wightman RM (2000) Subsecond adsorption and desorption of dopamine at carbon-fiber microelectrodes. Anal Chem 72:5994-6002.

Ciancone MT, Rebec GV (1989) A Simple Device for the Reliable Production of Varnish-Insulated, High-Impedance Tungsten Microelectrodes. Journal of Neuroscience Methods 27:77-79.

Cline KK, Mcdermott MT, Mccreery RL (1994) Anomalously Slow-Electron Transfer at Ordered Graphite-Electrodes - Influence of Electronic Factors and Reactive Sites. Journal of Physical Chemistry 98:5314-5319.

Cvacka J, Quaiserova V, Park J, Show Y, Muck A, Swain GM (2003) Boron-doped diamond microelectrodes for use in capillary electrophoresis with electrochemical detection. Analytical Chemistry 75:2678-2687.

Deakin MR, Stutts KJ, Wightman RM (1985) The Effect of Ph on Some Outer-Sphere Electrode-Reactions at Carbon Electrodes. Journal of Electroanalytical Chemistry 182:113-122.

El-Deab MS, Okajima T, Ohsaka T (2003) Electrochemical reduction of oxygen on gold nanoparticle-electrodeposited glassy carbon electrodes. Journal of the Electrochemical Society 150:A851-A857.

Fan FF (2004) Experimental Techniques of Electrogenerated Chemiluminescence. In: Electrogenerated Chemoluminescence (Bard AJ, ed), p 23. New York: Marcel Dekker.

Freeman JA (1969) A Simple Method for Producing in Quantity Metal Micro-Electrodes with a Desired Taper and Impedance. Electroencephalography and Clinical Neurophysiology 26:623-&.

Goodfellow-Cambridge-Limited (accessed April 2006) Techniqual database, www.goodfellow.com. In.

Hermans A, Seipel AT, Miller CE, Wightman RM (2006) Carbon-fiber microelectrodes modified with 4-sulfobenzene have increased sensitivity and selectivity for catecholamines. Langmuir 22:1964-1969.

Hockett LA, Creager SE (1993) A Convenient Method for Removing Surface Oxides from Tungsten Stm Tips. Review of Scientific Instruments 64:263-264.

Holder MN, Gardner CE, Macpherson JV, Unwin PR (2005) Combined scanning electrochemical-atomic force microscopy (SECM-AFM): Simulation and experiment for flux-generation at un-insulated metal-coated probes. Journal of Electroanalytical Chemistry 585:8-18.

Hubel DH (1957) Tungsten Microelectrode for Recording from Single Units. Science 125:549-550.

Ji XB, Banks CE, Crossley A, Compton RG (2006) Oxygenated edge plane sites slow the electron transfer of the ferro-/ferricyanide redox couple at graphite electrodes. Chemphyschem 7:1337-1344.

Kawagoe KT, Zimmerman JB, Wightman RM (1993) Principles of voltammetry and microelectrode surface states. Journal of neuroscience methods 48:225-240.

Kiema GK, Aktay M, McDermott MT (2003) Preparation of reproducible glassy carbon electrodes by removal of polishing impurities. Journal of Electroanalytical Chemistry 540:7-15.

Levivk WR (1971) Another tungsten Microelectrode. Med Biol Eng 10:510-515.

Lillard RS, Kanner GS, Butt DP (1998) The nature of oxide films on tungsten in acidic and alkaline solutions. Journal of the Electrochemical Society 145:2718-2725.

Loeb GE, Bak MJ, Salcman M, Schmidt EM (1977) Parylene as a Chronically Stable, Reproducible Microelectrode Insulator. Ieee Transactions on Biomedical Engineering 24:121-128.

Manica DP, Mitsumori Y, Ewing AG (2003) Characterization of electrode fouling and surface regeneration for a platinum electrode on an electrophoresis microchip. Analytical Chemistry 75:4572-4577.

Michael DJ, Joseph JD, Kilpatrick MR, Travis ER, Wightman RM (1999) Improving data acquisition for fast scan cyclic voltammetry. Analytical Chemistry 71:3941-3947.

Ottaviano L, Lozzi L, Santucci S (2003) Scanning Auger microscopy study of W tips for scanning tunneling microscopy. Review of Scientific Instruments 74:3368-3378.

Paparazzo E, Moretto L, Selci S, Righini M, Farne I (1999) Effects of HF attack on the surface and interface microchemistry of W tips for use in the STM microscope: a scanning Auger microscopy (SAM) study. Vacuum 52:421-426.

Park J, Show Y, Quaiserova V, Galligan JJ, Fink GD, Swain GM (2005) Diamond microelectrodes for use in biological environments. Journal of Electroanalytical Chemistry 583:56-68.

Ranganathan S, McCreery RL (2001) Electroanalytical performance of carbon films with near-atomic flatness. Anal Chem 73:893-900.

Ranganathan S, McCreery R, Majji SM, Madou M (2000) Photoresist-derived carbon for microelectromechanical systems and electrochemical applications. Journal of the Electrochemical Society 147:277-282.

Suzuki H, Hirakawa T, Sasaki S, Karube I (1999) An integrated three-electrode system with a micromachined liquid-junction Ag/AgCl reference electrode. Analytica Chimica Acta 387:103-112.

The PD George Company AVC Technical Bulletin, Epoxylite Insulator #6001.

Tu WY, Liu WJ, Cha CS, Wu BL (1998) Study of the powder/membrane interface by using the powder microelectrode technique I. The Pt-black/Nafion (R) interfaces. Electrochimica Acta 43:3731-3739.

Verhagen JV, Gabbott PL, Rolls ET (2003) A simple method for reconditioning epoxy-coated microelectrodes for extracellular single neuron recording. Journal of Neuroscience Methods 123:215-217.

Walsh DA, Fernandez JL, Mauzeroll J, Bard AJ (2005) Scanning electrochemical microscopy. 55. Fabrication and characterization of micropipet probes. Analytical Chemistry 77:5182-5188.

Wightman RM (2006) Probing cellular chemistry in biological systems with microelectrodes. Science 311:1570-1574.

Wightman RM, Wipf DO (1989) Voltammetry at microelectrodes. In: Electroanalytical Chemistry, A series of advances (Bard JA, ed), p 267. New York and Basel: Marcel Dekker, INC.

Zoski CG (2002) Ultramicroelectrodes: Design, fabrication, and characterization. Electroanalysis 14:1041-1051.

Zoski CG, Mirkin MV (2002) Steady-state limiting currents at finite conical microelectrodes. Analytical Chemistry 74:1986-1992.

CHAPTER 4

CARBON COATED TUNGSTEN MICROELECTRODES FOR DOPAMINE DETECTION *IN VITRO* AND *IN VIVO*

Introduction

In a previous study we demonstrated that tungsten microelectrodes can be used as a substrate for different electrode materials (Hermans and Wightman, 2006). We were able to produce functional gold and platinum microelectrodes via electroplating and carbon microelectrodes by deposition of pyrolzed photoresist films (PPF) on tungsten electrodes. Electrodes produced in this way showed identical electrochemical properties to glass-insulated microelectrodes fabricated from gold and platinum microwires or carbon fibers. Microelectrodes made from carbon fibers have been shown to have ideal properties for biological electrochemical recordings of catecholamines (Cahill et al., 1996). These electrodes are small in size and therefore cause minimal damage in biological tissues (Peters et al., 2004). Traditionally carbon fiber microelectrodes are produced by heat-pulling a glass capillary around the fiber (Kawagoe et al., 1993). While this approach yields functional electrodes, they are easily broken and unsuitable for chronic implantation. However, tungsten microelectrodes have several useful physical properties that make them advantageous over glass-encased electrodes such as a high rigidity, long life times, a small conical sensing area and a thin insulating layer which enables

the fabrication of electrodes that have a much smaller diameter over the whole length of the electrode. These properties make tungsten electrodes an ideal electrode for *in-vivo* applications. Indeed, tungsten electrodes have been used for decades by electrophysiologists for voltage sensing (Hubel, 1957; Levivk, 1971). Because of the high mechanical stability, tungsten electrodes are often chronically implanted for electrophysiological recordings (Loeb et al., 1977; Venkatachalam et al., 1999).

To conduct simultaneous electrophysiological recordings in more than one location, micro fabricated arrays with multiple electrophysiological recording sites on silicon (Blum et al., 1991) or ceramic (Moxon et al., 2004) substrates are widely used. This approach has been adapted for electrochemical *in-vivo* applications (Burmeister, 2000; Burmeister and Gerhardt, 2001, 2003). In these studies gold or platinum is usually used as electrode material. The electrode sites are coated with an enzyme layer to detect molecules such as glutamate. An alternative approach is to use metal mircowire electrodes to construct a multiwire array (Nicolelis et al., 1997; Nicolelis and Ribeiro, 2002; Polikov et al., 2005). Early microwire arrays were constructed from two wires as stereotrode (Mcnaughton et al., 1983) and later from 4 wires as tetrode (Wilson and Mcnaughton, 1993; Gray et al., 1995). For these arrays, Teflon insulated microwires were twisted together and cut to the desired length for recordings. Arrays with a higher numbers of recordings sites were constructed by aligning mirowires in rows containing either 8 or 16 microwires staggered at different lengths(Nicolelis et al., 1997). With this approach arrays with up to 128 microwires could be constructed (Nicolelis et al., 2003). Different methods

have been used to align the microwires: polystyrene chips with laser-induced grooves (Takahashi et al., 2005), grated wires (Williams et al., 1999), wooden sticks (Tsai et al., 1997) and, most commonly, microfabricated spacers (Bai et al., 2000; Kipke et al., 2003). Alternatively, the Utah Intracortical Electrode Array (UIEA), a micro-machined and acid-etched electrode array made from silicon chips, is also used for single unit recordings (Jones et al., 1992; Normann et al., 1997; Rousche and Normann, 1997, 1998).

An array of carbon fibers for electrochemical sensing has been fabricated by Adrian Michael and coworkers (Dressman et al., 2002). They encased one carbon fiber into each barrel of a 2- or 4-barrel glass capillary and pulled it into a fine tip. These sensors were able to detect dopamine during *in vivo* applications. This method, however, produced a fixed position of the electrodes relative to one another. Multiple mircowires on the other hand can used with microdrives, where each electrode is independently and driven into place (Sato et al., 2007) which enable recordings in multiple locations.

In this study we examine the capabilities of PFF tungsten microwire electrodes for dopamine detection *in vitro* and *in vivo* in comparison to traditionally used carbon-fiber microelectrodes. Furthermore, we propose a method to pattern these mirowires in an array for electrochemical measurements in multiple brain locations simultaneously.

EXPERIMENTAL SECTION

Chemicals

All chemicals for flow injection analysis were purchased from Sigma-Aldrich (St. Louis, MO) and used as received. Solutions were prepared using doubly distilled water (Megapure system, Corning, New York). Solutions for flow injection analysis were prepared in a TRIS buffer solution, pH 7.4 containing 15 mM TRIS, 140 mM NaCl, 3.25 mM KCl, 1.2 $CaCl_2$, 1.25 mM NaH_2PO_4, 1.2 mM $MgCl_2$ and 2.0 mM Na_2SO_4. This buffer mimics the ionic environment present in cerebral spinal fluid. Stock solutions of analyte were prepared in 0.1 M $HClO_4$, and were diluted to the desired concentration with TRIS buffer on the day of use.

PPF microelectrodes

PPF-microelectrodes were constructed similarly to the previous description (Hermans and Wightman, 2006). The fabrication process for PPF microelectrodes is outlined in figure 4.1. The substrate for the microelectrodes was an uninsulated tungsten wire (99.95 %, diameter 0.125mm, length 75mm, Advent Research Material, Eynsham, England). A conical tip was prepared by etching in a saturated sodium nitrite solution containing 1M NaOH at an AC potential of 12V (60Hz). The counter electrode was a stainless steel coil. The wires were lowered slowly into the etching solution until gas evolution was observed and raised again when the gas evolution stopped. After etching, the tungsten wires were cleaned for 10 seconds in hydrofluoric acid (48%, Sigma-Aldrich, St. Louis, MO) then electrolyzed for 30 sec at

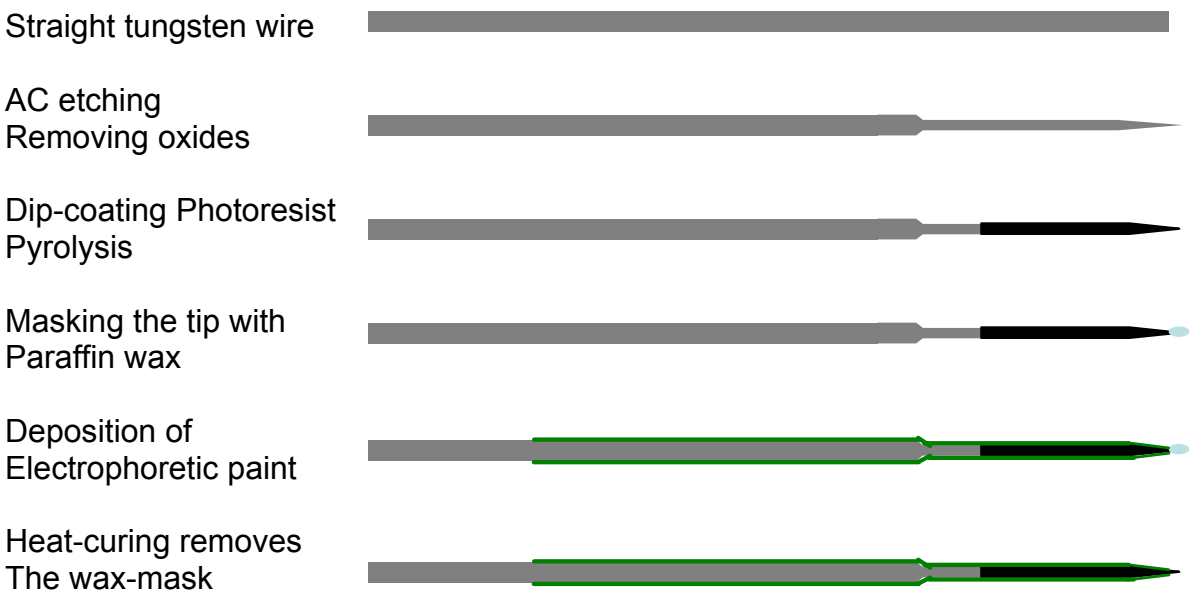

Figure 4.1. Fabrication process for PPF microelectrodes

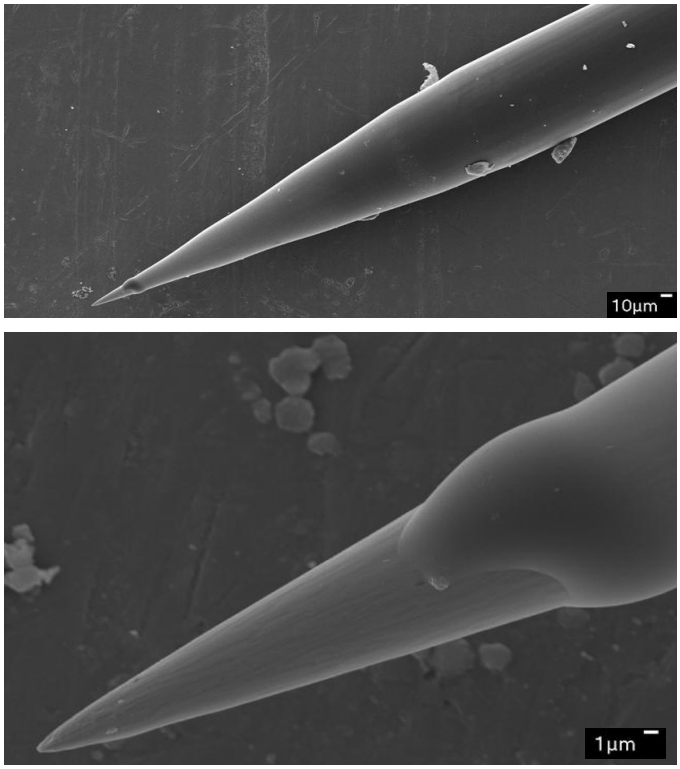

Figure 4.2. SEM micrograph of PPF microelectrodes. Top panel. Low magnification image showing the etched tip of the electrode Bottom panel. Higher magnification image of the tip of the PPF microelectrode indicating the insulation/PPF interface

50 °C in electrocleaning solution (Electrocleaner, Shor Int., Mt. Vernon, NY) at -5 V vs. a platinum or gold counter electrode. Multiple (up to 15) cleaned and etched tungsten wires were dipped 3 times into photoresist (AZ P4330-RS, Clariant, Sommerville, NJ) in 5 min intervals with a Burleigh micromanipulator (Burleigh Inchworm, CE-1000, fishers, NY). The electrodes were pulled out of the photoresist at a speed of 2mm/min. The electrodes were then transferred into a furnace oven (Lindberg Blue, TF55035A-1) fitted with a quartz tube. Forming gas (95% nitrogen, 5% hydrogen, National Specialty Gases) flowed though the tube furnace at an approximate rate of 100 ml/min. The tube was purged for 20 min at room temperature and then the temperature was increased linearly for 100 min to 1000 °C, held at 1000 °C for 2 hours, and then cooled to room temperature.

To insulate the electrodes, the tip was masked with paraffin wax (mp 53-57, Sigma-Aldrich). Paraffin wax was melted in a heating coil that was positioned under a stereoscope. The electrode was then carefully inserted into the wax with a micromanipulator to cover the desired surface area, and then the electrode was pulled back leaving a wax layer at the tip. As insulation material an anodic electrophoretic paint (ZQ-84-3225, PPG Industries, Milford, OH, USA) was used. Insulation of the working electrode was conducted by application of a +2 V DC potential in a 1:1 dilution of the electophoretic paint while simultaneously monitoring the current. A stainless steel coil, surrounding the working electrode, was used as counter electrode. The electrode was removed from the solution one minute after no further change in current flow could be observed. The electrodes were cured at 200˚C for 5 minutes. The paraffin wax evaporates during the curing process leaving

a non insulated electroactive area at the electrode tip behind. Figure 4.2 shows an SEM image of a PPF microelectrode. The electroactive area is directly determined by the area, which was covered by the wax mask. With the wax coating procedure presented here, the mask could be applied with an accuracy of approximately 10 µm on the tip of the electrode. With an aspect ratio, which is defined as height divided by the radius of the conical tip, of 4, we are able to produce electrodes with a geometrical area as small as 7.2×10^{-7} cm^2 with 10 µm wax coverage up to 13×10^{-6} cm^2 with a wax coverage of 40 µm.

Before use, the electrodes were soaked in 2-propanol purified with Norit A activated carbon (ICN, Costa Mesa, CA) for at least 20 min (Bath et al., 2000). Electrodes were electrochemically activated by triangular excursions from -0.4V to 1.3V vs. Ag/AgCl at a repetition frequency of 60Hz for 15 minutes followed by excursions from -0.4V to 1.3V vs. Ag/AgCl at a repetition frequency of 10Hz for 15 minutes before measurements were taken.

Construction of multiwire arrays

V-groove Microchips were purchase from OE/Land (Saint-Laurent, Quebec, Canada, 4 channels, 250 µm spacing, 12 x 2.25 mm). Insulated PPF microelectrodes were set in each channel of the microchip and aligned under a stereoscope. Electrodes were held in place by application of superglue to the microchip (Krazy Glue, Elmer's Products Inc, Columbus, OH, USA) and electrical contact was made directly to the insulated end of each single electrode.

Glass encased carbon fiber microelectrodes

For comparison, carbon fiber microelectrodes were fabricated as previously described (Kawagoe et al., 1993) with T-650 carbon fibers (Thornel, Amoco Corp., Greenville, SC, 5 μm diameter). A single fiber was aspirated into a glass capillary and pulled on a micropipette puller (Narashige, Tokyo, Japan). The carbon fiber was cut so that approximately 50 μm protruded from the glass seal. The microelectrodes were backfilled with electrolyte solution (4 M potassium acetate, 150 mM potassium chloride), and wires were inserted into the capillary for electrical contact. Before use, electrodes were soaked in isopropanol purified with Norit A activated carbon (ICN, Costa Mesa, CA) for at least 20 minutes (Bath et al., 2000). Electrodes were electrochemically activated by triangular excursions from -0.4V to 1.3V vs. Ag/AgCl at a repetition frequency of 60Hz for 15 minutes followed by excursions from -0.4V to 1.3V vs. Ag/AgCl at a repetition frequency of 10Hz for 15 minutes before measurements were taken.

For all experiments a Ag-AgCl reference electrode (Bioanalytical Systems, West Lafayette, ID) was used.

Flow cell measurements

For background-subtracted cyclic voltammograms the electrode was positioned at the outlet of a 6-port rotary valve. The loop injector was mounted on an actuator (Rheodyne model 5041 valve and 5701 actuator) that was controlled by a 12-V DC solenoid valve kit (Rheodyne, Rohnert Park, CA). This introduced the analyte to the electrode surface. Solution was driven with a syringe infusion pump

(2 cm/s, Harvard Apparatus Model 22, Holliston, MA) through the valve and the electrochemical cell.

Data acquisition and analysis

Cyclic voltammograms were acquired and analyzed using locally constructed hardware and software written in LabVIEW (National Instruments, Austin, TX) that has been described previously(Michael et al., 1999; Heien et al., 2003) All cyclic voltammograms presented in this study were low-pass filtered in the software at 2 kHz.

Units recorded were amplified (x1,000) and bandpass-filtered (300-3,000 Hz).and digitized with commercially available software (DIGITIZER, Plexon, Dallas)

Electrically evoked dopamine release in anesthetized rats

Male Sparague-Dawley rats (250g-400g; Charles River Laboratories, Wilmington, MA) were anesthetized with 50% w/w urethane in saline solution (0.3 mL per 100 g rat weight) and placed in a stereotaxic frame (Kopf Instruments, Tujunga, CA). After holes were drilled into the skull, a twisted bipolar stimulating electrode (Plastic One, Wallingford, CT) was lowered into the substantia niagra/ventral tegmental area: AP -5.2 mm, ML +1.0 mm, and DV -7.5 mm. The working electrode was placed into the caudate-putamen region striatum: anterior/posterior (AP) +1.2 mm, medial/lateral (ML) +2.0 mm, and dorsal/ventral (DV) -4.5 mm). To maintain the body temperature at 37°C a heating pad (Braintree, Braintree, MA) was used.

A Ag/AgCl reference electrode was positioned in the contralateral hemisphere. Dopamine release was evoked by constant current stimulation pulses through the stimulation electrode. To avoid electrical crosstalk, the stimulation occurred during the rest period between each cycle of the voltammogram. 60 biphasic stimulation pulses (+/- 125 μA, 2ms per phase) at a frequency of 60 Hz were used for all *in vivo* experiments. Between the end of the stimulus and the beginning of the next cyclic voltammogram, a 2 ms delay was inserted.

Single unit recording in freely moving rats

Male Sprague-Dawley rats implanted with a jugular vein catheter (300-450 g, Charles River Laboratories, Wilmington, MA) were housed individually on a 12:12 hour light cycle with ad libitum access to food and water. Procedures were as described previously (Phillips et al., 2003). Rats were anesthetized with ketamine hydrochloride (100 mg/kg i.p.) and xylazine hydrochloride (20 mg/kg i.m.) and placed in a stereotaxic frame for implantation surgery. A Ag/AgCl reference electrode was chronically implanted in the forebrain, and secured in place. A guide cannula (Bioanalytical Systems, West Lafayette, IN) was positioned above the substantia niagra/ventral tegmental area (AP -5.3 mm, ML +0.8 mm, and DV -7.5 mm relative to bregma)**.**

Following surgery, rats were allowed to recover for 48 hours during which time they received acetaminophen administered orally every 12 hours. Experiments were performed within one week of the implantation surgery. The electrodes were

connected to a light weight amplifier that is connected to a swivel linked to the remaining electronics. Rats were acclimated to the recording chamber for 1 h.

RESULTS AND DISCUSSION

Electrochemical detection of dopamine *in vitro*

Previous research indicated that PPF films initially form hydrogen terminated carbon surfaces. The surface can be activated by excursions to positive potentials (Ranganathan and McCreery, 2001). In a recent study (chapter 5) we have shown that a background signal at PPF microelectrodes obtained at high scan rates in buffer with no analyte present only showed a capacitive charging current. Figure 4.3a indicates that after electrochemical activation the background cyclic voltammogram for carbon fiber microelectrode and PPF microelectrodes are identical as observed previously (Hermans and Wightman, 2006). Both background signal show a broad peak around 0.2 V vs. Ag/AgCl which can be attributed to redox processes at the surface of the electrode (Chen and McCreery, 1996). The bigger signal at the PPF electrodes presented in the figures in this study arises from a bigger surface area of the PPF electrode compared to the carbon fiber electrode. The difference in surface area also explains the larger peak current observed in the background subtracted cyclic voltammogram for dopamine at PPF microelectrodes. Beside the difference in amplitude, the responses to dopamine are exactly identical with regard to peak separation and response time to a bolus injection of the analyte (figure 4.3c).

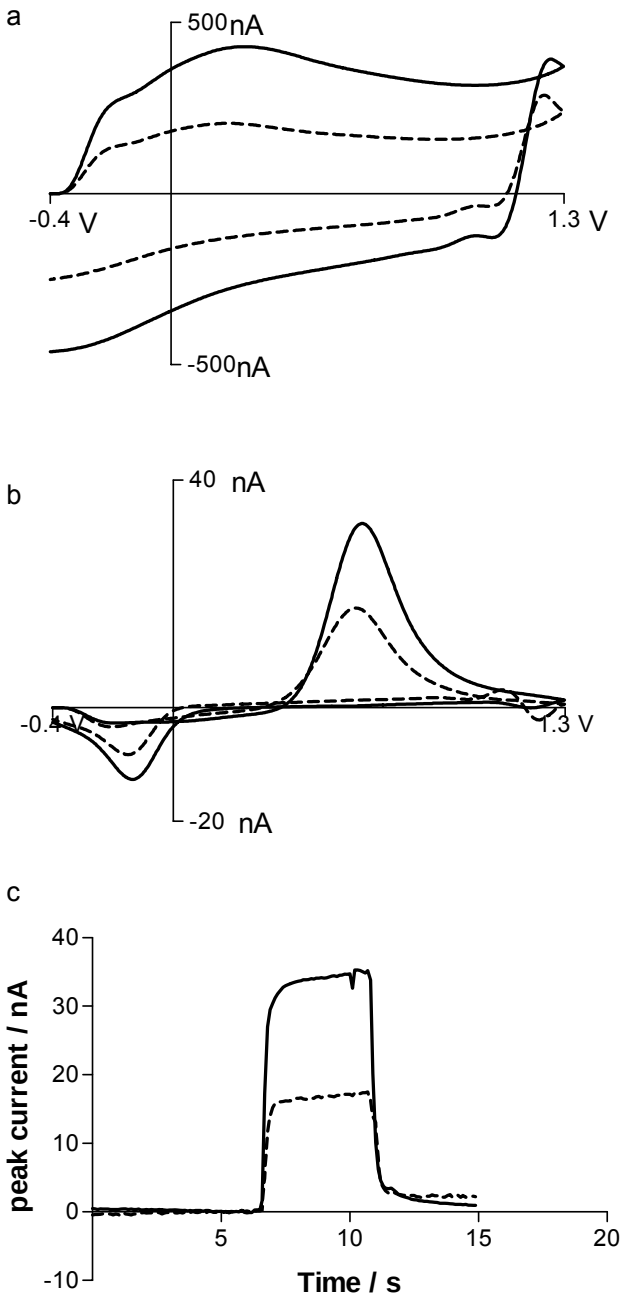

Figure 4.3. Response to dopamine at carbon fibers and PPF electrodes. Responses at PPF electrodes are represented with a solid line, Cylindrical carbon fiber microelectrodes are shown with a dashed line. Panel a. Background signal obtained in TRIS buffer at a scan rate of 400 V/s Panel b. Background subtracted voltammogram for 5μM dopamine Panel c. Peak oxidation current for dopamine for a bolus injection of 5μM dopamine

Electrochemical detection of other compounds *in vitro*

The cyclic voltammetric response at PPF microelectrodes to other electroactive species that are present in the brain and that might interfere with the detection of dopamine was examined. Dopamine and norepinephrine are both neurotransmitter that are derived from tyrosine. When dopamine is metabolized by monoamine oxidase (MAO), 3,4 dihydroxy phenyl acetic acid (DOPAC) is formed. Metabolism of dopamine by catecholamine-o-methyl transferase (COMT) leads to formation of 3-methoxytyramine (3MT). DOPAC can also be metabolized by COMT to homovanilic acid (HVA). . All of these dopamine metabolites are electroactive and can be detected electrochemically. The electrochemical responses to serotonin, a neurotransmitter derived from tryptophan, and to the serotonin metabolite,, 5-hydroxy indole acetic acid (5 HIAA), were also examined. Voltammograms for ascorbic acid and uric acid, electroactive compounds that are present in the brain but are not neurotransmitters, were also examined. Ascorbic acid concentrations in the extracellular fluid of the brain are 0.5 mM which is 10^4-10^6 times higher than the concentrations of catecholamines (Mefford et al., 1981; Nagy et al., 1982). However, as it can be seen in figure 4.4, the electron transfer kinetics for the oxidation of ascorbic acid are relatively slow at carbon electrodes so that it can be distinguished at high scan rates from other compounds, such as dopamine. In summary all electroactive interferences that we tested show identical voltammetric esponses at carbon fibers and PPF microelectrodes. The background voltammogram obtained at fast scan rates on carbon fiber microelectrodes varies with pH (Runnels et al., 1999). This way it is possible to measure pH changes when

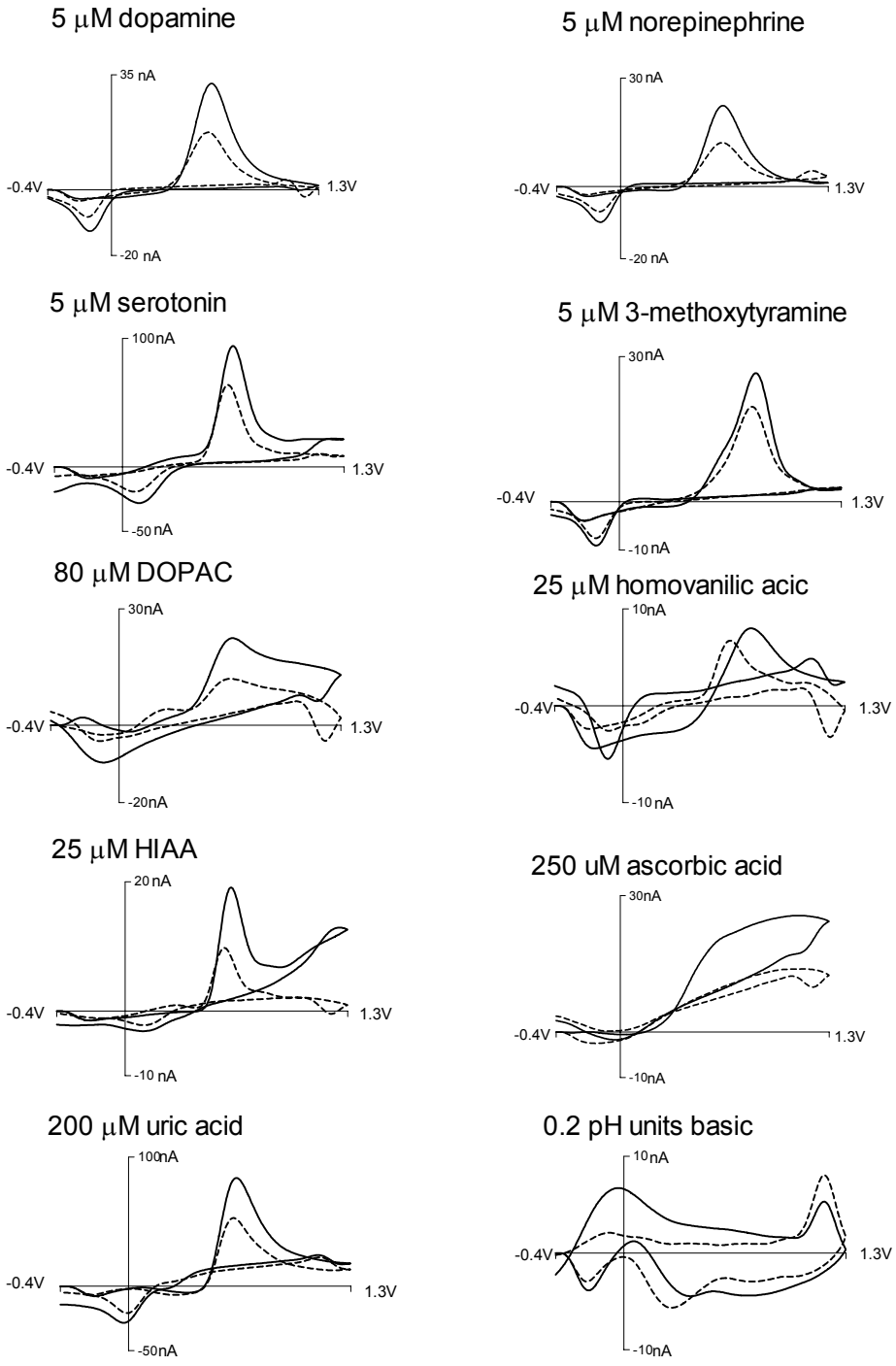

Figure 4.4. Background subtracted cyclic voltammograms for various compounds. Responses at PPF electrodes are represented with a solid line, Cylindrical carbon fiber microelectrodes are shown with a dashed line. The cyclic voltammograms were recorded in a flow injection cell 300 ms following the injection of the analyte.

using background subtracted voltammograms. The resulting voltammograms for pH changes at PPF electrodes also mimics the signals seen at conventional carbon fiber electrodes, which enables pH measurements at PPF microelectrodes when using fast scan cyclic voltammetry.

Electrochemical and electrophysiological measurements *in vivo*

The electrochemical performance of PPF microelectrodes *in-vivo* was tested. The working electrode was lowered into the caudate-putamen, a region where dopamine terminals are located. Dopamine release in from nerve terminals was evoked by biphasic electrical stimulations of the cell bodies of the corresponding dopaminergic neurons located in the ventral tegmental area (VTA). With all PPF microelectrodes tested (n = 4 electrodes) it was possible to obtain voltammograms associated with electrically evoked dopamine release. A representative voltammogram is shown in figure 4.5.

In addition, the capability of PPF electrodes for sensing extracellular voltage measurements was tested. For these unit recordings the electrode was lowered into the VTA of a freely moving rat and connected to a voltage follower. The signals detected had an average interspike interval of 0.25 s resulting in an average mean firing rate of 4Hz which is in very good agreement with literature reports for midbrain dopamine neurons(Hyland et al., 2002). However the shape of the waveform recorded differs between recordings with carbon fiber electrodes and PPF microelectrodes. Carbon fiber electrodes showed a triphasic signal with the first phase negative going (figure 4.5b) while PPF electrodes recorded a

a

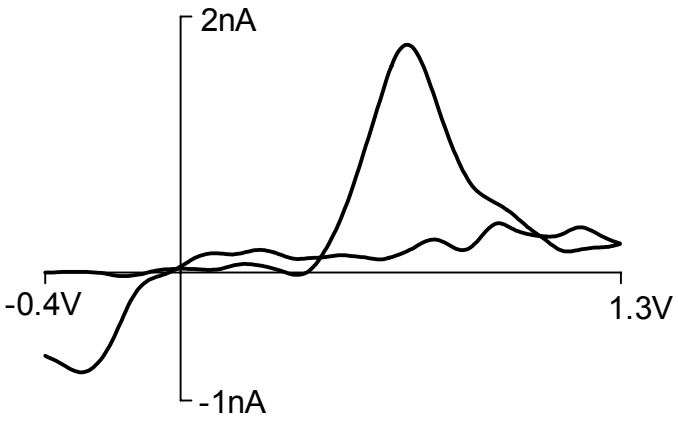

b

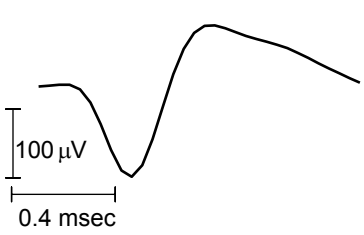

c

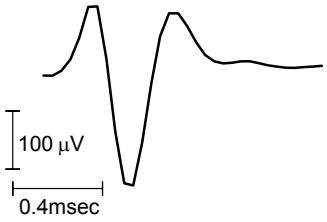

Figure 4.5. Electrochemical and electrophysiological measurements *in-vivo.* Panel a. Background subtracted cyclic voltammgram measured in the caudate-putamen following 60 biphasic stimulation pulses (+/- 125 μA, 2ms per phase) at a frequency of 60 Hz in the ventral tegmental area(VTA); Panel b. Extracellular action potential waveforms recorded in the VTA at carbon fiber microelectrodes; Panel c. Extracellular action potential waveforms recorded in the VTA at PPF microelectrodes

response where the first phase initially went positive (figure 4.5c). The waveform detected with PPF electrodes, however, is identical in shape and length to signals recorded with metal microelectrode arrays (Hyland et al., 2002). The difference in signal between these two electrode types is most likely due to different electrode resistances. The resistance of the cylindrical carbon fiber microelectrodes for unit recordings has been reported to be 500 kΩ at 1 kHz, which is relatively low impedance compared to metal electrodes that are traditionally used for eletrophysiological recordings. Commercially available electrodes for extracellular recordings have resistances ranging from 0.5 to 12 MΩ. The PPF electrodes used for single unit recordings in this study were therefore constructed with small surface areas, using a small amount of wax during the construction process. This probably resulted in electrodes with higher impedance, which might be the reason for the different shape of the waveforms recorded. Further reasons for the differences in signals might include the shape of the voltage sensor. PPF microelectrodes seem preferable over carbon fiber microelectrodes for unit recordings because the signals are better comparable to conventional metal microelectrode recordings.

Construction of PPF-microelectrode arrays

V-groove chips were used as a method to align the tungsten electrodes and produce a multiwire array. V-groove chips are commercially produced for use in different applications in telecommunication, data transmission, and switching. They are also used for diode pumped lasers and other general fiber

a

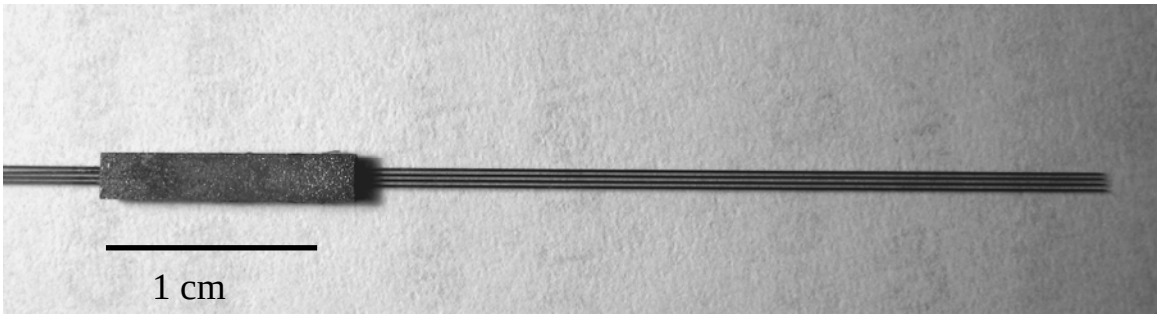

b

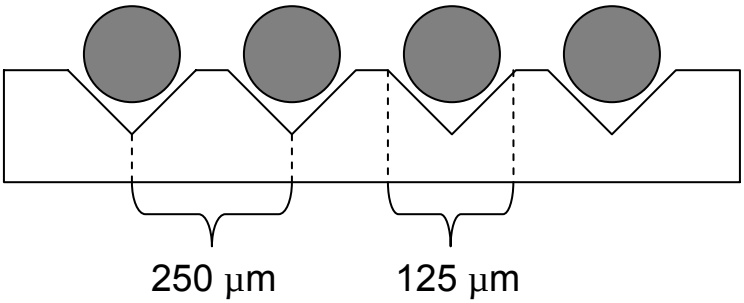

c

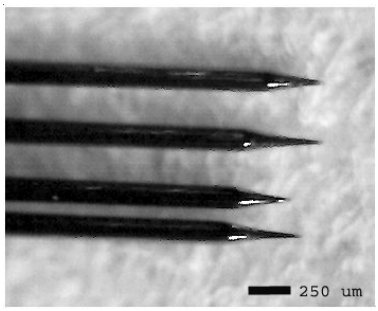

Figure 4.6. Construction of multiwire array. Panel a complete assembly of v-groove chip with 4 PPF electrodes; Panel b. Cross section of V-groove chip used in this study; Panel c. Light micrograph of tips of the multiwire array

optic instrumentation (Fiberguide-Industries, July 2007). V-groove chips are formed from silicon substrates with multiple parallel channels, V-shaped in cross section, along the chip. Figure 4.6b shows a cross section of the silicon used in this study to align the 4 microwires. As can be seen in figure 6a the microwires are parallel to each other over their whole length. Because the v-groove chip is constructed from silicon and therefore conductive, it is of high importance that each single wire is completely insulated with electro paint at the area of contact with the chip to minimize crosstalk between each individual channel. Indeed, *in-vitro* experiments with this array had no cross talk. V-groove chips are commercially mass produced. This makes the method presented here an easy, inexpensive and accurate procedure to fabricate multiwire arrays.

Summary

Here, we show that PPF microelectrodes can be used as an alternative to carbon fiber microelectrodes for biological measurements of catecholamines, such as dopamine, with fast scan cyclic voltammetry. The electrochemical response to all analytes tested in this study is identical at the two types of electrode. It was possible to detect dopamine release *in-vivo* with PPF microelectrodes. Furthermore, PPF microelectrodes could be used for external unit recordings, resulting in signals that are more comparable to conventional electrophysiological measurements in the literature than signals recorded with carbon fibers. Finally, a simple and inexpensive method to fabricate mircowire

arrays from PPF microelectrodes and commercially available v-groove microchips is presented.

REFERENCES

Bai Q, Wise KD, Anderson DJ (2000) A high-yield microassembly structure for three-dimensional microelectrode arrays. Ieee Transactions on Biomedical Engineering 47:281-289.

Bath BD, Michael DJ, Trafton BJ, Joseph JD, Runnels PL, Wightman RM (2000) Subsecond adsorption and desorption of dopamine at carbon-fiber microelectrodes. Anal Chem 72:5994-6002.

Blum NA, Carkhuff BG, Charles HK, Edwards RL, Meyer RA (1991) Multisite Microprobes for Neural Recordings. Ieee Transactions on Biomedical Engineering 38:68-74.

Burmeister JJ, Gerhardt GA (2001) Self referencing ceramic based multisite microelectrodes for the detection and elimination of interferences from the measurement of L-glutamate and other analytes. Analytical Chemistry 73:1037-1042.

Burmeister JJ, Gerhardt GA (2003) Ceramic-based multisite microelectrode arrays for in vivo electrochemical recordings of glutamate and other neurochemicals. Trac-Trends in Analytical Chemistry 22:498-502.

Burmeister JJ, Moxon, Karen, Gerhardt, Greg A. (2000) Ceramic-Based Multisite Microelectrodes for Electrochemical Recordings. Anal Chem 72:187-192.

Cahill PS, Walker QD, Finnegan JM, Mickelson GE, Travis ER, Wightman RM (1996) Microelectrodes for the measurement of catecholamines in biological systems. Analytical Chemistry 68:3180-3186.

Chen P, McCreery RL (1996) Control of electron transfer kinetics at glassy carbon electrodes by specific surface modification. Analytical Chemistry 68:3958-3965.

Dressman SF, Peters JL, Michael AC (2002) Carbon fiber microelectrodes with multiple sensing elements for in vivo voltammetry. Journal of Neuroscience Methods 119:75-81.

Fiberguide-Industries (July 2007) Fiberguide Industries - V grooves In. http://www.fiberguide.com/Products/VGrooves.html#Applications.

Gray CM, Maldonado PE, Wilson M, McNaughton B (1995) Tetrodes markedly improve the reliability and yield of multiple single-unit isolation from multi-unit recordings in cat striate cortex. Journal of Neuroscience Methods 63:43-54.

Heien ML, Phillips PE, Stuber GD, Seipel AT, Wightman RM (2003) Overoxidation of carbon-fiber microelectrodes enhances dopamine adsorption and increases sensitivity. Analyst 128:1413-1419.

Hermans A, Wightman RM (2006) Conical tungsten tips as substrates for the preparation of ultramicroelectrodes. Langmuir 22:10348-10353.

Hubel DH (1957) Tungsten Microelectrode for Recording from Single Units. Science 125:549-550.

Hyland BI, Reynolds JN, Hay J, Perk CG, Miller R (2002) Firing modes of midbrain dopamine cells in the freely moving rat. Neuroscience 114:475-492.

Jones KE, Campbell PK, Normann RA (1992) A Glass Silicon Composite Intracortical Electrode Array. Annals of Biomedical Engineering 20:423-437.

Kawagoe KT, Zimmerman JB, Wightman RM (1993) Principles of voltammetry and microelectrode surface states. Journal of neuroscience methods 48:225-240.

Kipke DR, Vetter RJ, Williams JC, Hetke JF (2003) Silicon-substrate intracortical microelectrode arrays for long-term recording of neuronal spike activity in cerebral cortex. Ieee Transactions on Neural Systems and Rehabilitation Engineering 11:151-155.

Levivk WR (1971) Another tungsten Microelectrode. Med Biol Eng 10:510-515.

Loeb GE, Bak MJ, Salcman M, Schmidt EM (1977) Parylene as a Chronically Stable, Reproducible Microelectrode Insulator. Ieee Transactions on Biomedical Engineering 24:121-128.

Mcnaughton BL, Okeefe J, Barnes CA (1983) The Stereotrode - a New Technique for Simultaneous Isolation of Several Single Units in the Central Nervous-System from Multiple Unit Records. Journal of Neuroscience Methods 8:391-397.

Mefford IN, Oke AF, Adams RN (1981) Regional Distribution of Ascorbate in Human-Brain. Brain Research 212:223-226.

Michael DJ, Joseph JD, Kilpatrick MR, Travis ER, Wightman RM (1999) Improving data acquisition for fast scan cyclic voltammetry. Analytical Chemistry 71:3941-3947.

Moxon KA, Leiser SC, Gerhardt GA, Barbee KA, Chapin JK (2004) Ceramic-based multisite electrode arrays for chronic single-neuron recording. Ieee Transactions on Biomedical Engineering 51:647-656.

Nagy G, Rice ME, Adams RN (1982) A New Type of Enzyme Electrode - the Ascorbic-Acid Eliminator Electrode. Life Sciences 31:2611-2616.

Nicolelis MA, Ribeiro S (2002) Multielectrode recordings: the next steps. Curr Opin Neurobiol 12:602-606.

Nicolelis MA, Ghazanfar AA, Faggin BM, Votaw S, Oliveira LM (1997) Reconstructing the engram: simultaneous, multisite, many single neuron recordings. Neuron 18:529-537.

Nicolelis MA, Dimitrov D, Carmena JM, Crist R, Lehew G, Kralik JD, Wise SP (2003) Chronic, multisite, multielectrode recordings in macaque monkeys. Proc Natl Acad Sci U S A 100:11041-11046.

Normann RA, Maynard EM, Rousche PJ, Nordhausen CT, Warren DJ, Guillory KS (1997) The Utah 100 microelectrode array: An experimental platform for a cortically based vision prosthesis. Investigative Ophthalmology & Visual Science 38:192-192.

Peters JL, Miner LH, Michael AC, Sesack SR (2004) Ultrastructure at carbon fiber microelectrode implantation sites after acute voltammetric measurements in the striatum of anesthetized rats. Journal of Neuroscience Methods 137:9-23.

Phillips PE, Robinson DL, Stuber GD, Carelli RM, Wightman RM (2003) Real-time measurements of phasic changes in extracellular dopamine concentration in freely moving rats by fast-scan cyclic voltammetry. Methods Mol Med 79:443-464.

Polikov VS, Tresco PA, Reichert WM (2005) Response of brain tissue to chronically implanted neural electrodes. Journal of Neuroscience Methods 148:1-18.

Ranganathan S, McCreery RL (2001) Electroanalytical performance of carbon films with near-atomic flatness. Anal Chem 73:893-900.

Rousche PJ, Normann RA (1997) Chronic intracortical microstimulation of cat auditory cortex using a 100 penetrating electrode array. Journal of Physiology-London 499P:P87-P88.

Rousche PJ, Normann RA (1998) Chronic recording capability of the Utah Intracortical Electrode Array in cat sensory cortex. Journal of Neuroscience Methods 82:1-15.

Runnels PL, Joseph JD, Logman MJ, Wightman RM (1999) Effect of pH and Surface Functionalities on the Cyclic Voltammetric Responses of Carbon-Fiber Microelectrodes. Analytical Chemistry 71:2782-2789.

Sato T, Suzuki T, Mabuchi K (2007) A new multi-electrode array design for chronic neural recording, with independent and automatic hydraulic positioning. Journal of Neuroscience Methods 160:45-51.

Takahashi H, Suzurikawa J, Nakao M, Mase F, Kaga K (2005) Easy-to-prepare assembly array of tungsten microelectrodes. Ieee Transactions on Biomedical Engineering 52:952-956.

Tsai ML, Chai CY, Yen CT (1997) A simple method for the construction of a recording-injection microelectrode with glass-insulated microwire. Journal of Neuroscience Methods 72:1-4.

Venkatachalam S, Fee MS, Kleinfeld D (1999) Ultra-miniature headstage with 6-channel drive and vacuum-assisted micro-wire implantation for chronic recording from the neocortex. Journal of Neuroscience Methods 90:37-46.

Williams JC, Rennaker RL, Kipke DR (1999) Long-term neural recording characteristics of wire microelectrode arrays implanted in cerebral cortex. Brain Research Protocols 4:303-313.

Wilson MA, Mcnaughton BL (1993) Dynamics of the Hippocampal Ensemble Code for Space. Science 261:1055-1058.

CHAPTER 5

MONITORING BRAIN DOPAMINE FLUCTUATIONS WITH FAST-SCAN CYCLIC VOLTAMMETRY FOR MULTIPLE MINUTES

Introduction

Fast-scan cyclic voltammetry (FSCV) is a useful tool to follow rapid chemical changes (Howell and Wightman, 1984). FSCV has been used in a variety of applications including the study of rapid electron-transfer kinetics (Wightman and Wipf, 1990; Mirkin et al., 1993; Clegg et al., 2004), monitoring evaporation of microdroplets (Neugebauer et al., 2004), and chromatographic detection (Soucazeguillous et al., 1993; Song et al., 2004). The method has been particularly useful for the monitoring of secretion neurotransmitters *in vitro* (Sulzer and Pothos, 2000; Swamy and Venton, 2007) and *in-vivo* (Millar et al., 1985; Robinson et al., 2003; Venton and Wightman, 2003). In all of these applications, ultramicroelectrodes are employed because small currents are generated even at high scan rates, and this minimizes distortion of the cyclic voltammograms by ohmic drop. Except for experiments on the nanosecond time domain, (Amatore and Lefrou, 1990; Amatore and Maisonhaute, 2005) the instrumentation can be quite simple.

A shortcoming of FSCV is the large size of the background current. The current required to charge the double layer and arising from surface attached redox

reactions is proportional to scan rate (Bard and Faulkner, 2001). In contrast, for a diffusion controlled electrochemical reaction, the faradaic current is proportional to the square root of the scan rate. Thus, optimum ratios of the faradaic to background current are not achieved with FSCV. Several methods have been used to minimize the contribution of the background. Early experiments used two separate, but identical electrochemical cells, one cell containing only the background solution and the other containing background solution and sample, and the signals were subtracted by analog means (Wang and Dewald, 1984). Data digitizers simplified this procedure allowing recordings in background solution to be subtracted from recordings with the electroactive species present, both recorded in the same electrochemical cell (Howell et al., 1986). This digital subtraction procedure is the one used by most investigators in this field. More recently, Yoo and Park (Yoo and Park, 2005) described a method to subtract background signals electronically during a fast scan potential sweep by customizing the applied waveform. The waveform was chosen so that it generated a flat background current. The current was then converted into a voltage and subtracted by a voltage limiter. This method enabled amplification of the background-subtracted current so that an improved dynamic range from the current to voltage converter could be achieved, minimizing quantization noise. This procedure led to improved detection limits for the catecholamine neurotransmitter, dopamine. However, information was only obtained on the anodic sweep and the cathodic current was discarded.

In this work we present an improved background subtraction approach and demonstrate its utility to follow the concentration of dopamine in the brain of a

behaving animal. The procedure involves analog removal of the background signal before it is digitized. This is accomplished by first recording a background cyclic voltammogram, and then playing it back from a digital-to-analog convertor into the current-to-voltage transducer. In this way, the inverted, digitized version is added to the electrode current at the transducer input, in the analog domain, an approach that is analogous to the procedure used in noise cancellation headphones. It has two advantages for monitoring low concentrations of dopamine. First, the input gain of the analog-to-digital converter can be increased, diminishing quantization noise. Second, the removal of the majority of background current allowed the components that remain, which drift, to be digitized and removed with principal component analysis (PCA). Background-currents at carbon-fiber microelectrodes during FSCV are documented to drift over time-scales of minutes (Hsueh et al., 1997; Hayes et al., 1998), limiting the time over which digital background subtraction is useful. Even after a conditioning period of several minutes, background drift is sufficient that subtraction fails to yield a recognizable voltammetric signal for voltammograms separated by more than 90 s (Heien et al., 2005). With the subtraction of the signal before digitization, and extraction of the drift components with principal component analysis, stable signals were monitored for 30 minutes, a 20-fold increase over existing methods.

EXERIMENTAL SECTION

Chemicals

All chemicals for flow injection analysis were purchased from Sigma-Aldrich (St. Louis, MO) and used as received. Solutions were prepared using doubly distilled water (Megapure system, Corning, New York). Flow injection analysis was done in a TRIS buffer solution, pH 7.4 containing 15 mM TRIS, 140 mM NaCl, 3.25 mM KCl, 1.2 $CaCl_2$, 1.25 mM NaH_2PO_4, 1.2 mM $MgCl_2$ and 2.0 mM Na_2SO_4. This buffer mimics the ionic environment present in cerebral spinal fluid. Stock solutions of dopamine were prepared in 0.1 M $HClO_4$, and were diluted to the desired concentration with TRIS buffer on the day of use.

Data acquisition and background correction

Cyclic voltammograms were acquired and analyzed using locally constructed hardware and software written in LabVIEW (National Instruments, Austin, TX) that has been described previously (Michael et al., 1999; Heien et al., 2003). Data was acquired with a digital to analog converter interface (PCI-6052, 16 bit, National instruments, Austin TX) with a personal home computer. For fast-scan cyclic voltammetric measurements, the rest potential was held at -0.4 V vs. Ag/AgCl. Triangular excursions were made to 1.3 V at a scan rate of 400 V/s and repeated at a frequency of 10 Hz. The measurements were conducted inside a grounded Faraday cage to minimize electrical noise.

Figure 5.1 shows a simplified schematic of the current-to voltage transducer used in this work. The triangular waveform (E_{in}) is applied to the non-inverting input of the operational amplifier. The working electrode is connected to the inverting input and the reference electrode is held at ground. This arrangement is advantageous because it can be used with multiple electronic devices (ion-selective electrodes, single unit recording electrodes, etc.) while all are biased against the same reference electrode. The inverting input of the amplifier is also connected to a resistor (R_1, impedance equal to R_f, the feedback resistor) into which the background signal, collected and digitized from previous scans, E_1, can be input. The output of the amplifier, E_3, is given by:

$$E_3 = E_{in} - (E_1/R_1 + I)R_f \qquad (1)$$

where I is the working electrode current.

The background correction process consists of two steps. First, the background signal is recorded while the digitized background signal input is held at ground (E_1 = 0 V). The digitized signal measured is solely due to the background signal and the applied voltage:

$$E_3 = E_{in} - (IR_f) \qquad (2)$$

Next this signal is applied as E_1. Due to the inverting property of the input, the output has both the applied voltage and background signal removed yielding a flat line. If the background alters from the value stored in E_1, it will cause the output to deviate from the flat line behavior.

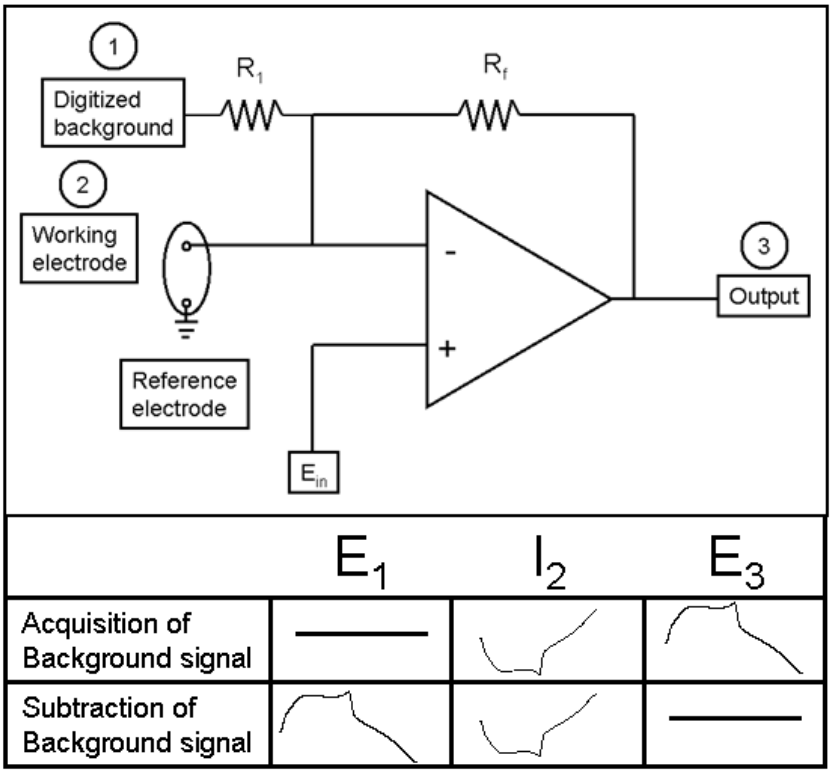

Figure 5.1. Electronic setup for digital background subtraction. The background is subtracted in a 2 step process: **1st Step: Acquisition of background signal**: The waveform is applied to E_{in} and driven to the electrode through the operational amplifier while second the input (E_1) is held at ground. **2nd step: Subtraction of background signal.** The waveform is applied to E_{in} and driven to the electrode through the operational amplifier while the background signal which was recorded during the 1st step is applied to input (E_1). The current obtained at the working electrode (I_2) is cancelled out at the summing point resulting in a flat signal at the output (E_3)

To provide appropriate removal of the background, the triangular waveform and the digitized background must be applied synchronously. However, digital-to-analog converters, typically have a time delay when switching between two output channels. This time delay can cause spurious results in the form of sharp spikes, particularly at the beginning and switching potentials where the rate of background change is the greatest. To account for the time delay the digitized background signal was time-shifted with software until the current spikes were minimized.

Flow-injection analysis

For flow–injection analysis the electrode was positioned at the outlet of a six-port rotary valve. A loop injector mounted on an actuator (Rheodyne model 5041 valve and 5701 actuator) and controlled by a 12-V DC solenoid valve kit (Rheodyne, Rohnert Park, CA) was used to introduce a bolus of analyte to the electrode. The flow rate was controlled by a syringe infusion pump (2 ml/min, Harvard Apparatus Model 22, Holliston, MA).

Electrode preparation

The microelectrodes were fabricated as previously described(Kawagoe et al., 1993) with T-650 carbon fibers (Thornel, Amoco Corp., Greenville, SC, 5 μm diameter). A single fiber was aspirated into a glass capillary and pulled on a micropipette puller (Narashige, Tokyo, Japan). The carbon fiber was cut so that approximately 50 μm protruded from the glass seal. The microelectrodes were backfilled with electrolyte solution (4 M potassium acetate, 150 mM potassium

chloride), and wires were inserted into the capillary for electrical contact. Before use, electrodes were soaked in isopropanol purified with Norit A activated carbon (ICN, Costa Mesa, CA) for at least 20 minutes.(Bath et al., 2000) Before recording electrodes were cycled at a repetition rate of 60 Hz for 15 minutes from -0.4V to 1.3 V for 15 minutes following 30 minutes of cycling at 10 Hz with the same scan parameters.

For all measurements Ag/AgCl reference electrodes were used.

Noise analysis

To evaluate quantization noise, a triangular waveform at 400 V/s from -0.4V to 1.3V was applied to an equivalent electrochemical cell consisting of a resistor (1 MΩ) and capacitor (400 pF) in series. The values for resistance and capacitance mimic the response of the microelectrodes used in this work. After the background signal was removed, the input range of the analog-to-digital converter was increased and the noise level in three different systems was measured as a standard deviation. The noise values were then normalized to the original noise obtained with the lowest gain.

In vivo measurements in anesthetized rats

Male Sprague-Dawley rats (225-350g; Charles River, Wilmington, MA) were anesthetized with urethane (1.5 g/kg, i.p.) and placed in a stereotaxic frame (Kopf, Tujunga, CA). A heating pad (Harvard Apparatus, Holliston, MA) maintained body temperature at 37°C. Holes were drilled in the skull for the working, reference, and

stimulating electrodes using coordinates (relative to bregma) from the brain atlas of Paxinos and Watson (Paxinos and Watson, 1998). The carbon-fiber microelectrode was placed in the striatum: anterior/posterior (AP) +1.2 mm, medial/lateral (ML) +2.0 mm, and dorsal/ventral (DV) -4.5 mm). The stimulating electrode was placed in the substantia nigra: AP -5.2 mm, ML +1.0 mm, and DV -7.5 mm. A Ag/AgCl reference electrode was inserted in the opposite hemisphere. The DV position of both the stimulating and working electrodes was adjusted to find sites that supported maximal dopamine release. The stimulation consisted of 40 biphasic pulses delivered at 60 Hz frequency (± 125 μA, 2 ms per phase).

In vivo measurements in freely moving rats

Male Sprague-Dawley rats implanted with a jugular vein catheter (300-450 g, Charles River Laboratories, Wilmington, MA) were housed individually on a 12:12 hour light cycle with ad libitum access to food and water. Procedures were as described previously(Phillips et al., 2003a). Rats were anesthetized with ketamine hydrochloride (100 mg/kg i.p.) and xylazine hydrochloride (20 mg/kg i.m.) and placed in a stereotaxic frame for implantation surgery. A Ag/AgCl reference electrode was chronically implanted in the forebrain, and secured in place. A guide cannula (Bioanalytical Systems, West Lafayette, IN) was positioned above the contralateral NAc (1.7 mm AP, 0.8 mm ML, -2.5 mm DV relative to bregma)**.** A bipolar stimulating electrode was lowered toward the VTA (-5.4 mm AP, 1.0 mm ML, -8.0 mm DV relative to bregma). All items were affixed to the skull with machine screws and cranioplastic cement, and secured in place**.**

Following surgery, rats were allowed to recover for 48 hours during which time they received acetaminophen administered orally every 12 hours. Experiments were performed within one week of the implantation surgery. Experiments were conducted in an operant box containing an infusion pump for drug delivery through the jugular catheter. The electrodes were connected to a light weight amplifier that is connected to a swivel linked to the remaining electronics. Rats were acclimated to the recording chamber for 1 h. Once baseline voltammetric recordings were made, the rats were given a 6 sec infusion of either saline or cocaine (3 mg/kg).

Histological Verification of Electrode Placement

The tip of the carbon-fiber is too small (5 μm diameter) to be seen histologically. Therefore, following experiments each rat was deeply anesthetized with urethane and a constant current was applied to an electrode to lesion the area. The animal was then perfused transcardially with phosphate buffered saline, followed by a 4% formalin solution. The brain was extracted and stored in a 4% formalin solution. The fixed tissue was finally frozen and sliced on a cryostat at 40 μm sections. Placement of the electrode tip was verified by microscopic inspection of the section.

Data analysis

Data analysis was performed with local software written in NI LabVIEW and MathWorks MATLAB. Principal component analysis (PCa) analysis was conducted as described previously. (Heien et al., 2004) Malinowski's F-test was used (p =

0.05) to determine the number of relevant eigenvectors. (Malinowski, 1988, 1990) For analysis of flow cell injections, calibration sets for dopamine were constructed with varying concentrations ranging from 0.5 μM to 2 μM. For *in vivo* experiments calibration sets for dopamine were constructed from electrically evoked stimulations with varying number of stimulation pulses. Calibrations for pH changes during *in-vivo* experiments were also obtained from pH shifts following electrical stimulation (Venton et al., 2003). The calibration set for background drift was constructed from the cyclic voltammograms obtained for the background drift 10 minutes before and for 10 minutes after each of the recordings.

Quantitative comparison between components

To quantitatively compare the signals for each of the components, an RMS current value was calculated for each. To obtain the RMS currents classical-least squares (CLS) was used (Kramer, 1998). CLS can be expressed in matrix representation as

$$\mathbf{A} = \mathbf{KC} \qquad (4)$$

where **A** is a matrix of measurement values, **C** is a matrix of concentration values, and **K** is a matrix containing pure component spectra. In this study, **A** is an $n \times m$ matrix containing cyclic voltammograms measured at n potentials and m time points, **C** is an $l \times m$ concentration matrix of l components, and **K** is an $n \times l$ matrix containing pure component cyclic voltammograms for each component.

K is calculated using cyclic voltammograms and concentrations from calibration sets according to

$$\mathbf{K = AC^T(CC^T)} \qquad (5)$$

where the superscript **T** represents transposed matrices. Concentration traces for each component and cyclic voltammograms at *m* time points were constructed using only the relevant eigenvectors. The eigenvectors were determined from principal component regression and were used as the training set to calculate K as shown in equation (5). Once pure component cyclic voltammograms have been ascertained, cyclic voltammograms at *m* time points for the j^{th} component ($\mathbf{A_j}$) were generated according to

$$\mathbf{A_j = k_j c_j} \qquad (6)$$

where $\mathbf{k_j}$ and $\mathbf{c_j}$ are the pure component cyclic voltammograms and concentration traces for the j^{th} component, respectively. With equation (6) it is possible to separate each data set into its pure components.

The RMS current value (I_{RMS}) for each component at each time point was determined by summing across each cyclic voltammogram according to

$$I_{RMS} = \left[\frac{1}{T} \sum_{0}^{T} i^2(t) \right]^{1/2} \qquad (7)$$

where i(t) is the current at each potential and T is the length of time of the potential sweep.(Simpson, 1987) The RMS current traces give precise information of how much each of the compounds contributes to the total current measured.

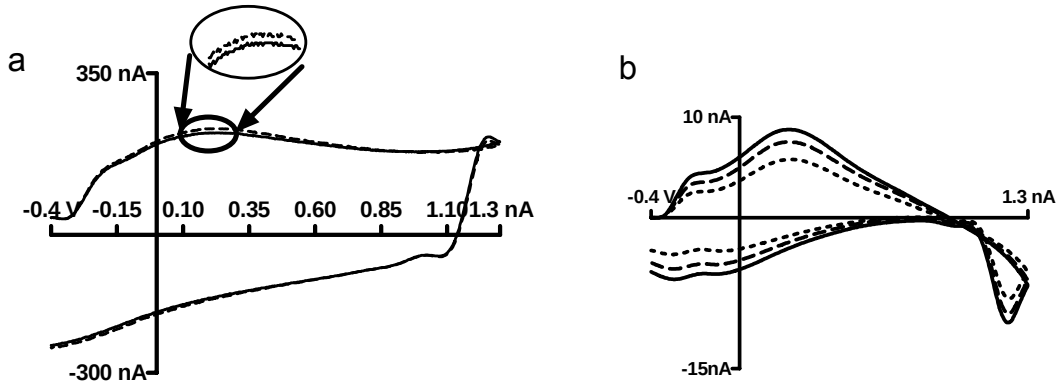

Figure 5.2. Background change. Panel a. Background signal obtained after conditioning of continuous cycling from -0.4V to 1.3V vs. Ag/AgCl with a repetition frequency of 60 Hz for 15 minutes following cycling at a frequency of10 Hz for 30 minutes (solid line) or for 60 minutes (dashed line); Panel b. Cyclic voltammograms obtained for changes in background current. Background current was subtracted after conditioning for 15 minutes from -0.4V to 1.3V vs. Ag/AgCl with a repetition frequency of 60 Hz following cycling at a frequency of 10 Hz for 30 minutes. The cyclic voltammograms were obtained 10 minutes (dotted line), 20 minutes (dashed line) and 30 minutes (solid line) after digital background subtraction occurred.

RESULTS AND DISCUSSION

Noise reduction

The current to voltage transducer has to be used with a relatively low gain so that the background current remains on scale. For example the background shown in Figure 5.2a requires an input range of ± 350 nA. In contrast, the sensitivity for dopamine is ~ 7 nA/μM, and biologically meaningful concentrations of dopamine monitored during behavior are ~50 nM (Phillips et al., 2003b), yielding 350 pA excursions. When the uncorrected background signal is digitized with a 16 bit analog-to-digital convertor, the minimum resolvable current will be $(700/2^{16})$ nA or 10.7 pA. Because each value of the analog-to-digital converter is separated by this magnitude, this results in what is termed quantization noise. A reduction in the background amplitude allows the gain to be increased, lowering the nose. This is shown by the dashed line in Figure 5.3 that is taken from the specifications of the interface board. With a smaller input range, corresponding to a larger gain, the quantization noise decreases.

The analog background subtraction technique described here allows removal of this noise source. As illustrated in Figure 5.2b, the amplitude of the background signal is dramatically diminished following analog subtraction, and it can be observed using a ± 15 nA range. This 24-fold increase in gain reduces the quantization noise proportionately. As shown in figure 5.3, the measured noise levels off at around 35% of the original noise at the highest gain settings. At these settings other noise sources predominate over quantization noise.

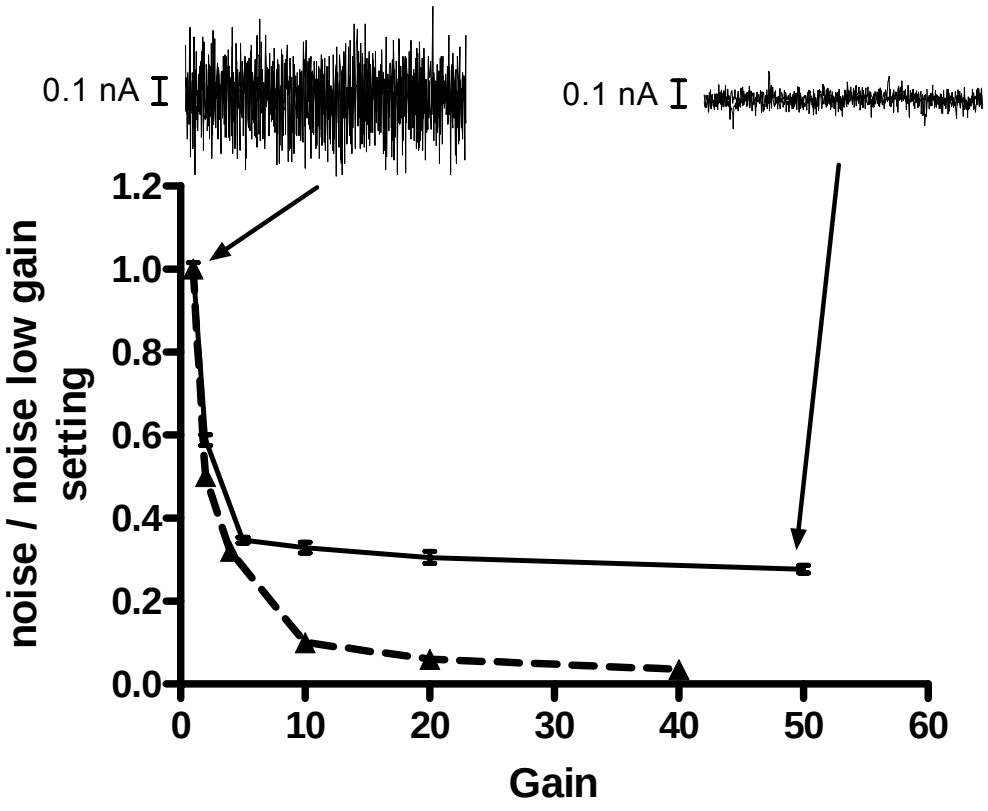

Figure 5.3. Noise characterization. Plot of noise measured at different input ranges of the analog-to-digital converter. The data is normalized for the noise level measured at the highest input range. Solid line: Noise level measured in the system, Dashed line: quantization noise of analog-to-digital converter according to specifications(National-Instruments-Corporation, 2005). Insets indicate a typical cyclic voltammogram recorded to determine the noise levels at the highest input range and the lowest input range.

Effect of drift of the background

During FSCV the background at carbon-fiber microelectrodes changes with time. Indeed, at the start of use, the electrode is usually cycled with the triangular wave to obtain a stable background. The initial changes in the background current are large, but become smaller as the cycling is continued. However, even after 1.5 hours of continuous triangular wave application the background signal does not fully stabilize (Hsueh et al., 1997). With the waveform used in this work, the background current continued to increase, which we attribute to an ongoing oxidation of the carbon surface. This drift is a significant problem for measurements with FSCV because it sets the time limit over which changes can be monitored. In measurements for dopamine in vivo, we have had to restricted measurement times to less than 90 s to minimize distortion of cyclic voltammetric signals by the drift.

In this work, electrodes were cycled for 15 min with a triangular waveform from -0.4 V to 1.3 V and back vs. Ag/AgCl at a repetition rate of 60 Hz. The repetition rate subsequently was lowered to 10 Hz for 30 min prior to recordings. In figure 5.2a a background cyclic voltammogram recorded immediately after pretreatment is compared to one recorded 30 minutes later. When viewed on an expanded scale, differences between these two background signals are evident indicating the drift is continuing.

The analog background subtraction approach allows the changes in the background to be examined more closely. Following preconditioning, analog background subtraction was initiated. Cyclic voltammograms recorded at 10 minute intervals following the initiation of the analog subtraction reveal the extent and nature

of the drift (Figure 5.2b). These data show that the change in background current is potential dependent. An oxidation peak around 0.2V vs. Ag/AgCl emerges that appears surface associated. In addition, there is a current spike at the anodic switching potential that is distorted by the filtering employed. Thus, even after 45 minutes of preconditioning, the current at the carbon-fiber electrode has not reached an equilibrium condition. In prior work, compensation for background drift has been achieved by subtracting current at a potential where the analyte is not electroactive from the current at a potential where the analyte is electroactive (Borland and Michael, 2004). The present results show that this is an inappropriate method because of the potential dependence of the background changes.

PCA has been used to remove the background from cyclic voltammograms (Reich et al., 1990). However, this approach did not succeed in our application because the background signal is much larger than the faradaic signals (Heien et al., 2004). The analog background subtraction approach diminishes the amplitude of the recorded background so that only the drift remains. A calibration set for this component can be obtained from cyclic voltammograms that were recorded before and after the data collection in the interval of interest. This approach was evaluated in a flow-injection analysis experiment with the electrode continuously cycling for 15 minute. At 1 min intervals, 2 μM dopamine was injected for 5 s into the system. Figure 5.4a shows the current from successive voltammograms recorded at the dopamine oxidation potential. Upward drift is clearly apparent as are the superimposed rapid changes arising from the dopamine injections. This set of cyclic voltammograms was evaluated by PCA with a training set for dopamine and another

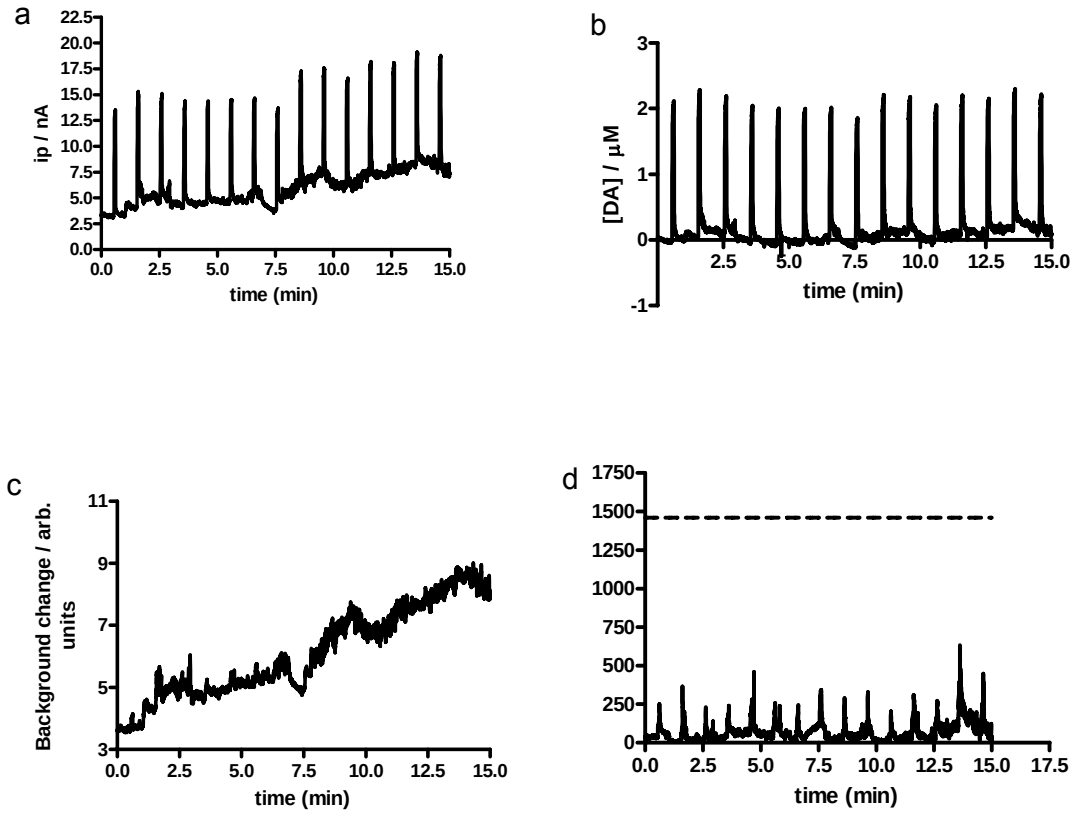

Figure 5.4. Dopamine injections *in vitro.* 2 µM of dopamine was injected for 5 seconds every minute in a flow cell experiment. Panel a. Current vs. time trace at the dopamine oxidation potential; Panel b. Concentration vs. time trace for dopamine obtained after correction for background drift with principal component regression. Panel c. Extracted component of background drift; Panel d. Residual data is within the 95% confidence interval as indicated by the dashed line

set for the drift. This procedure separates the voltammograms into two different components (figure 5.4b,c) and the residual (Figure 5.4d). The baseline for the dopamine concentration is essentially flat (figure 5.4b), while the drift is placed in the background (figure 5.4c). The residual (figure 5.4d) shows a spike at the beginning of every dopamine injection. This arises from a slight changes in shape of the dopamine signal as it adsorbs compared to the training set (Heien et al., 2004). However, this error is never higher than 5% of the total signal measured throughout the whole data collection. The dashed line in figure 5.4d represents the 95% confidence limit, and the residual is clearly below that limit. Indeed, dopamine could be monitored for longer than 1 hour before the residual value crossed the 95% confidence interval.

Monitoring dopamine concentrations in vivo

To test the method in vivo, the electrode was implanted in the caudate-putamen of an anesthetized rat, and stimulations of cell bodies of dopaminergic neurons were repeated every 2 minutes. The results were quite similar to those obtained in the flow-injection analysis system. When the current was monitored in successive analog subtracted, cyclic voltammograms at the potential for dopamine oxidation there was an increase in oxidation current at each stimulation, and these changes were superimposed on an upward drift. With suitable training sets, PCA could resolve the background drift from the dopamine concentration (figure 5.5a,b), and the residual remained low over the 20 minute interval. Recall, with the

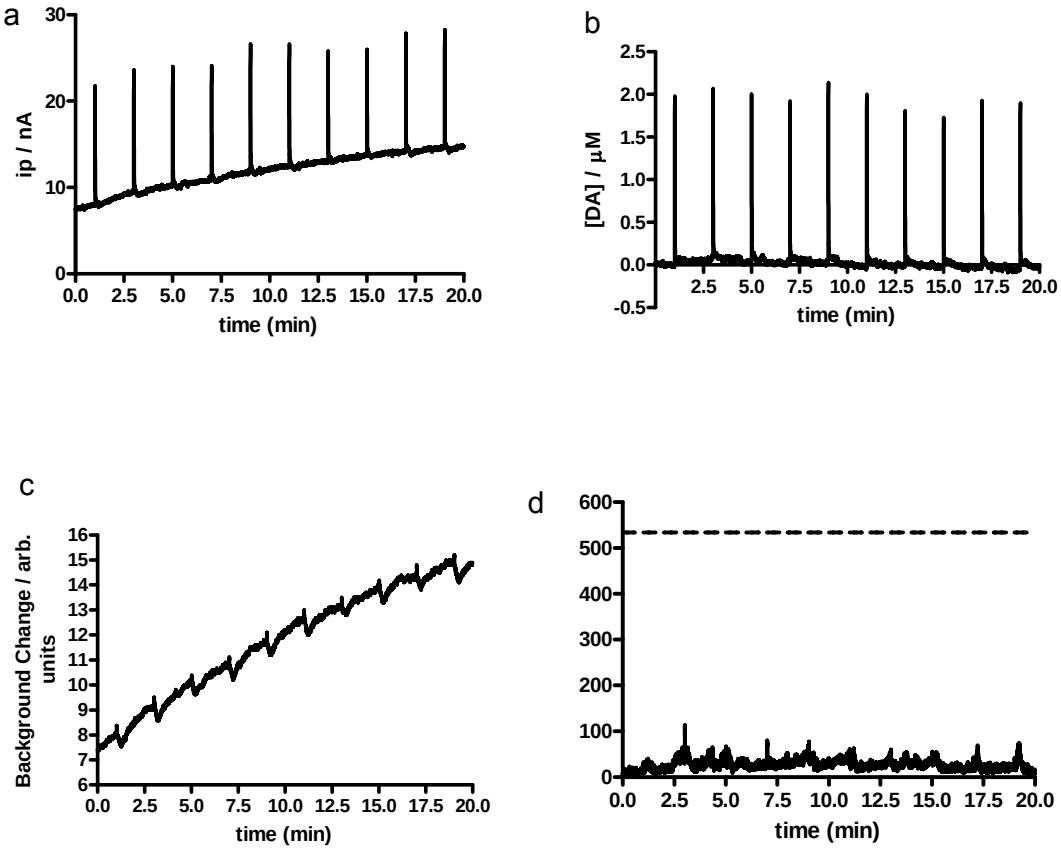

Figure 5.5. Dopamine stimulations *in vivo* A stimulation of 40 biphasic pulses at 60 Hz frequency (± 125 µA, 2ms per phase) every 2 minutes was used to evoke dopamine release. Panel a. Current vs. time trace at the dopamine oxidation potential; Panel b. Concentration vs. time trace for dopamine obtained after correction for background drift with principal component regression. Panel c. Extracted component of background drift; Panel d. Residual data is within the 95% confidence interval as indicated by the dashed line

traditional digital subtraction of the background, signals could only be monitored for 90 s.

As a second test of the analog subtraction procedure, we measured changes in the brain following an intravenous dose of cocaine administered to an ambulatory rat. Cocaine is a dopamine uptake blocker and increases extracellular dopamine concentration in the striatum. While early microdialysis studies suggested that dopamine levels are elevated for hours (Bradberry and Roth, 1989; Pettit et al., 1990), recent results have shown that the dopamine concentrations in the nucleus accumbens are elevated for around 20 minutes (Shou et al., 2006) and closely follow the time course of elevated cocaine levels in the brain.(Pan et al., 1991) In prior cyclic voltammetric recordings using digital background correction we were only able to capture the maximum dopamine change before the 90 s window caused by drift precluded further analysisb(Heien et al., 2005).

Analog subtracted cyclic voltammograms were collected for 30 min with cocaine administered at 12 min. PCA was conducted on these data similarly to the flow-injection and stimulation experiments, except that the responses to pH changes were also included in the calibration set. The resulting concentration trace for dopamine (figure 5.6a) shows a long term concentration change occurring within 1 minute after the cocaine injection. The time course observed matches well recent microdialysis recordings(Shou et al., 2006) as well as with the pharmacokinetic model (Pan et al., 1991) for cocaine concentrations (dashed line, figure 5.6a). Also time-locked with dopamine administration, the pH of the brain region changes to more basic values and then returns to near starting levels. Shifts in pH correlate

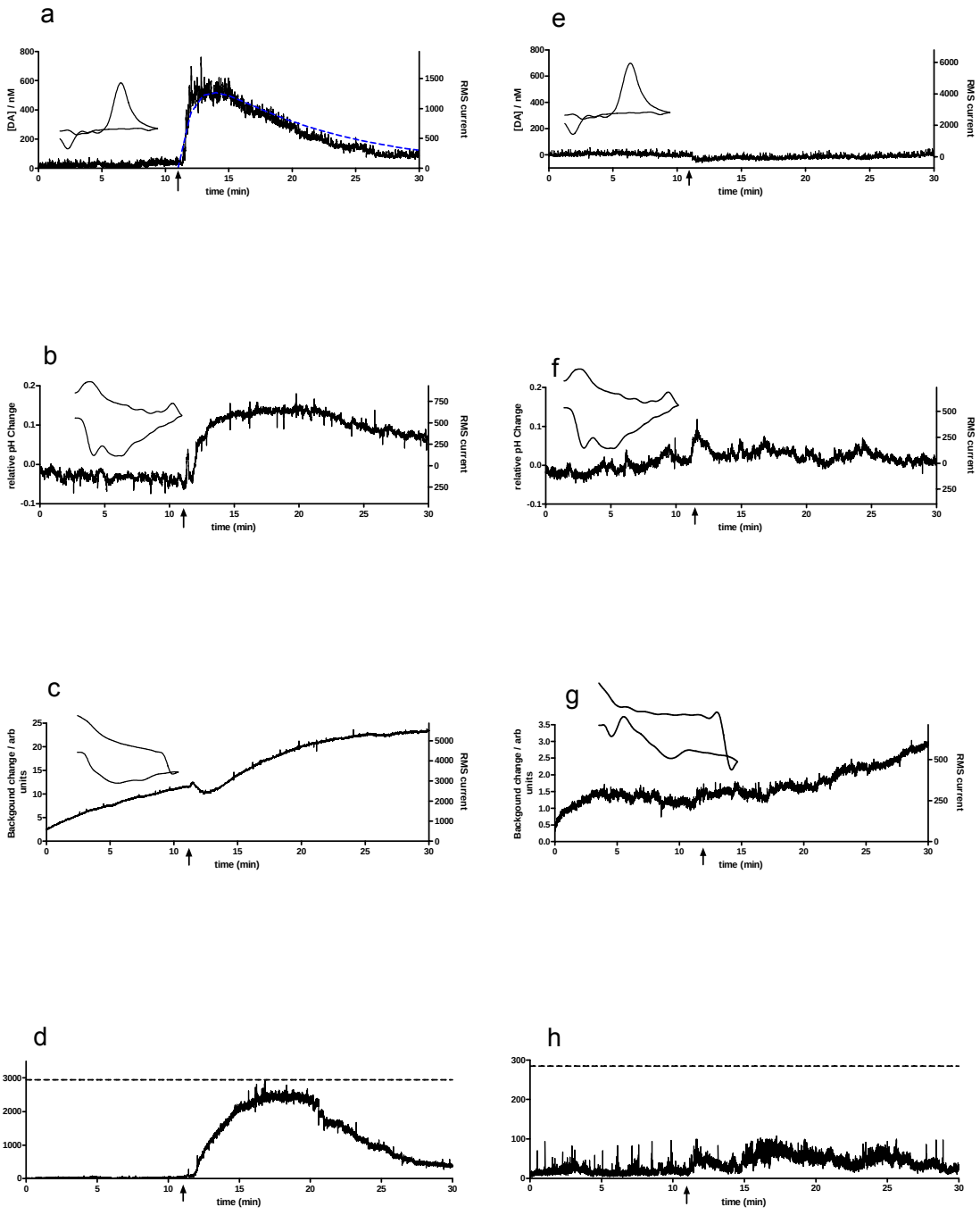

Figure 5.6. Response to iv cocaine and saline injections. Left panels show time traces obtained with principal component regression for cocaine injection at approximately 11 minutes (indicated by arrow); Right panels show time traces obtained with principal component regression for saline control injection at approximately 11 minutes (indicated by arrow); Insets show a representative cyclic voltammogram that was used for the calibration set; Panel a,e. Concentration / RMS current vs. time trace for dopamine, in panel a the concentration trace for

dopamine is overlaid with concentration trace for cocaine in the brain (dashed line) obtained after pharmacokinetic modeling(Pan et al., 1991); Panel b,f. pH change / RMS current vs time; Panel c,g. Background drift / RMS current vs time; Panel d,h. Residual data is within the 95% confidence interval as indicated by the dashed line

with the local oxygen level and are caused in part by dilation of blood vessels (Venton et al., 2003). The residual increases after the cocaine injection, although it does not cross the 5 % uncertainty value. The changing residual might be due to other chemical substances, not included in the training set, that change in response to cocaine. Alternatively, the presence of increase dopamine may have altered the background, causing the shift. A definitive conclusion requires further experimentation. Responses following saline injections were also examined. As apparent in figure 5.6 (right panel) with saline injection no significant change in dopamine concentration or pH shifts could be observed. However, background drift was still observed and could be accounted for.

Both saline and cocaine experiments were replicated in 5 animals. All showed similar traces to those shown in figure 5.6. However the amplitude and length of the of the long term dopamine concentration change showed differences between each experiment. The maximal change in dopamine concentration after cocaine administration ranged from 100 nM to 600 nM and the dopamine concentration remained elevated for between 10 and 20 minutes. These shorter time traces do not agree with microdialysis measurements. This discrepancy could be explained with the different size of the microelectrode compared to the microdialysis probe. The microelectrode samples a much smaller area than the microdialysis probe which gives more importance to the heterogeneity of the brain. A recording closer to a release site would result in a different concentration profile then a sample taken further away from a release site. Furthermore, it has been reported that because of the relatively large size of microdialysis probes a trauma

layer forms around the probe (Clapp-Lilly et al., 1999; Khan and Michael, 2003) which might explain differences between voltammetric recordings and microdialysis recordings (Bungay et al., 2003; Borland et al., 2005). All traces shown in figure 5.6 are collected at a 10 Hz sampling rate. Accordingly all traces presented here have a resolution of 100ms and the time-traces of figure 5.6 consist of a total of 18000 points. For microdialysis the fastest sampling rates have reported to be on the order of 1-2 minutes(Jenkins and Becker, 2003; Bradberry and Rubino, 2004; Shou et al., 2006) resulting in around 20 sampling points per 30 minute trace.

Investigation of chemical fluctuations

The dopamine trace exhibits an increase in fluctuations immediately after cocaine administration (figure 5.6a), a change that is not so apparent in the pH, background, or residual responses. These cocaine induced concentration transients have been reported before, and appear to arise because of cocaine's unique actions on dopamine neurons (Heien et al., 2005; Stuber et al., 2005). To characterize further the cocaine induced fluctuations in each channel, we used the CLS method to unravel the set of cyclic voltammogram for dopamine, pH, and background. An example is shown for a one minute segment in Figure 5.7. The color plot in the top panel of figure 5.7 shows the current after the unused eigenvectors have been discarded. This can be broken down into a set of distinct cyclic voltammograms for each component that are shown as color plots for each component (Figure 5.7, lower panels). These plots are a representation of the A_j- matrices of the current values. The root mean square of each reconstructed cyclic voltammogram was

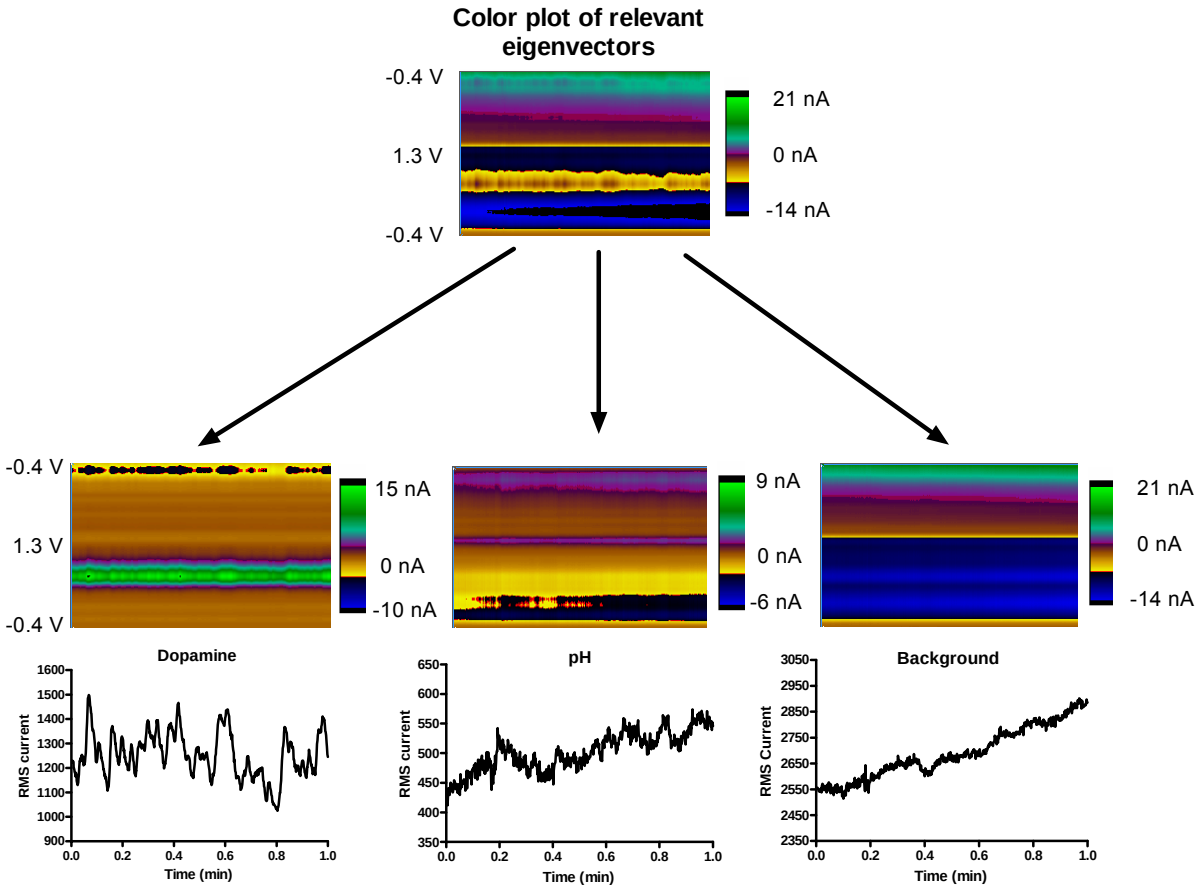

Figure 5.7. Construction of pure component color plots and RMS traces. This figure shows representative data obtained 2 minutes after cocaine administration. For all color representations the current is shown in false color, time on x-axis, potential on the y-axis. Top panel: Color representation of the recorded data after discarding the non-important principal components. Middle panel: Color representations of pure component spectra. Bottom panel: RMS traces for each of the components

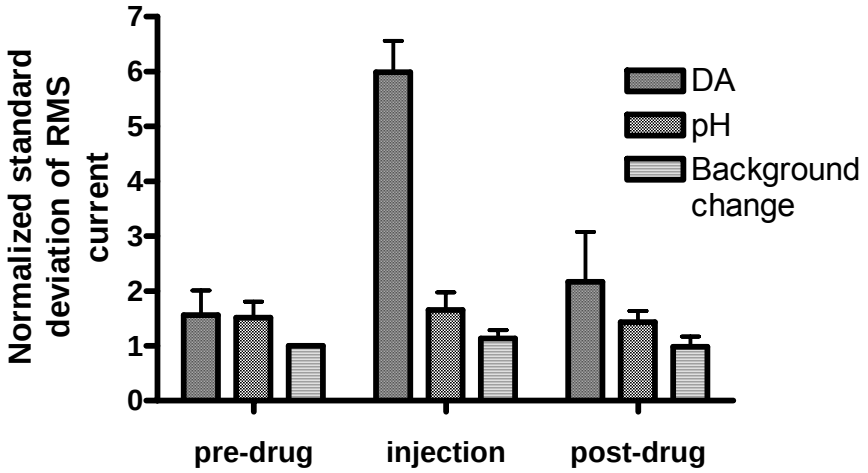

Figure 5.8: Standard-deviation of RMS-current traces. Standard deviations are shown for the RMS current traces for dopamine (DA), pH change (pH), and background change (BG). Data was collected for 3 minutes pre-drug, for 3 minutes after drug injection and for 3 minutes 20 minutes after drug administration. All values are normalized to the standard deviation of background current pre-drug. (n=3 animals, error bars: SEM)

taken as the relevant value for comparison between channels. When time varying data contains information about the process of interest can be viewed as a fluctuation but it is better termed “noise” when the measured data decreases the probability to obtain useful information (Bezegh and Janata, 1987).

The variation in these signals was evaluated as a standard deviation for each trace over the time of interest, normalized to the standard deviation for the background. The temporal variations measurements were in 3 minute intervals. The times selected were before cocaine administration, immediately after cocaine administration, and 20 minutes after cocaine administration. Before cocaine administration the standard deviation for the dopamine signal and the pH signal are slightly elevated in comparison to the signal for background change, indicating that chemical fluctuations might be present in these two traces. After cocaine administration the fluctuations drastically increase in the dopamine signal while they are unchanged for the pH and background signals. Thus, even though a pH change occurs following cocaine administration, unlike dopamine, an increase in pH fluctuations does not occur. The fluctuations in the dopamine trace 20 minutes after cocaine are still elevated, but are approaching pre-cocaine levels.

Summary

In this study we have demonstrated an analog method to subtract the background currents that occur during cyclic voltammetric scans at high scan rates. This subtraction enables the use of higher gains before the analog-to-digital conversion, lowering quantization noise. Furthermore, by monitoring the drift and

compensation of these background changes with PCA, FSCV measurements can be made for longer time scales. This enabled dopamine and pH concentrations to be monitored over time windows that previously have been accessible only to microdialysis but with a time resolution that is 600-times greater. With this high time resolution we were able to monitor short term fluctuations in concentrations. The data indicates that an increase in fluctuations in dopamine concentrations accompany the slow concentration changes in dopamine after administration of cocaine.

REFERENCES

Amatore C, Lefrou C (1990) Is Cyclic Voltammetry above a Few Hundred Kilovolts Per Second Still Cyclic Voltammetry. Journal of Electroanalytical Chemistry 296:335-358.

Amatore C, Maisonhaute E (2005) When voltammetry reaches nanoseconds. Anal Chem 77:303A-311A.

Bard AJ, Faulkner LR (2001) Electrochemical Methods, Fundamentals and Applications, 2 Edition. New York: John Wiley.

Bath BD, Michael DJ, Trafton BJ, Joseph JD, Runnels PL, Wightman RM (2000) Subsecond adsorption and desorption of dopamine at carbon-fiber microelectrodes. Anal Chem 72:5994-6002.

Bezegh A, Janata J (1987) Information from Noise. Analytical Chemistry 59:A494-&.

Borland LM, Michael AC (2004) Voltammetric study of the control of striatal dopamine release by glutamate. Journal of Neurochemistry 91:220-229.

Borland LM, Shi GY, Yang H, Michael AC (2005) Voltammetric study of extracellular dopamine near microdialysis probes acutely implanted in the striatum of the anesthetized rat. Journal of Neuroscience Methods 146:149-158.

Bradberry CW, Roth RH (1989) Cocaine Increases Extracellular Dopamine in Rat Nucleus Accumbens and Ventral Tegmental Area as Shown by Invivo Microdialysis. Neuroscience Letters 103:97-102.

Bradberry CW, Rubino SR (2004) Phasic alterations in dopamine and serotonin release in striatum and prefrontal cortex in response to cocaine predictive cues in behaving rhesus macaques. Neuropsychopharmacology 29:676-685.

Bungay PM, Newton-Vinson P, Isele W, Garris PA, Justice JB (2003) Microdialysis of dopamine interpreted with quantitative model incorporating probe implantation trauma. J Neurochem 86:932-946.

Clapp-Lilly KL, Roberts RC, Duffy LK, Irons KP, Hu Y, Drew KL (1999) An ultrastructural analysis of tissue surrounding a microdialysis probe. Journal of Neuroscience Methods 90:129-142.

Clegg AD, Rees NV, Klymenko OV, Coles BA, Compton RG (2004) Marcus theory of outer-sphere heterogeneous electron transfer reactions: Dependence of the standard electrochemical rate constant on the hydrodynamic radius from high precision measurements of the oxidation of anthracene and its

derivatives in nonaqueous solvents using the high-speed channel electrode. Journal of the American Chemical Society 126:6185-6192.

Hayes MA, Kristensen EW, Kuhr WG (1998) Background-subtraction of fast-scan cyclic staircase voltammetry at protein-modified carbon-fiber electrodes. Biosensors & Bioelectronics 13:1297-1305.

Heien ML, Phillips PE, Stuber GD, Seipel AT, Wightman RM (2003) Overoxidation of carbon-fiber microelectrodes enhances dopamine adsorption and increases sensitivity. Analyst 128:1413-1419.

Heien MLAV, Johnson MA, Wightman RM (2004) Resolving neurotransmitters detected by fast-scan cyclic voltammetry. Analytical Chemistry 76:5697-5704.

Heien MLAV, Khan AS, Ariansen JL, Cheer JF, Phillips PEM, Wassum KM, Wightman RM (2005) Real-time measurement of dopamine fluctuations after cocaine in the brain of behaving rats. Proceedings of the National Academy of Sciences of the United States of America 102:10023-10028.

Howell JO, Wightman RM (1984) Ultra-fast voltammetry and voltammetry in highly resistive solutions with microvoltammetric electrodes. AnalChem 56:524-529.

Howell JO, Kuhr WG, Ensman RE, Wightman RM (1986) Background Subtraction for Rapid Scan Voltammetry. Journal of Electroanalytical Chemistry 209:77-90.

Hsueh C, Bravo R, Jaramillo AJ, BrajterToth A (1997) Surface and kinetic enhancement of selectivity and sensitivity in analysis with fast scan voltammetry at scan rates above 1000 V/s. Analytica Chimica Acta 349:67-76.

Jenkins WJ, Becker JB (2003) Dynamic increases in dopamine during paced copulation in the female rat. European Journal of Neuroscience 18:1997-2001.

Kawagoe KT, Zimmerman JB, Wightman RM (1993) Principles of voltammetry and microelectrode surface states. Journal of neuroscience methods 48:225-240.

Khan AS, Michael AC (2003) Invasive consequences of using micro-electrodes and microdialysis probes in the brain. Trac-Trends in Analytical Chemistry 22:503-508.

Kramer R (1998) Chemometric Techniques for Quantitative Analysis. New York: Marcel Dekker, Inc.

Malinowski ER (1988) Journal of Chemometrics 3:49-60.

Malinowski ER (1990) Journal of Chemometrics 4:102.

Michael DJ, Joseph JD, Kilpatrick MR, Travis ER, Wightman RM (1999) Improving data acquisition for fast scan cyclic voltammetry. Analytical Chemistry 71:3941-3947.

Millar J, Stamford JA, Kruk ZL, Wightman RM (1985) Electrochemical, Pharmacological and Electrophysiological Evidence of Rapid Dopamine Release and Removal in the Rat Caudate-Nucleus Following Electrical-Stimulation of the Median Forebrain-Bundle. European Journal of Pharmacology 109:341-348.

Mirkin MV, Bulhoes LOS, Bard AJ (1993) Determination of the Kinetic-Parameters for the Electroreduction of C-60 by Scanning Electrochemical Microscopy and Fast Scan Cyclic Voltammetry. Journal of the American Chemical Society 115:201-204.

National-Instruments-Corporation (2005) NI 6052E Family Specifications. NI 6052E Family Specifications.

Neugebauer S, Evans SR, Aguilar ZP, Mosbach M, Fritsch I, Schuhmann W (2004) Analysis in ultrasmall volumes: Microdispensing of picoliter droplets and analysis without protection from evaporation. Analytical Chemistry 76:458-463.

Pan HT, Menacherry S, Justice JB (1991) Differences in the Pharmacokinetics of Cocaine in Naive and Cocaine-Experienced Rats. Journal of Neurochemistry 56:1299-1306.

Paxinos W, Watson C (1998) The Rat Brain in stereotaxic coordiantes. Academic Press, Orlando, Florida.

Pettit HO, Pan HT, Parsons LH, Justice JB (1990) Extracellular Concentrations of Cocaine and Dopamine Are Enhanced during Chronic Cocaine Administration. Journal of Neurochemistry 55:798-804.

Phillips PE, Robinson DL, Stuber GD, Carelli RM, Wightman RM (2003a) Real-time measurements of phasic changes in extracellular dopamine concentration in freely moving rats by fast-scan cyclic voltammetry. Methods Mol Med 79:443-464.

Phillips PE, Stuber GD, Heien ML, Wightman RM, Carelli RM (2003b) Subsecond dopamine release promotes cocaine seeking. Nature 422:614-618.

Reich G, Wolf J, Long JT, Weber SG (1990) Recovery of voltammograms by target factor analysis of current-time data in electrochemical detection. Anal Chem 62:2643-2646.

Robinson DL, Venton BJ, Heien ML, Wightman RM (2003) Detecting subsecond dopamine release with fast-scan cyclic voltammetry in vivo. Clin Chem 49:1763-1773.

Shou MS, Ferrario CR, Schultz KN, Robinson TE, Kennedy RT (2006) Monitoring dopamine in vivo by microdialysis sampling and on-line CE-laser-induced fluorescence. Analytical Chemistry 78:6717-6725.

Simpson RE (1987) Alternating Current Circuits. In: Introductory electronics for scientists and engineers, 2 Edition, pp 54-56. Englewood Cliffs: Prentice-Hall, Inc.

Song Y, Heien MLAV, Jimenez V, Wightman RM, Murray RW (2004) Voltammetric detection of metal nanoparticles separated by liquid chromatography. Analytical Chemistry 76:4911-4919.

Soucazeguillous B, Kutner W, Kadish KM (1993) Amperometric and Fast Scan-Rate Cyclic Voltammetry Detection at a Microelectrode for Gel-Permeation High-Performance Liquid-Chromatography of Fullerenes. Analytical Chemistry 65:669-672.

Stuber GD, Wightman RM, Carelli RM (2005) Extinction of cocaine self-administration reveals functionally and temporally distinct dopaminergic signals in the nucleus accumbens. Neuron 46:661-669.

Sulzer D, Pothos EN (2000) Regulation of quantal size by presynaptic mechanisms. Reviews in the Neurosciences 11:159-212.

Swamy BEK, Venton BJ (2007) Subsecond detection of physiological adenosine concentrations using fast-scan cyclic voltammetry. Analytical Chemistry 79:744-750.

Venton BJ, Wightman RM (2003) Psychoanalytical electrochemistry: dopamine and behavior. Analytical Chemistry 75:414A-421A.

Venton BJ, Michael DJ, Wightman RM (2003) Correlation of local changes in extracellular oxygen and pH that accompany dopaminergic terminal activity in the rat caudate-putamen. Journal of Neurochemistry 84:373-381.

Wang J, Dewald HD (1984) Background-Current Subtraction in Voltammetric Detection for Flow-Injection Analysis. Talanta 31:387-390.

Wightman RM, Wipf DO (1990) High-speed cyclic voltammetry. Accounts of Chemical Research 23:64-70.

Yoo JS, Park SM (2005) Programmed potential sweep voltammetry for lower detection limits. Analytical Chemistry 77:3694-3699.

CHAPTER 6

CHANGES IN BACKGROUND SIGNAL AT CARBON MICROELECTRODES DURING FAST SCAN CYCLIC VOLTAMMETRY

Introduction

Fast scan cyclic voltammetry with carbon fiber microelectrodes can be used for electrochemical detection of easily oxidized neurotransmitters such as dopamine and serotonin in the brain (Cragg et al., 2000; Robinson et al., 2003; Venton and Wightman, 2003; Wightman, 2006). Carbon-fiber microelectrodes are suitable for *in vivo* application because they are sufficiently small that tissue damage is minimized (Khan and Michael, 2003; Peters et al., 2004). The small size also means that the chemical events that are recorded arise from a local micoenvironment with dimensions in the micrometer range. To increase sensitivity and selectivity for the neurotransmitters of interest, surface coatings are often applied to the electrode. Nafion, a perfluorinated cation-exchange polymer, can be coated on the electrode surface to increase the dopamine signal and minimize interfering signal, such as ascorbic acid (Gerhardt et al., 1984; Cahill et al., 1996). Similar effects have been shown with coating of overoxidized polypyrrole (Witkowski and Brajter-Toth, 1992; Pihel et al., 1996).

Another way to achieve increased sensitivity and selectivity is to use electrochemical pretreatments that promote oxidation of the carbon surface. In

early studies overoxidation was conducted by repetitive excursions to + 3 V vs. Ag/AgCl at 70 Hz (Gonon et al., 1980; Gonon et al., 1981). Electrodes treated in this way showed much higher sensitivity for catecholamines than untreated electrodes. However, besides increasing the amount of surface oxides, this surface treatment drastically increased the surface area of the electrode (Swain and Kuwana, 1991). A more recent study showed that electrodes that are oxidized at a potential of 1.4 V vs. Ag/AgCl exhibit higher sensitivity to positively charged analytes (Heien et al., 2003). This is due to an increased adsorption of cations to the carbon surface. A five-fold increase in sensitivity has been reported for dopamine *in vitro* when using FSCV at these overoxidized carbon fibers. However, the overoxidized electrodes show a slower time response and lower selectivity than electrodes that have not been exposed to high oxidizing potentials. Interestingly, the signal during *in-vivo* applications following carbon surface oxidation was increased almost twice as much as in vitro with a nine-fold increase in sensitivity when compared to the pre-oxidized surface. This finding suggests further electrode activation in biological tissue. Indeed, carbon-paste electrodes have been reported to exhibit faster electron-transfer kinetics for ferrocyanide (Ormonde and Oneill, 1989) and dopamine (Blaha and Jung, 1991) following contact with brain tissue. Those studies, however, do not provide an explanation for this observation beside non-specific adsorption of biomolecules.

In fast scan voltammetric measurements a large background current is produced. This background current is composed of the current required to charge the double layer and the current arising from redox reactions of surface

groups (Chen and McCreery, 1996; Bard and Faulkner, 2001). Electrochemical activation as well as a biological activation happens on a long time scale of minutes, much longer than the length of one voltammetric sweep at fast scan rates. Changes in the electrochemical response caused by activation processes, such as a change in capacitance or surface oxidation, would not be observable in a background subtracted voltammogram but should be observable as a change in the background current. In this study, a novel method of background subtraction (Chapter 5) is used to reveal changes in the background current that occur over a time scale of minutes during electrochemical and biological activation.

EXPERIMENTAL SECTION

Chemicals

All chemicals for flow injection analysis were purchased from Sigma-Aldrich (St. Louis, MO) and used as received. Solutions were prepared using doubly distilled water. Flow injection analysis was done in a TRIS buffer solution, pH 7.4 containing 15 mM TRIS, 140 mM NaCl, 3.25 mM KCl, 1.2 $CaCl_2$, 1.25 mM NaH_2PO_4, 1.2 mM $MgCl_2$ and 2.0 mM Na_2SO_4. This buffer mimics the ionic environment present in cerebral spinal fluid. Stock solutions of dopamine were prepared in 0.1 M $HClO_4$, and were diluted to the desired concentration with TRIS buffer on the day of use.

Data acquisition and electrochemical pretreatment

Cyclic voltammograms were acquired and analyzed using locally constructed hardware and software written in LabVIEW (National Instruments, Austin, TX) that has been described previously (Michael et al., 1999; Heien et al., 2003). Data was acquired with a digital to analog converter interface (PCI-6052, 16 bit, National instruments, Austin TX) with a personal home computer. A modified current to voltage transducer (Chapter 5) was used to enable the possibility to examine changes in background current. All fast scan voltammetric data was filtered with a software-lowpass filter at 2kHz.

For electrochemical pretreatments, the rest potential was held at -0.4 V vs. Ag/AgCl. Triangular excursions were made to 1.3 V at a scan rate of 400 V/s and repeated for the first 15 minutes at a frequency of 60 Hz following triangular excursions at a repetition frequency of 10Hz for 30 minutes. The measurements were conducted inside a grounded Faraday cage to minimize electrical noise.

Flow-injection analysis

For flow–injection analysis the electrode was positioned at the outlet of a six-port rotary valve. A loop injector mounted on an actuator (Rheodyne model 5041 valve and 5701 actuator) and controlled by a 12-V DC solenoid valve kit (Rheodyne, Rohnert Park, CA) was used to introduce a bolus of analyte to the electrode. The flow rate was controlled by a syringe infusion pump (2 ml/min, Harvard Apparatus Model 22, Holliston, MA).

Electrode preparation

Carbon fiber microelectrodes were fabricated as previously described(Kawagoe et al., 1993) with T-650 carbon fibers (Thornel, Amoco Corp., Greenville, SC, 5 µm diameter). A single fiber was aspirated into a glass capillary and pulled on a micropipette puller (Narashige, Tokyo, Japan). The carbon fiber was cut so that approximately 50 µm protruded from the glass seal. The microelectrodes were backfilled with electrolyte solution (4 M potassium acetate, 150 mM potassium chloride), and wires were inserted into the capillary for electrical contact. Before use, electrodes were soaked in isopropanol purified with Norit A activated carbon (ICN, Costa Mesa, CA) for at least 20 minutes.(Bath et al., 2000)

PPF-microelectrodes were constructed as previously described (Hermans and Wightman, 2006). As insulation material a cathodic electrophoretic paint (ZQ-84-3225, PPG Industries, Milford, OH, USA) was used instead of epoxylite. Insulation of the working electrode was conducted by application of a +2V DC potential in a 1:1 dilution of the electrophoretic paint while simultaneously monitoring the current. A stainless steel coil, surrounding the working electrode, was used as counter electrode. The electrode was removed from the solution 1 minute after no further change in current flow could be observed. The electrodes were cured at 200˚C for 5 minutes and used immediately.

For all measurements Ag/AgCl reference electrodes were used (Bioanalytical systems, West Lafayette, IN, USA).

In vivo measurements in anesthetized rats

Male Sprague-Dawley rats (225-350g; Charles River, Wilmington, MA) were anesthetized with urethane (1.5 g/kg, i.p.) and placed in a stereotaxic frame (Kopf, Tujunga, CA). A heating pad (Harvard Apparatus, Holliston, MA) maintained body temperature at 37°C. Holes were drilled in the skull for the working, reference, and stimulating electrodes using coordinates (relative to bregma) from the brain atlas (Paxinos and Watson, 1998). The carbon-fiber microelectrode was placed in the striatum: anterior/posterior (AP) +1.2 mm, medial/lateral (ML) +2.0 mm, and dorsal/ventral (DV) -4.5 mm). A Ag/AgCl reference electrode was inserted in the opposite hemisphere. For recordings in the cortex, the carbon-fiber microelectrode was placed anterior/posterior (AP) +1.2 mm, medial/lateral (ML) +2.0 mm, and dorsal/ventral (DV) -0.5 mm)

RESULTS AND DISCUSSION

Electrochemical activation of pyrolyzed photoresist films

Pyrolyzed photoresist films (PPF) have been shown to have a carbonaceous surface that has similar properties to glassy carbon electrodes (Ranganathan et al., 2000) and carbon fibers (Hermans and Wightman, 2006). PPF films are formed under a reducing hydrogen atmosphere, a condition that forms a carbon surface that is almost completely hydrogen terminated. Before any electrochemical treatment the oxygen/carbon ratio at the surface of PPF

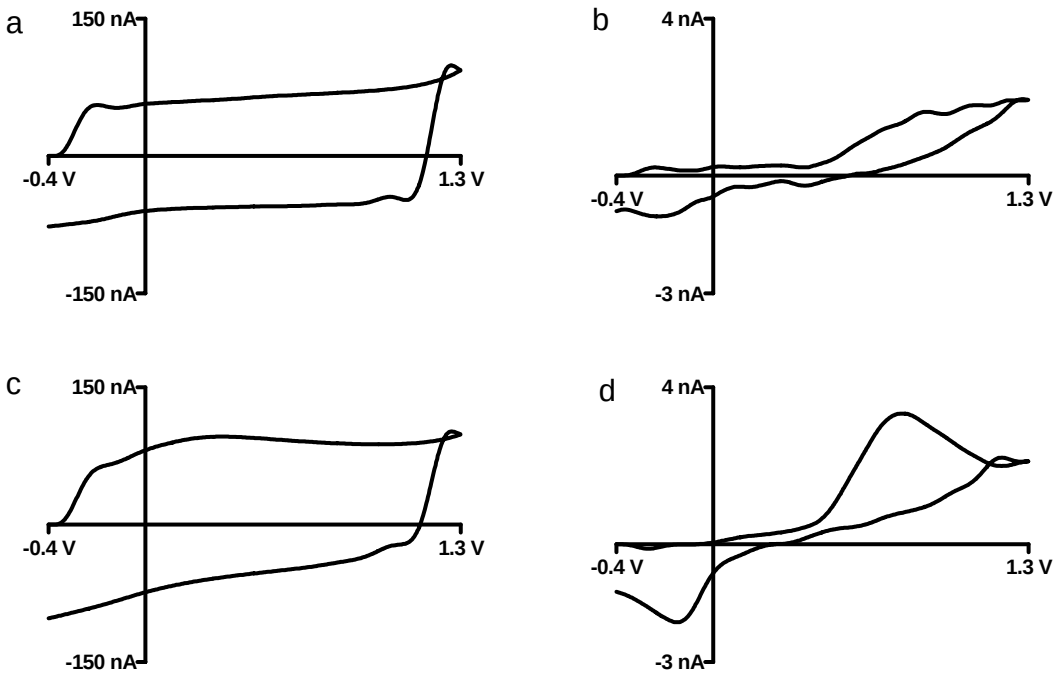

Figure 6.1. Electrochemical activation of PPF microelectrodes. Panel a. Background cyclic voltammogram at untreated PPF microelectrode in Tris-buffer; Panel b. Background subtracted cyclic voltammogram for 1 µM dopamine at an untreated PPF microelectrode; Panel c. Background cyclic voltammogram at PPF microelectrode in Tris-buffer after 15 minutes of voltammetric cycling at a repetition frequency of 60 Hz; Panel d. Background subtracted cyclic voltammogram for 1 µM doapmine at PPF microelectrode in Tris-buffer after 15 minutes of voltammetric cycling at a repetition frequency of 60Hz

films has been reported to be less than 2% (Ranganathan and McCreery, 2001). 6.1a shows the initial non-subtracted cyclic voltammetric response of a PPF microelectrode. The cyclic voltammogram has the rectangular shape expected for charging of the electric double layer (Bard and Faulkner, 2001), without other pronounced features except at the switching potential (1.3 V) where hysteresis caused by filtering is apparent. After repetitive cycling for 15 minutes at a repetition frequency of 60 Hz, an increase in oxidative current around 0.2 V vs. Ag/AgCl can be observed (Figure 6.1c). This surface wave is thought to be due to the growth of surface functional groups on the electrode surface such as quinones (Fagan et al., 1985; Chen and McCreery, 1996; Runnels et al., 1999) that are formed by the oxidation of the carbon electrode.

Electrochemical activation has been shown to increase electron-transfer kinetics at glassy carbon electrodes (Chen and McCreery, 1996), carbon-fiber microelectrodes (Runnels et al., 1999; Strein et al., 1999), and large size PPF electrodes(Ranganathan and McCreery, 2001). Here, we report similar effects at PPF microelectrodes. As seen in the right panel of figure 6.1, the background subtracted cyclic voltammogram for dopamine at untreated PPF microelectrodes has a broad separation of the anodic and cathodic peaks indicative of slow electron-transfer kinetics. However, after electrochemical activation the background-subtracted cyclic voltammogram for dopamine is similar with regards to the kinetics and shape of the voltammogram to that obtained with carbon-fiber microelectrodes treated in the same way (Baur et al., 1988). It has been shown that dopamine absorbs to carbon-fiber microelectrodes (Bath et al., 2000). The

oxide groups on the carbon surface are thought to function as adsorption sites for dopamine. Indeed, it has been shown that electrochemical oxidation of carbon fibers to high positive potentials increases adsorption of dopamine (Heien et al., 2003). The symmetrical shape of the oxidative and reductive peaks in figure 6.1d are a consequence of dopamine adsorption that causes the increase in sensitivity.

Background changes at carbon-fiber microelectrodes *in vitro*

Carbon fibers inherently have a larger amount of surface oxides than untreated PPF films. Nevertheless, in many voltammetric applications, carbon-fiber microelectrodes undergo electrochemical pretreatment until a relatively stable background signal is obtained (Borland et al., 2005; Swamy and Venton, 2007). Previous studies (Hsueh et al., 1997) have shown that the background current at carbon fibers which were continuously cycled from -0.8V to 1.2V vs. SCE at a rate of 100 V/s significantly change during the first 30 minutes. An apparent increase in capacitance as well as the formation of an oxidative peak at 0.2 V, similar to the peak observed in figure 6.1, was observed. Further cycling showed stabilization of the background signal – only a little drift was observed.

To examine the changes in background current at carbon fibers more closely we used analog background subtraction during the electrochemical pretreatment (Chapter 5). This approach allowed subtraction of the background

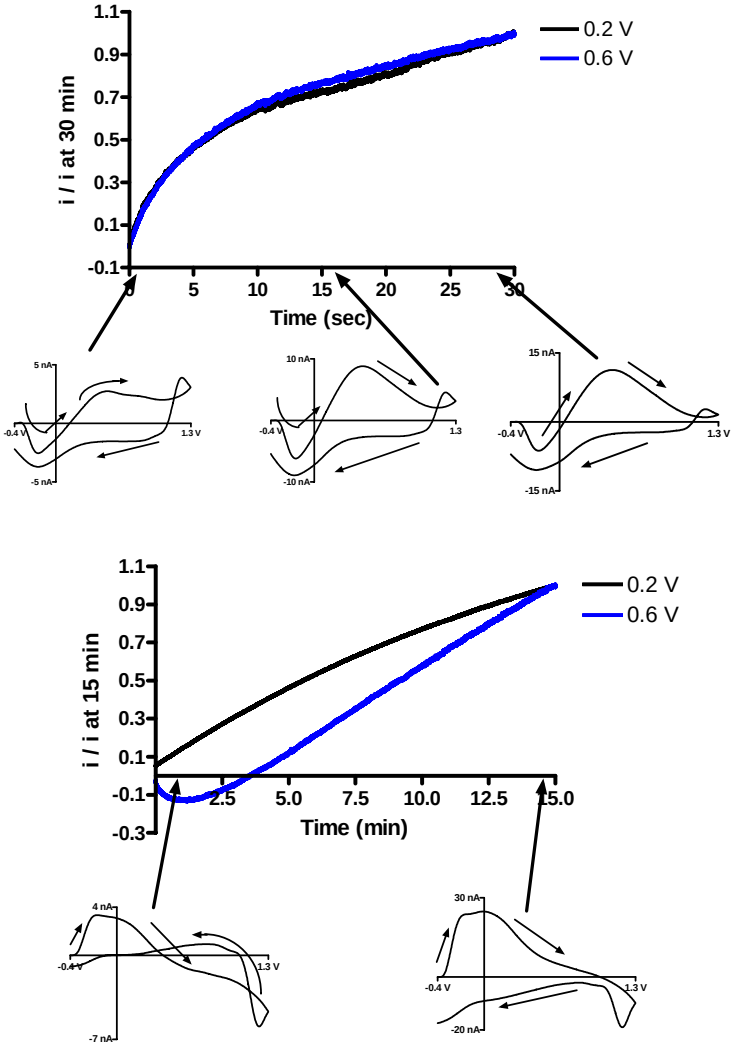

Figure 6.2. Changes in background signal at carbon-fiber microelectrodes *in vitro*. Top panel. Carbon-fiber microelectrodes were cycled for 15 minutes at a repetition frequency of 60 Hz and a scan rate of 400 V/s. The change in background current with time at 0.2 V and 0.6 V vs. Ag/AgCl on the anodic sweep were normalized to the current at each respective potential at the end of the experiment (average response n=4 electrodes). Representative cyclic voltammograms for background change are shown at different time points. Bottom panel. Following conditioning for 15 minutes at a repetition frequency of 60Hz electrodes the current was rezeroed. Then the changes in background current were followed during cycling for 30 minutes at a repetition of 10 Hz and a scan rate of 400 V/s.

at the beginning of the experiment, removing the large capacitive contribution. Subsequent observations of the remaining background current allowed its changes to be followed. The current at two potentials on the anodic excursion was monitored: the current at 0.2 V vs. Ag/AgCl, the voltage where the surface wave grows in, and at 0.6V vs. Ag/AgCl, the potential where dopamine oxidation occurs.

The cyclic voltammograms in figure 6.2, upper panel, show the change in background signal measured in a pH 7.4 Tris buffer during the first 15 minutes while cycling at 400 V/s from -0.4 V to 1.3 V vs. Ag/AgCl with a repetition frequency of 60 Hz. This waveform is a commonly used electrochemical pretreatment before data collection for *in vivo* applications (Cheer et al., 2005) to achieve a stable background signal. Interestingly, the background does not change uniformly during the 15 minute interval as can be seen in the different shape of voltammogram taken 1 minute and 14 minutes after the cycling started. The current at 0.2V increases with time in an exponential manner, while the current at 0.6 V decreases initially and then increases after approximately 1.5 minutes of cycling. The main feature, that can be observed during the first 15 minutes is an increase in oxidative current around a potential of 0V vs. Ag/AgCl. This potential change is probably due to oxidation of surface oxide groups. However, only a small change in background current was observed at all other potentials. The finding that the currents at 0.6V and for 0.2V change in quite different ways demonstrates the electrochemical oxidation of the electrode results in potential dependent changes, an expected result for a permanent

chemical alteration of the surface. In addition, this result demonstrates that a linear compensation for the initial background drift is inappropriate.

After the initial cycling at 60 Hz to achieve electrochemical conditioning, the triangular potential was applied at a repetition frequency of 10 Hz while the electrode was held at the cathodic limit between scans (Cheer et al., 2005). This waveform is used for dopamine detection. In the time between scans dopamine adsorbs to the electrode surface and pre-concentrates resulting in the high sensitivity (Bath et al., 2000). In contrast to the initial conditioning at 60Hz, the change in background signal during 10 Hz cycling is more uniform over the 30 minute observation period. The relative changes in the currents at 0.2 V and at 0.6 V are superimposable. After a steep initial increase when the 10 Hz repetition frequency is initiated, the drift at both potential levels off to a linear increase with a slope of 1.5% signal change per minute. Therefore, we suggest waiting for 15 minutes until the linear region of the background change is reached before data is collected.

During this conditioning period the main change in the background is an increase in anodic current around the potential of 0.4V vs. Ag/AgCl. Additionally, both anodic and cathodic currents decrease at around -0.2V vs. Ag/AgCl. Overall, however, the changes in background are more modest than during the 60 Hz cycling period. These differences in background changes observed at the two repetition frequencies correlate with the difference in the average potential applied to the electrode with varying repetition rates of the -0.4 V to 1.3 V triangular wave at 400 V/s. When this waveform is repeated at 60 Hz, the

average potential applied to the electrode is 33 mV vs. Ag/AgCl, while the average potential for a 10 Hz repetition frequency is -328 mV vs. Ag/AgCl. Thus, on average, the electrode is held at a much more positive potential with the 60 Hz repetition rate allowing for greater formation of surface oxide groups. At the less frequent repetition rate less oxidation of the electrode occurs so the background becomes more stable.

Background changes at carbon fiber microelectrodes *in-vivo*

The experiment in figure 6.2 was repeated *in vivo* in the cortex of anesthetized rats to examine whether brain tissue could affect the background changes. During the initial application of the triangular waveform at a repetition frequency of 60 Hz the background changes were similar to those *in vitro* (compare Figure 6.3, top panel, with Figure 6.2, top panel). The shape of the cyclic voltammograms that arise from the background changes during this conditioning period are virtually identical *in vivo* and *in vitro,* although the time course of the background changes seems slightly slower is *in vivo.* In the second conditioning interval with cycling at 10 Hz, the changes in background current obtained *in vivo* differ significantly from those obtained *in vitro*. A decrease in the oxidative current around 0.2V occurs indicating diminished surface oxides. The differences in background changes obtained *in vivo* and *in vitro* application are likely due to the different chemical environments. The buffer used for *in vitro* experiments mimics the ionic environment of the cerebral spinal fluids but does not include any of the electroactive substances present in the

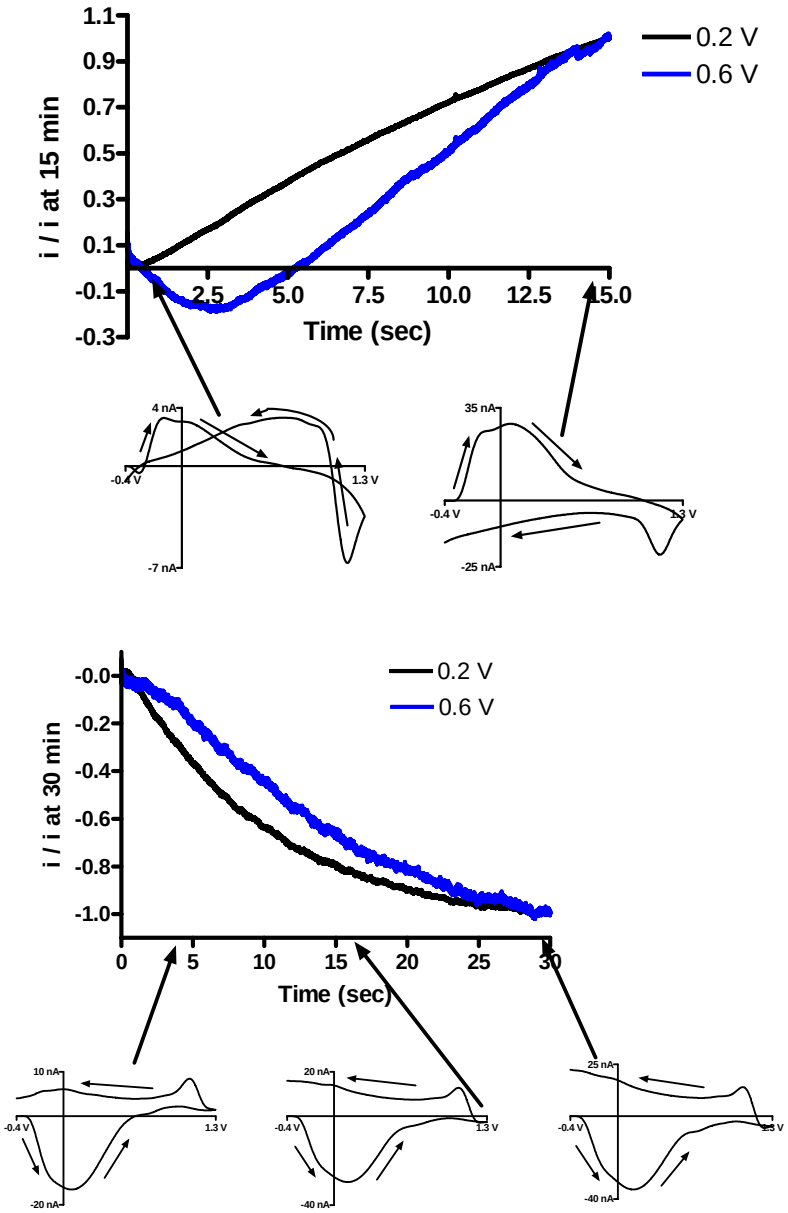

Figure 6.3. Changes in background signal at carbon fiber microelectrodes *in vivo (cortex)*. Top panel. Carbon fiber microelectrodes were cycled for 15 minutes at a repetition frequency of 60 Hz. Bottom panel. Following conditioning for 15 minutes at a repetition frequency of 60 Hz electrodes were cycled for 30 minutes at a repetition of 10 Hz. The background signal was subtracted before measurements were taken. The current for background change at 0.2 V vs. Ag/AgCl and 0.6 V vs. Ag/AgCl at the anodic sweep were normalized to the current at each respective potential at the end of the experiment and plotted vs. time. (average response n=4 electrodes) Representative cyclic voltammograms for background change are shown at different time points.

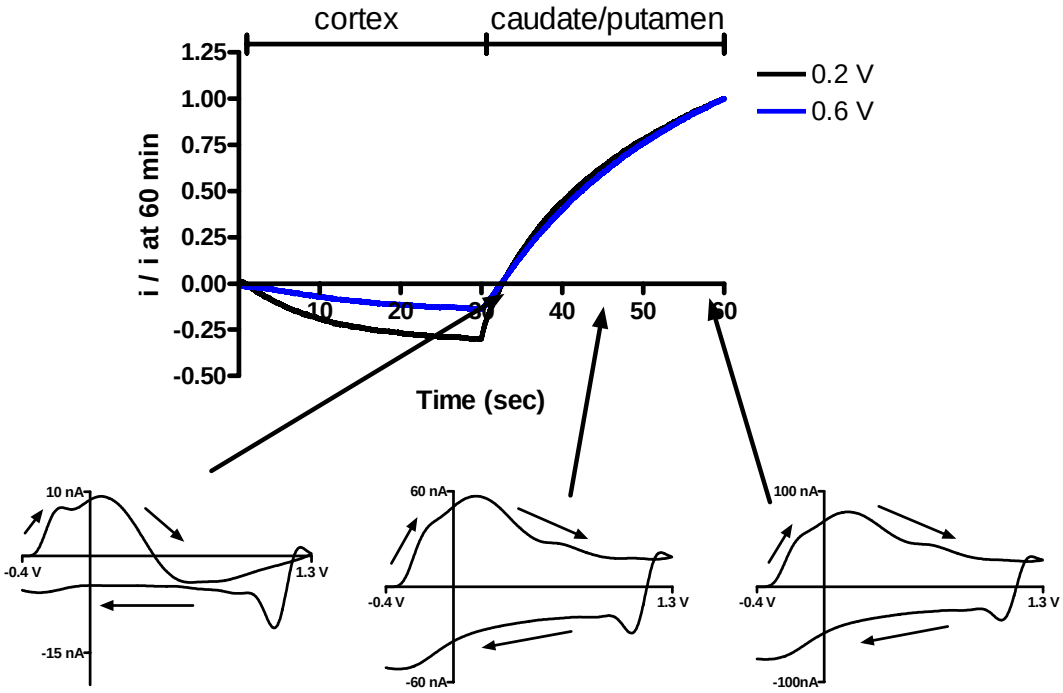

Figure 6.4. Background changes in caudate/putamen. Carbon fiber microelectrodes were cycled for 15 minutes at a repetition frequency of 60Hz before conditioning for 30 minutes at a repetition of 10 Hz in the cortex. The background signal was subtracted and the electrode was lowered in into the caudate/putamen. The current for background change at 0.2 V vs. Ag/AgCl and 0.6 V vs. Ag/AgCl at the anodic sweep were normalized to the current at each respective potential at the end of the experiment and plotted vs. time (average response n=4 electrodes). Representative cyclic voltammograms for background change after lowering the electrodes are shown at different time points .

brain such as ascorbic acid or glutathione that could react with surface functional groups. In addition, the *in vitro* experiment does not include proteins that can absorb to the electrode surface, changing the background signal. Furthermore, the oxygen level of the *in vitro* buffer and the extracellular fluid of the brain differ.

The time course in figure 6.3, lower panel, shows that the changes in background current are relatively stable during the last 15 minutes of cycling at 10 Hz. The current changes linearly with a slope of 1.1% signal change per minute at 0.2 V and 2.8% signal change per minute at 0.6 V during the during the last 5 minutes. At the end of this equilibration period in the cortex, the background signal was subtracted again and the electrode was lowered into the caudate/putamen of the rat. Lowering the electrode into the caudate-putamen caused a dramatic increase in the background (Figure 6.4). There was a large increase in the oxidation current at about 0.2 V that resembled the background changes observed during the initial 60 Hz cycling. Additionally an overall increase in capacitance of the electrode as well as the emergence of a small oxidative current peak at 0.6 V was observed. The latter feature occurs where dopamine adsorbs suggesting that the presence of dopamine in the caudate-putamen may be responsible for altering the background response.

Dopamine induced background changes

To investigate whether extracellular dopamine in the caudate/putamen could affect the background, experiments were conducted in physiological buffer into which small concentrations of dopamine were purposely added. First,

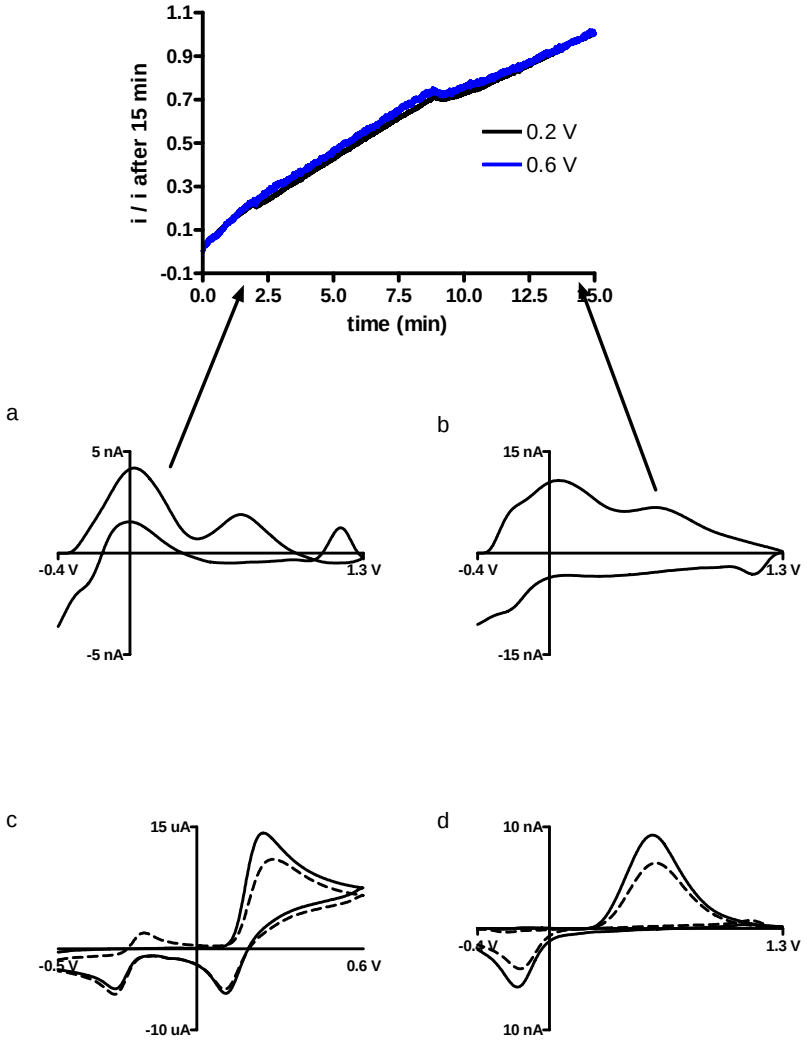

Figure 6.5. Dopamine induced background changes *in vitro*. Carbon fiber microelectrodes were cycled for 15 minutes at a repetition frequency of 60 Hz before conditioning for 30 minutes at a repetition of 10 Hz. The background signal was subtracted and the electrode was 100 nM dopamine was introduced into the background solution. The current for background change at 0.2 V vs. Ag/AgCl and 0.6 V vs. Ag/AgCl at the anodic sweep were normalized to the current at each respective potential at the end of the experiment and plotted vs. time (average response n=3 electrodes) Panel a,b. Background change 2and 15 minutes after introduction of dopamine; Panel c. response to injection of 1 µM dopamine before (dashed line) and after (solid line) conditioning in 100 nM dopamine solution for 15 minutes; Panel d. Cyclic volatmmogram at glassy carbon electrode for 1 mM dopamine at a scan rate of 100 mV/s (first cycle: solid line, second cycle: dashed line)

electrodes were cycled for 15 minutes in physiological buffer at a repetition frequency of 60 Hz following by 30 minute cycling at 10 Hz analogous to the experiment in figures 6.2 and 6.3. We then wished to add dopamine to the physiological buffer at a concentration that mimicked the basal concentrations of dopamine in the rat caudate-putamen. However, this value is not well established. While early studies with microdialysis sampling reported 1-2 µM concentrations of basal dopamine (Lindefors et al., 1989; Benviste and Huttemeier, 1990), later studies estimated basal level concentrations of around 25 nM (Shou et al., 2006). In the present work we used 100 nM.

After the preconditioning the background signal was subtracted again and 100 nM dopamine was introduced. The oxidative current at about 0 V increased following exposure to dopamine and there was a smaller increase in oxidation current at 0.6 V occurred. The current at 0.6 V is due to dopamine oxidation. Overall, the background changes observed 15 minutes after addition of dopamine (figure 6.5b) are similar to the signal observed in the caudate/putamen (figure 6.4, middle panel). To examine if these dopamine-induced background changes influence the sensitivity of the electrode, cyclic voltammograms for 1 µM dopamine were taken before dopamine was introduced into the buffer. This response was compared with the voltammogram obtained for 1µM dopamine after 15 minutes of cycling (figure 6.5c). The average response for dopamine showed a 35% ± 15% increase in peak current after the dopamine treatment.

Polymerization of dopamine

After electrochemical oxidation catecholamines such as dopamine undergo secondary reactions (Adams, 1969; Lane and Hubbard, 1976). The most important secondary reaction is the intracyclization of the orthoquinone to the 5-6 dihydroxyindoline. A slow scan cyclic voltammogram of dopamine, which shows the formation of 5-6 dihydroxyindoline, is shown in figure 6.5d. The 5-6 dihydroxyindoline is more easily oxidized than dopamine to produce an aminochrome, which is known to readily polymerize to melanin-like products as shown in previous research (Lane and Hubbard, 1976). These early studies reported a poisoning of the electrode surface by formation of the melanin layer at platinum electrodes. Polymer films created by dopamine polymerization on gold electrodes have been used for capacitive sensing of dopamine via molecular imprinting within the film (Liu et al., 2006). However, recent research showed that melanin layers on glassy carbon electrodes formed from L-dopa (Rubianes and Rivas, 2001; Gonzalez et al., 2004) or directly from dopamine (Chang et al., 2006) via electrochemical polymerization increase sensitivity and selectivity for dopamine. Polymerization of dopamine on gold electrodes showed similar effects (Li et al., 2006) of cationic selectivity within the polymer film. In all of these studies (Rubianes and Rivas, 2001; Gonzalez et al., 2004; Chang et al., 2006; Li et al., 2006) the melanin layer was found to exclude ascorbic acid while retaining or increasing the electrochemical activity for dopamine. These layers have been created using millimolar concentration of the monoamine monomer.

The formation of a melanin like polymer on the electrode surface is most likely responsible for the background changes and the increased sensitivity to dopamine seen in both *in-vitro* and *in-vivo* experiments in this present study. Melanin is naturally formed within the human brain causing the dark coloring of the substantia nigra. It has been reported that 95% of the neurons in the this brain region contain melanin-like species (Gibb, 1992). Although QCM measurements of the formation of melanin from dopamine at gold electrodes reported that no mass change was detected at monomer concentrations below (Li et al., 2006), this study showed visible effects with dopamine concentration in the nanomolar range.

Even though the formation of 5-6 dihydroxyindoline is kinetically slow and therefore not directly observed in the cyclic voltammogram for dopamine when fast scan rates are applied (figure 6.1d), it is plausible that 5-6 dihydroxyindoline slowly forms from dopamine orthoquinone on the electrode surface over time. One indication for the presence of 5-6 dihydroxyindoline is the voltammogram obtained 2 minutes after introduction of dopamine into the background buffer (figure 6.5a). This voltammogram shows peaks in the negative potential region that can be attributed to the redox reaction of 5-6 dihydroxyindoline to the aminochrome. Formation of a melanin like polymer is also in agreement with the increase in capacitance of the electrode (figure 5.5 and 6.5b). Although the results in this study do not provide a direct proof of polymerization of dopamine at the electrode surface at high scan rates, the cyclic voltammograms of the background changes give strong evidence for the formation of a melanin type

structure on the electrode surface. Because of the similarities to the results between the *in-vitro* and *in-vivo* experiments we can assume that a similar process also occurs when the electrode is lowered into the caudate/putamen.

Summary

In this study we demonstrate that carbon microelectrodes used with fast scan cyclic voltammetry can undergo two different types of activation: Electrochemical activation and activation in brain tissue. These activations were monitored by measuring the changes in the background signals obtained with fast-scan cyclic voltammetry. Triangular excursions to 1.3V vs. Ag/AgCl caused an increase in oxidative current around the potential region between 0 V and 0.2V vs. Ag/AgCl resulting from formation of surface oxide groups. This electrochemical activation was necessary for hydrogen terminated PPF electrodes in order to detect dopamine. Electrochemical activation of carbon fibers was conducted in the cortex resulting in similar changes for the background current compared to changes *in-vitro*. Lowering electrodes after electrochemical activation into the caudate/putamen caused large background drift. These drifts were mimicked *in-vitro* by addition of dopamine to the background solution. We hypothesize that the background drift is caused by polymerization of dopamine to a melanin like structure. The presence of this layer also enhances sensitivity to dopamine and could explain previous observations which reported activation of electrodes after treatment with brain tissue.

REFERENCES

Adams RN (1969) Anodic Oxidation Pathways of Aromatic Hydrocarbons and Amines. Accounts of Chemical Research 2:175-&.

Bard AJ, Faulkner LR (2001) In: Electrochemical Methods, 2nd Ed., p 18. New York: Wiley.

Bath BD, Michael DJ, Trafton BJ, Joseph JD, Runnels PL, Wightman RM (2000) Subsecond adsorption and desorption of dopamine at carbon-fiber microelectrodes. Anal Chem 72:5994-6002.

Baur JE, Kristensen EW, May LJ, Wiedemann DJ, Wightman RM (1988) Fast-scan voltammetry of biogenic amines. Analytical Chemistry 60:1268-1272.

Benviste H, Huttemeier PC (1990) Microdialysis - Theory and Application. Prog Neurobiol 33:195-215.

Blaha CD, Jung ME (1991) Electrochemical Evaluation of Stearate-Modified Graphite Paste Electrodes - Selective Detection of Dopamine Is Maintained after Exposure to Brain-Tissue. Journal of Electroanalytical Chemistry 310:317-334.

Borland LM, Shi GY, Yang H, Michael AC (2005) Voltammetric study of extracellular dopamine near microdialysis probes acutely implanted in the striatum of the anesthetized rat. Journal of Neuroscience Methods 146:149-158.

Cahill PS, Walker QD, Finnegan JM, Mickelson GE, Travis ER, Wightman RM (1996) Microelectrodes for the measurement of catecholamines in biological systems. Analytical Chemistry 68:3180-3186.

Chang HY, Kim D, Park YC (2006) Electrochemically degraded dopamine film for the determination of dopamine. Electroanalysis 18:1578-1583.

Cheer JF, Heien MLAV, Garris PA, Carelli RM, Wightman RM (2005) Simultaneous dopamine and single-unit recordings reveal accumbens GABAergic responses: Implications for intracranial self-stimulation. Proceedings of the National Academy of Sciences of the United States of America 102:19150-19155.

Chen P, McCreery RL (1996) Control of electron transfer kinetics at glassy carbon electrodes by specific surface modification. Analytical Chemistry 68:3958-3965.

Cragg SJ, Hille CJ, Greenfield SA (2000) Dopamine release and uptake dynamics within nonhuman primate striatum in vitro. Journal of Neuroscience 20:8209-8217.

Fagan DT, Hu IF, Kuwana T (1985) Vacuum Heat-Treatment for Activation of Glassy-Carbon Electrodes. Analytical Chemistry 57:2759-2763.

Gerhardt GA, Oke AF, Nagy G, Moghaddam B, Adams RN (1984) Nafion-Coated Electrodes with High Selectivity for Cns Electrochemistry. Brain Research 290:390-395.

Gibb WRG (1992) Melanin, Tyrosine-Hydroxylase, Calbindin and Substance-P in the Human Midbrain and Substantia-Nigra in Relation to Nigrostriatal Projections and Differential Neuronal Susceptibility in Parkinsons-Disease. Brain Research 581:283-291.

Gonon F, Buda M, Cespuglio R, Jouvet M, Pujol JF (1980) Invivo Electrochemical Detection of Catechols in the Neostriatum of Anesthetized Rats - Dopamine or Dopac. Nature 286:902-904.

Gonon FG, Fombarlet CM, Buda MJ, Pujol JF (1981) Electrochemical Treatment of Pyrolytic Carbon-Fiber Electrodes. Analytical Chemistry 53:1386-1389.

Gonzalez R, Sanchez A, Chicharro M, Rubianes MD, Rivas GA (2004) Dopamine and glucose sensors based on glassy carbon electrodes modified with melanic polymers. Electroanalysis 16:1244-1253.

Heien MLAV, Phillips PEM, Stuber GD, Seipel AT, Wightman RM (2003) Overoxidation of carbon-fiber microelectrodes enhances dopamine adsorption and increases sensitivity. Analyst 128:1413-1419.

Hermans A, Wightman RM (2006) Conical tungsten tips as substrates for the preparation of ultramicroelectrodes. Langmuir 22:10348-10353.

Hsueh C, Bravo R, Jaramillo AJ, BrajterToth A (1997) Surface and kinetic enhancement of selectivity and sensitivity in analysis with fast scan voltammetry at scan rates above 1000 V/s. Analytica Chimica Acta 349:67-76.

Kawagoe KT, Zimmerman JB, Wightman RM (1993) Principles of voltammetry and microelectrode surface states. Journal of neuroscience methods 48:225-240.

Khan AS, Michael AC (2003) Invasive consequences of using micro-electrodes and microdialysis probes in the brain. Trac-Trends in Analytical Chemistry 22:503-508.

Lane RF, Hubbard AT (1976) Differential Double Pulse Voltammetry at Chemically Modified Platinum-Electrodes for Invivo Determination of Catecholamines. Analytical Chemistry 48:1287-1293.

Li YL, Liu ML, Xiang CH, Xie QJ, Yao SZ (2006) Electrochemical quartz crystal microbalance study on growth and property of the polymer deposit at gold electrodes during oxidation of dopamine in aqueous solutions. Thin Solid Films 497:270-278.

Lindefors N, Amberg G, Ungerstedt U (1989) Intracerebral Microdialysis .1. Experimental Studies of Diffusion Kinetics. Journal of Pharmacological Methods 22:141-156.

Liu K, Wei WZ, Zeng JX, Liu XY, Gao YP (2006) Application of a novel electrosynthesized polydopamine-imprinted film to the capacitive sensing of nicotine. Analytical and Bioanalytical Chemistry 385:724-729.

Michael DJ, Joseph JD, Kilpatrick MR, Travis ER, Wightman RM (1999) Improving data acquisition for fast scan cyclic voltammetry. Analytical Chemistry 71:3941-3947.

Ormonde DE, Oneill RD (1989) Altered Response of Carbon Paste Electrodes after Contact with Brain-Tissue - Implications for Modified Electrode Use Invivo. Journal of Electroanalytical Chemistry 261:463-469.

Paxinos W, Watson C (1998) The Rat Brain in stereotaxic coordiantes. Academic Press, Orlando, Florida.

Peters JL, Miner LH, Michael AC, Sesack SR (2004) Ultrastructure at carbon fiber microelectrode implantation sites after acute voltammetric measurements in the striatum of anesthetized rats. Journal of Neuroscience Methods 137:9-23.

Pihel K, Walker QD, Wightman RM (1996) Overoxidized polypyrrole-coated carbon fiber microelectrodes for dopamine measurements with fast-scan cyclic voltammetry. Analytical chemistry 68:2084-2089.

Ranganathan S, McCreery RL (2001) Electroanalytical performance of carbon films with near-atomic flatness. Anal Chem 73:893-900.

Ranganathan S, McCreery R, Majji SM, Madou M (2000) Photoresist-derived carbon for microelectromechanical systems and electrochemical applications. Journal of the Electrochemical Society 147:277-282.

Robinson DL, Venton BJ, Heien ML, Wightman RM (2003) Detecting subsecond dopamine release with fast-scan cyclic voltammetry in vivo. Clin Chem 49:1763-1773.

Rubianes MD, Rivas GA (2001) Highly selective dopamine quantification using a glassy carbon electrode modified with a melanin-type polymer. Analytica Chimica Acta 440:99-108.

Runnels PL, Joseph JD, Logman MJ, Wightman RM (1999) Effect of pH and Surface Functionalities on the Cyclic Voltammetric Responses of Carbon-Fiber Microelectrodes. Analytical Chemistry 71:2782-2789.

Shou MS, Ferrario CR, Schultz KN, Robinson TE, Kennedy RT (2006) Monitoring dopamine in vivo by microdialysis sampling and on-line CE-laser-induced fluorescence. Analytical Chemistry 78:6717-6725.

Strein TG, Ximba BJ, Hamad AH (1999) Steady-state voltammetry of catechol and guaiacol analogues at carbon fiber microdisk electrodes following laser and electrochemical activation procedures. Electroanalysis 11:37-46.

Swain GM, Kuwana T (1991) Electrochemical Formation of High Surface-Area Carbon-Fibers. Analytical Chemistry 63:517-519.

Swamy BEK, Venton BJ (2007) Subsecond detection of physiological adenosine concentrations using fast-scan cyclic voltammetry. Analytical Chemistry 79:744-750.

Venton BJ, Wightman RM (2003) Psychoanalytical electrochemistry: dopamine and behavior. Anal Chem 75:414A-421A.

Wightman RM (2006) Probing cellular chemistry in biological systems with microelectrodes. Science 311:1570-1574.

Witkowski A, Brajter-Toth A (1992) Overoxidized polypyrrole films: a model for the design of permselective electrodes. Anal Chem 64:635-641.

CHAPTER 7

ELECTROCHEMICAL MEASUREMENT OF PH SHIFTS AND DOPAMINE RELEASE IN PRIMATES DURING REWARD DELIVERY

Introduction

In recent years many studies have been conducted to examine neurophysiological and neurochemical phenomena during prediction and delivery of reward. The most common techniques to examine brain activity during reward delivery are electrophysiological studies, fMRI measurements, and electrochemical recordings. While electrophysiological data can give direct information about the neuronal activity, the biological meaning of the signal obtained with fMRI has been discussed greatly. Changes in cerebral blood flow are at the heart of brain imaging signals (Raichle and Mintun, 2006). With blood oxygen dependent (BOLD) fMRI it is possible to directly monitor the oxygen dissociation from hemoglobin (Ogawa et al., 1990). Electrochemical recordings are able to give information about changes in neurotransmitter concentrations(Cahill et al., 1996) as well as local changes in oxygen concentrations (Venton et al., 2003a) and pH (Runnels et al., 1999). Electrophysiological and electrochemical recordings both use implanted microelectrodes so they are invasive techniques. However, they provide micrometer spatial and subsecond temporal resolution. Neuroimaging techniques such as fMRI

are advantageous because they are noninvasive and can be used in humans. However, voxel sizes for fMRI techniques are normally on the order of 1 mm^3 (Hyde et al., 2001) with time resolutions of a few seconds (Kim et al., 1997).

Electrophysiological studies in primates have shown that midbrain dopamine neurons in the ventral tegmental area (VTA) and their projections to the to the ventral striatum burst fire during reward delivery (Schultz, 2002). After reward-based classical conditioning VTA dopamine neurons fire in response to cues that predict reward (Schultz, 1998) and during anticipation of reward (Fiorillo et al., 2003). The actual value of a reward is influenced by its magnitude, probability, and timing (immediate or delayed). VTA dopaminergic neurons have the ability to encode for the probably of the reward as well as for the value of the reward delivered (Tobler et al., 2005). Similar observations have been made with fMRI measurements that have shown activation of the nucleus accumbens of humans with different reward magnitudes (Knutson et al., 2001a; Knutson et al., 2001b). Electrochemical studies with fast-scan cyclic voltammetry in rats have detected phasic increases in dopamine concentration during operant responding for drugs of addiction (Phillips et al., 2003) like cocaine as well as for natural rewards (Roitman et al., 2004).

Successful voltammetric recordings in primate brain tissue have only been reported from brain slices (Cragg et al., 2000; Cragg, 2003). In this study we used specially designed carbon fiber microelectrodes to record pH-shifts and changes in dopamine concentration in behaving primates with fast-scan cyclic voltammetry. Recordings were conducted during delivery of an unpredicted free reward and

during the delivery of reward following a reward-predicting cue which was associated with 3 different reward probabilities.

EXPERIMENTAL SECTION

Chemicals

All chemicals were purchased from Sigma-Aldrich (St. Louis, MO) and used as received. Solutions were prepared using doubly distilled water (Megapure system, Corning, New York). For flow injection experiments phosphate buffered saline (150 nM NaCl, 10 mM Na_2HPO_4, 1.2 mM $CaCl_2$) was used. Stock solutions of dopamine were prepared in 0.1 M HCl, and were diluted to the desired concentration with PBS-buffer on the day of use. 4-sulfobenzenediazonuim tetrafluoroborate was synthesized as previously described(Hermans et al., 2006).

Electrode preparation

The carbon-fiber microelectrodes were fabricated from two different types of carbon fibers: 12 µm diameter carbon fibers (Thornel P55, Amoco, Greenville, SC) and 33 µm diameter carbon fibers (Textron Systems Division, Wilmington, MA). The carbon fibers were supported on tungsten wires. The tips of tungsten wires (125 µm diameter, 15 cm length, Advent research Materials, Oxford, England) were etched to a conical tip in a 1.0 M NaOH solution that was saturated with $NaSO_2$. The etched tips were cleaned, using electrocleaning solution (Grobet USA, Carlstadt, NJ) (Hermans and Wightman, 2006). Carbon-fibers were attached along the whole length of the tungsten wire with conductive silver epoxy (Epo-tek, Billerica, MA)

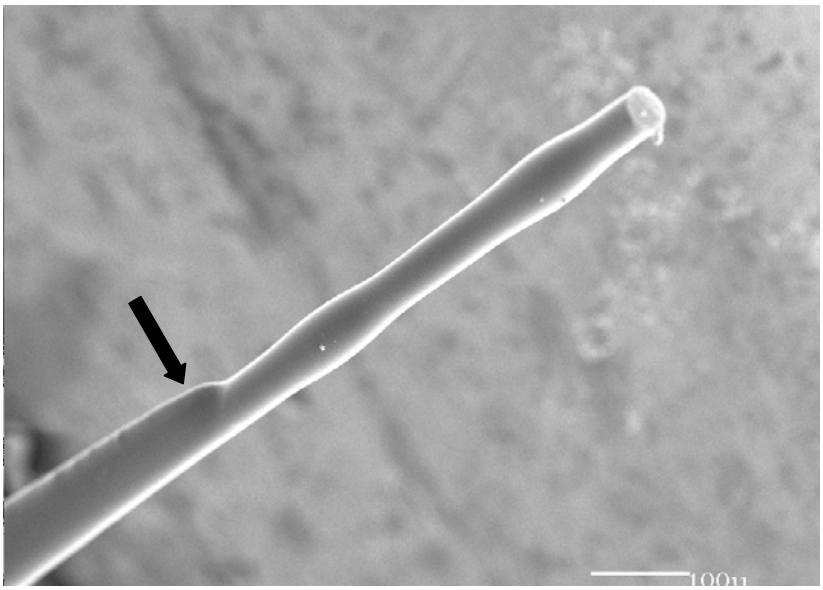

Figure 7.1. SEM image of electrodes for primate recordings. SEM image of **a** 33 µm carbon fiber attached to an etched tungsten wire encased in a glass capillary. The arrow indicates the joint between tungsten wire and the carbon fibers

extending from the tip of the tungsten wire. After the epoxy was cured, the assembly was inserted into a glass capillary and pulled in a horizontal electrode puller (Narishige, East Meadow, NY). During the pulling the end of the capillary that contained the etched tungsten was mounted in a stationary holder while the other end was attached to a movable holder. After the heating element reached a temperature sufficient to soften the glass, the movable end was slowly pulled resulting in a very thin (~5µm) flexible glass-insulating layer over the whole length of the tungsten wire with attached carbon fiber. After inspection under a microscope to ensure a smooth transition of the glass over the tip of the tungsten wire and the carbon fiber, the carbon fiber and the glass were cut with a scalpel blade approximately 250 µm from the end of the tungsten tip. The electrode was then further insulated by dipping it into epoxylite insulation (The Epoxylite Corporation, St. Louis) at 40°C for 1 minute (Verhagen et al., 2003) and then slowly withdrawn. The electrodes were cured for 8 hours at 80°C.

Following curing, the electrodes were polished at a 25° angle on a micropipette beveller (Sutter instrument, Novato, CA). The electrodes were then cycled in PBS buffer from -0.4V to 1.3 V vs. Ag/AgCl for several minutes and the background current was examined to ensure that the electrodes were well insulated. In addition, this pretreatment activates the electrode(Heien et al., 2003).

Following the electrochemical pretreatment, P-55 microelectrodes were coated with 4-sulfobenzene following procedures described elsewhere (Hermans et al., 2006). A potential of -1V Vs Ag/AgCl was applied to the electrode for 5 minutes in a 3 mM solution of 4-sulfobenzenediazonium tetrafluoroborate dissolved in 0.1 M

HCl. Electrodes manufactured from 33 µm diameter fiber did not undergo this treatment. Both electrode types were then dip-coated with Nafion as described previously (Kawagoe et al., 1993). An example SEM image of the electrode polished at a 90° angle is displayed in figure 7.1.

Flow-injection apparatus

Before use in the brain, the response for each electrode to dopamine was tested in a flow cell experiment. For flow–injection analysis the electrode was positioned at the outlet of a 6-port rotary valve (Rheodyne model 5041 valve). The solution flow rate was approximately 2 ml/s and was driven by gravity. The analyte was loaded into an injection loop and pushed to the surface of the electrode following manual switching of the 6-pot valve.

Data acquisition and analysis

Fast-scan cyclic voltammograms were acquired and analyzed using locally constructed hardware and software written in LabVIEW (National Instruments, Austin, TX) that has been described previously (Michael et al., 1999; Heien et al., 2003). The rest potential was -0.6V or -0.4 V vs. Ag/AgCl. Triangular excursions were to values between 1.0 V and 1.4V at a scan rate of 400 V/s. The waveform was repeated at a frequency of 10 Hz. The recorded signal was filtered at 10 kHz before being digitized. The behavior was synchronized to the voltammetric recordings by measuring TTL pulses at the onset of each event in the behavioral sequence.

Color representations were used to visualize the data(Michael et al., 1998) with the applied potential as ordinate and time as abscissa. The current is represented on a non-linear color scale to visualize the changes in current. Cyclic voltammograms were sorted according to specific recording locations and then background subtraction and signal averaging was performed.

In vivo recordings

In vivo experiments were performed in collaboration with Wolfram Schultz and coworkers in Cambridge, England. The basic experimental design and the individual animals in this are similar to experiments reported previously (Tobler et al., 2003; Tobler et al., 2005). Recordings were made in two Macaca mulatta monkeys that were mildly fluid deprived. The reward was a sweetened liquid delivered by a computer controlled liquid valve through a spout at the animal's mouth in fixed quantities of around 0.2 ml. Licking behavior was monitored by tongue interruptions of an infrared photobeam 4 mm below the spout. Licking histograms were constructed by aligning the data around the time of the reward presentation. The DIO outputs for each file were then added to obtain the histogram. Data was collected from 2 animals. Recordings were conducted in 67 striatal regions in animal 1 and in 46 striatal locations in animal 2. The recording locations were confirmed by histological examination of stereotaxically oriented coronal brain sections for animal 1. Therefore, we mainly focussed the analysis in this study on this animal 1. In each location approximately 90 single trials were performed, resulting in around 30 trials for each given probability. Given this number for each

location only 1 or 2 rewarded 5% trials and 1 or 2 non-rewarded 95% trials were recorded.

Presentation of free reward

Unpredicted reward was delivered in a set of 15 consecutive trials. The time between each reward delivery was variable but averaged 9 s, and consisted of 4 seconds plus an exponentially distributed interval with a mean of 5 s. The time between each set of trials was at least 30 minutes. The free reward trial was performed at all of the 113 recording locations after successful completion of the 90 predicted reward trials. Each session consisted of 15 free rewards per recording location. For later analysis, the 15 responses at each location were averaged around the time of reward delivery.

Presentation of predictable reward

In a second type of experiment the animals were trained in a pavlovian training procedure to distinguish different visual stimuli that coded the probability of subsequent reward delivery. Three different visual cues encoded for a 5%, 50% or 95% probability. The temporal sequence for the behavioral task is outlined in figure 7.2. At the beginning of the trial a center-fixation spot was shown on the computer screen. The monkey had been trained to focus on the center of the video screen in response to this cue. His eye movement to this cue was monitored by a separate camera. At the appearance of the center-fixation spot the monkey was supposed to initiate movement of its hand towards a keytouch within 500 ms. The cue indicating

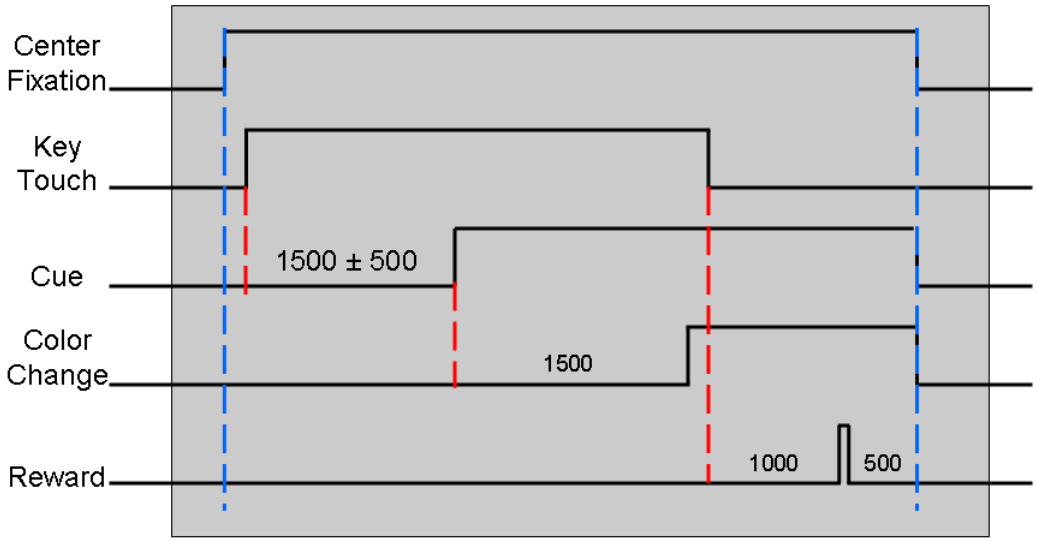

Figure 7.2. Timing diagram of the behavioral tasks performed by monkeys during predicted reward delivery. The center-fixation spot marks the beginning of each trial and indicates that the monkey should touch a key touch within the next 500 ms. If the key touch is not performed the trial is aborted. After a variable interval a cue is presented which encodes three different reward probabilities (5%, 50% and 95%). 1.5 seconds later the color of the center fixation spot changes initiation the release of the key touch. If the trial is a rewarded trial, the reward is given to the monkey. The next trial is initiated 3.5 ± 0.5 s after completion of a trial. Times on the diagram are in s.

the probability of reward appeared between 1.5 and 2 s after the keytouch. Another 1.5 s later the color of the center fixation spot changed, prompting the monkey to release the key touch. The reward delivery was initiated 1 s after the key was released. The screen was turned blank 500 ms after the reward was delivered and the next trial was initiated 3.5 ± 0.5 s later. This procedure was continued for 90 trials.

RESULTS

Responses to pH changes at carbon fiber microelectrodes

Background subtracted fast-scan cyclic voltammetry is responsive to changes in pH (Runnels et al., 1999). A representative signal for a basic pH-changes recorded in vitro at the electrodes used for these studies can be seen in figure 7.3. This cyclic voltammogram is similar to the voltammograms reported previously for pH changes with the same scan parameters (Heien et al., 2003). Similar signals for pH changes have been measured *in vivo* following electrical stimulation of dopamine neurons (Venton et al., 2003a) and after drug administration (Heien et al., 2005).

pH changes in vivo during delivery of free reward

Figure 7.4a shows a representative color plot that is the average of 15 trials obtained during free reward presentation at animal 1. The response is centered on the reward presentation that occurs at the 0 s time stamp. The background signal was taken from averaged scans 1.5 to 0.5 s before the reward was presented. The

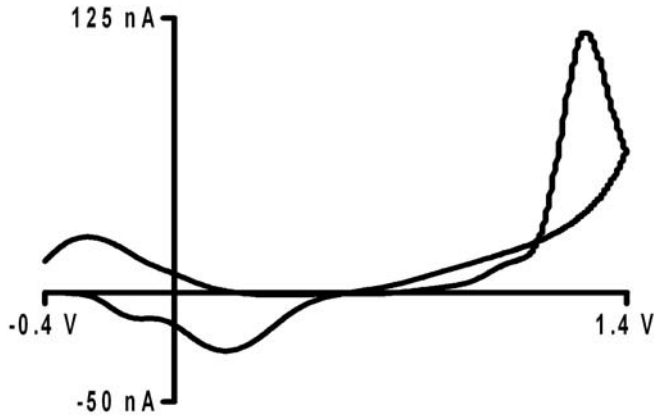

Figure 7.3. Cyclic voltammetric response to a basic pH change *in vitro.*
Background subtracted cyclic voltammogram for an approximate 2 pH unit change in the basic direction obtained in a flow cell experiment

pH trace shown in figure 7.4b represents relative pH changes. Absolute values could not be determined, because a post-calibration for the electrodes was not conducted. Reward delivery is preceded by a basic pH shift in the extracellular fluid and it is followed by an acidic pH shift shortly thereafter. This shift lasts for about 5 s. Figure 7.4c shows an averaged cyclic voltammogram obtained at the maximum basic pH shift. This shape of this cyclic voltammogram agrees with one recorded during an authentic basic pH shift measured *in vitro* (Hermans et al., 2006, figure3) and in prior *in vivo* measurements (Heien et al., 2005) . This pattern of pH changes was observed in ~85% percent of the recordings in animal 1 during free reward in striatal brain regions. The other 15% did not show any significant pH changes associated with reward presentation. The pH traces measured in animal 2 showed similar pattern to the traces observed in animal 1 with an acidic shift after delivery of the reward in 43% of the recordings. However, in 26 locations (57% of the recordings) the voltammetric recordings could not be assigned to a pH shift. There was no correlation of the pH shifts with the spatial position of the recording electrode within the striatum. Also, a larger time delay between reward delivery and the start of the acidic pH shifts was observed in the traces recorded in animal 2 compared to animal 1.

Correlation between pH changes and behavior during delivery of free reward

To find whether there was a correlation between pH changes measured during free reward and the animals' behavior, the licking pattern was analyzed. The licking pattern can serve as an indicator of behavioral reactions and learning (Rolls

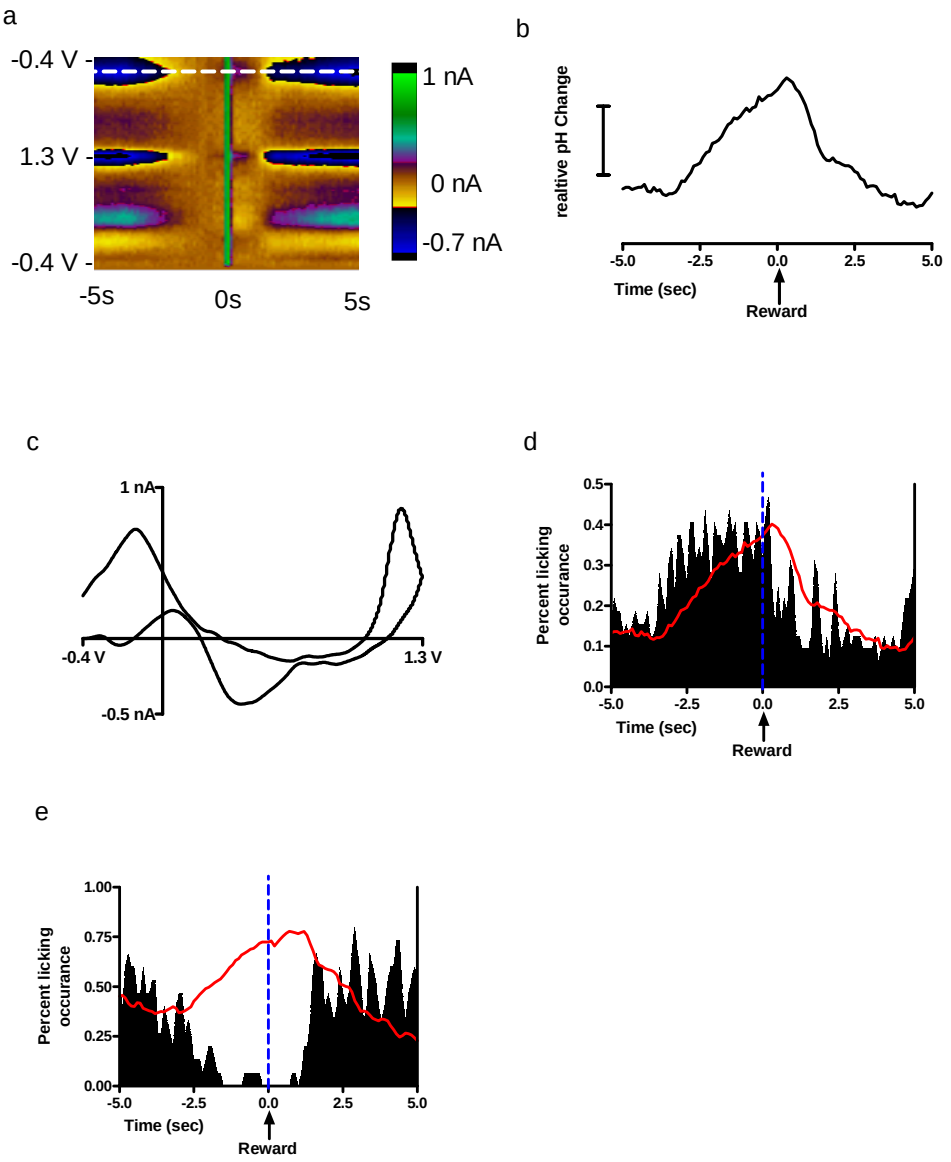

Figure 7.4. Delivery of free reward. The panels show averaged responses from 15 consecutive trials in the same location. The time between rewards averaged 9 s. Thus, the beginning and end of the recordings contain activity from the previous and subsequent trials, respectively. Panels a to d show data obtained from animal 1; Panel e shows data obtained from animal 2; a. All voltammograms shown in the form of a color plot. The horizontal line indicates the current that was used for construction of pH traces in panel b; b. Time trace for relative pH changes during delivery of free reward; c. Average cyclic voltammogram for basic pH shift obtained *in vivo*; d,e. Licking behavior of the monkey during delivery of free reward, pH trace is shown as red line (representative data from animal 1 is shown in panel d, data from animal 2 is shown in panel e)

et al., 1993; Aosaki et al., 1994). The licking histogram for animal 1 associated with the chemical changes in Figure 7.4a is shown in Figure 7.4d. The rate of licking begins to increase 3.5 s before reward delivery at which time it decreases. Immediately before the reward the licking level is approximately 30%, which means that the infrared light beam is broken 30% of the time. Licking starts to increase again relative to pre-reward levels at the beginning of the next trial. The time course of licking correlates well with the observed pH shifts. These trends in pH and licking behavior were present in 91% of all recording locations in animal 1. The remaining 9% of the files did not show a specific licking behavior time-locked to the reward.

However, licking behavior recorded for animal 2 showed a completely different pattern as indicated in figure 7.4e with an increase in licking after the reward was given. This pattern was observed in all free reward trials for this animal. As figure 7.4e indicates, licking was evoked about one second after delivery of the reward. These behavioral differences might result from a different length of behavioral training between the two animals.

pH changes during presentation of predicted reward

In contrast to free reward delivery, data obtained from animals 1and 2 show identical trends in behavior and electrochemical recordings during the tasks involving a predicted reward. The representative data shown in study was recorded with animal 1. To examine pH changes at different times during the predicted-reward task (Figure 7.2), the voltammetric data were averaged around each of the

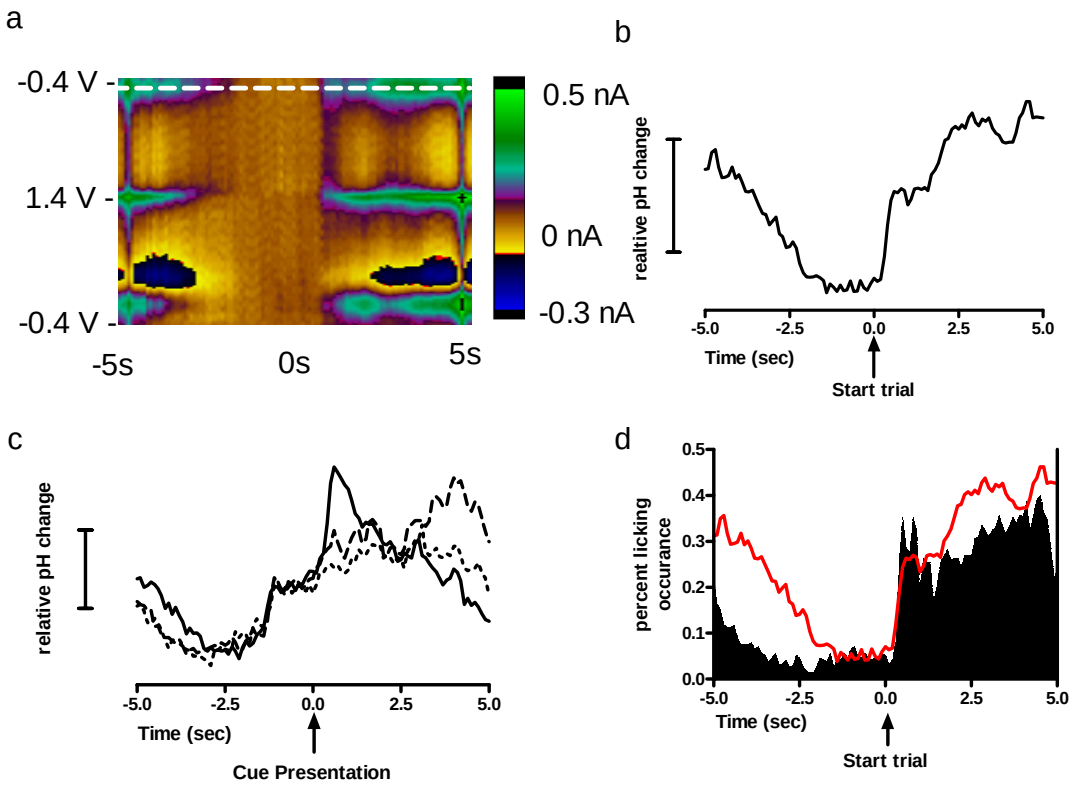

Figure 7.5. Delivery of predicted reward. Panels a and b show an averaged response from ~90 consecutive trials at a single location. The following trial was initiated 4 ± 0.5 s after reward delivery. In a, b, and d panels the center-fixation spot occurs at the 0 s time stamp. a. Voltammetric data in the form of a color plot. The horizontal line indicates the current that was used for construction of pH traces in panel b,c, and d. b. Time trace for relative pH changes around presentation of center fixation spot. c. Averaged time trace for relative pH changes during presentation of reward predicting cue. The time of cue presentation is at the 0 second time stamp. The traces are shown according to the probability of the reward indicated by the cue (dashed line 95%, dotted line 50%, solid line 5%, 15 trials each). d. Licking histogram centered around presentation of center fixation spot (90 trials total), red line represents the pH changes.

distinct events (appearance of the color fixation spot, presentation of the reward-predicting cue, color change of the center fixation spot, and time of reward delivery) at a single location. In addition, data from each location were sorted according to the reward probability indicated by the cue and according to the occurrence (or lack) of reward delivery.

An average color plot centered on the presentation of the center-fixation spot is shown in figure 7.5a. This plot consists of 90 trials and includes all probability trials. The center-fixation spot initiates a new trial and, because of the experimental design, indicates a probability of 50% reward delivery. The current at the potential where pH changes can be detected is shown in Figure 7.5b. A basic pH change is initiated with the presentation of the center fixation spot. This response was seen in all 113 recording locations in both animals.

Next the same pH data were separated into the reward probability of that trial and each of these 30 trials were averaged using the presentation of the reward predicting cue as the center point. For all three probabilities, the presentation of the cue occurs as the pH is shifting to basic values. However, for the 5% probability there is a sharp increase in alkalization followed by an acidification following the reward predicting cue. This trend was observed in around 35% of recording sites (39 = locations for both animals); in the remainder the pH continued to increase gradually. In the 95 % trials there was a further increase in alkalization observed after the reward that was followed by an acidification.

The pH appears to remain constant in the 50 % trials around reward delivery. However, to evaluate this further the trials following the presentation of the 50% cue

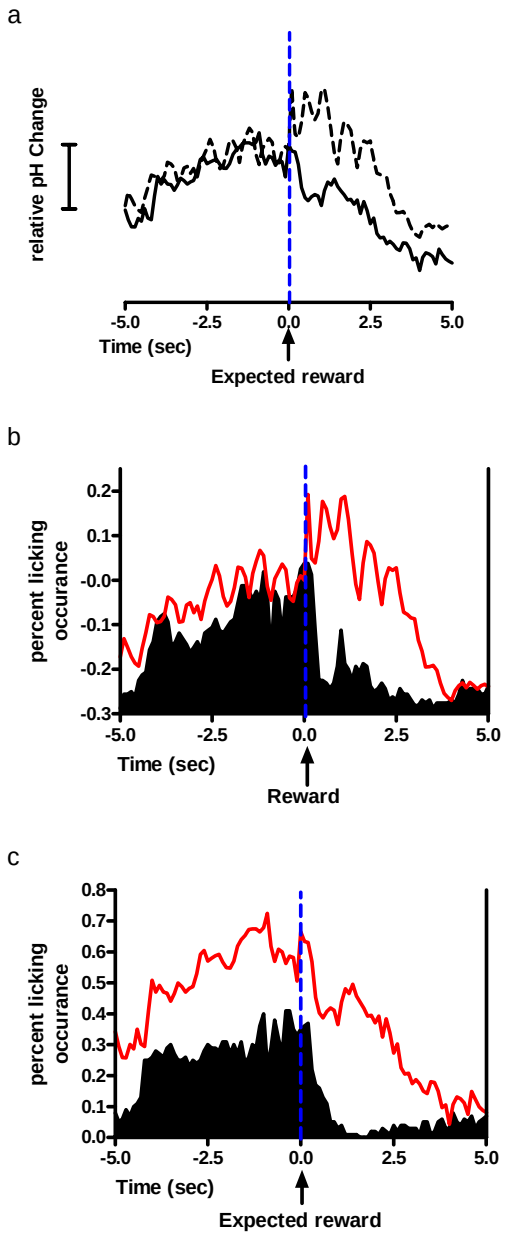

Figure 7.6. Delivery and non-delivery of predicted reward with 50% probability. Panel a. Averaged time trace for relative pH changes during time of reward delivery after presentation of 50% indicating cue. The time of reward is at the 0 second time stamp. The traces are shown according to the occurrence or non-occurrence of the reward (dashed line: rewarded trials, solid line: non- rewarded trials, 15 trials each) Panel b. Licking histogram for rewarded trials centered around presentation of reward of (15 trials total). Panel c. Licking histogram for non-rewarded trials centered around time where the reward would have been presented (15 trials total). pH traces are shown as red line

were separated into rewarded and unrewarded trials and the presentation of the reward was used as the center point for averaging (Figure 7.6a). For the rewarded trials the average shows an alkalization following reward delivery. For the unrewarded trials, an acidification occurred at the time when reward was anticipated. Very similar trends were seen in licking behavior.

Correlation between pH changes and behavior during delivery of predicted reward

Similar to the observation made during the free reward presentation, pH changes seem to correlate very well with the licking behavior of both animals. As seen during free reward delivery, basic pH shifts seem to coincide with an increase in licking. This licking increase is highly time locked to the presentation of the occurrence of the center-fixation spot (Figure 7.6d). The frequency of licks is then elevated until the time when the reward is delivered or the delivery is denied (figure 7.6 b, c). When no reward was delivered the monkey stop licking instantaneously (figure 7.6b) while in the cases when reward was given more licking occurred about one second after the delivery of the reward. These results also correlate well with the observation made at the pH changes where a further basic pH shift occurred after reward delivery.

Dopamine release during reward delivery

The large pH changes observed during both behavioral tasks are the main interfering signal for the observation of dopamine changes in all locations. In 14% of

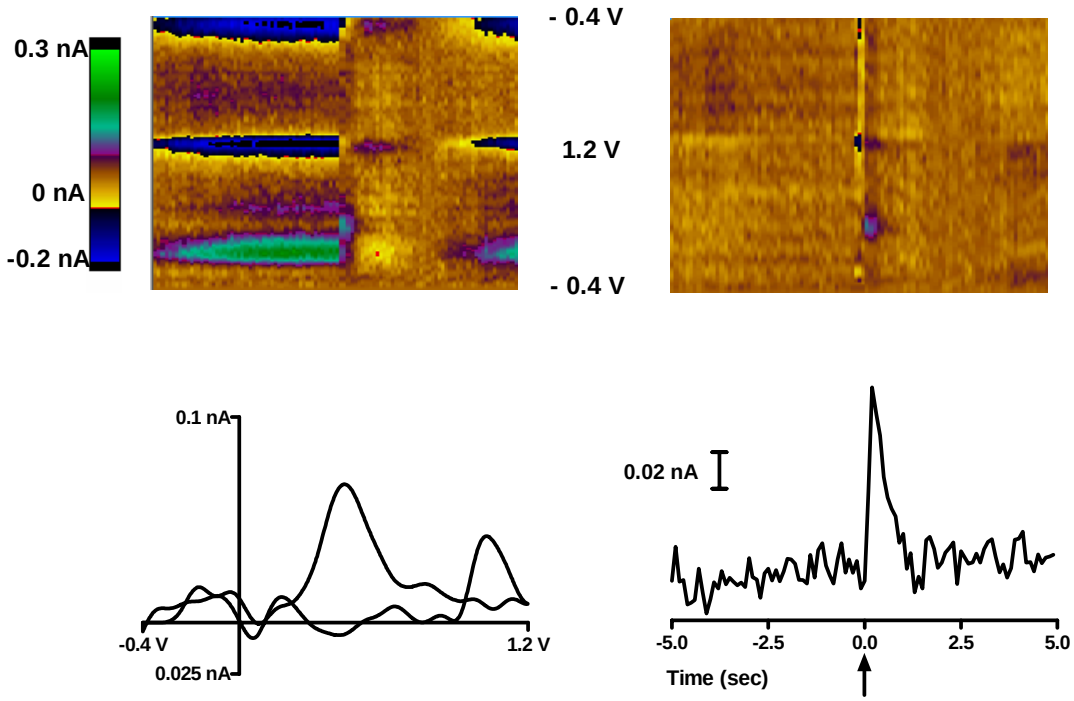

Figure 7.7. Detection of dopamine during free reward. Upper left panel. Raw color plot obtained during free reward delivery; Upper right panel. Color plot after removal of pH signal; Lower left panel. Cyclic voltammogram obtained after free reward delivery; Lower right panel. Current vs. time trace for the dopamine oxidation point

the locations a dopamine-like signal has been observed immediately after delivery of a free unpredicted reward. However, the dopamine responses were all masked by a change in pH overlapping with the signal for dopamine (top left panel figure 7.7). Principal component regression (PCR) was used to resolve the dopamine signal from the pH signal. PCR was conducted analogous to the method reported previously (Heien et al., 2004). The signal obtained for the pH shift was used as first and only principal component to perform PCR. Following PCR all non-used principal components were used to reconstruct cyclic voltammograms. A color representation of these cyclic voltammograms is shown in the top right panel of Figure 7. 7. This plot contains the signals from which the first principal component, the pH signal, was removed. An oxidative current around the oxidation potential for dopamine occurs right after delivery of the unpredicted reward. The cyclic voltammogram resembles that for dopamine at carbon-fiber electrodes (Venton and Wightman, 2003). The current at the dopamine oxidation potential shows that it exhibits a transient change immediately after reward delivery (Figure 7.7 bottom panel). The interference of pH shifts with the dopamine signal is most likely the reason that dopamine could only be observed in the minority of the recording locations. Comments about the absolute values of concentration changes are not possible, because post-calibrations of the electrodes were not conducted.

Dopamine release during delivery of predicted reward

Electrophysiological data shows that burst firing of dopaminergic neurons shifts from the time of reward presentation to the conditioned stimulus (Schultz,

1998). When the stimulus is associated with a reward probability, neuronal firing also occurs during the anticipation period following cues associated with high uncertainty (Fiorillo et al., 2003). Based on these results, dopamine release was expected after presentation of the cue indicating 95% reward probability and it was expected to gradually after presentation of the cue indicating a 50% reward probability. However, even after removal of the pH signal, changes in dopamine concentration were not observed. As figure 7.5 shows, the presentation of the reward predicting cue occurs while a steep pH-shift occurs, and this is likely to mask any underlying dopamine change. In about 10% of the trials a change in dopamine concentration was recorded at the time of delivery of an unpredicted reward (during 5% reward probability trials).

DISCUSSION

Previous studies have shown neuronal activation of dopaminergic neurons during administration of rewards with both electrophysiological measurements (Schultz, 2002) and human fMRI imaging (Berns et al., 2001). In the present study at the terminal regions of dopaminergic neurons, dopamine changes are seen in a few locations. However, the data are dominated by an acidic shift that is observed within one second after delivery of the reward, both for expected and unexpected rewards. The time traces of activity in the caudate nucleus obtained with fMRI imaging during reward delivery show an increase in signal intensity at the beginning of a trial and the presentation of a reward-predicting cue (Delgado et al., 2000; Zink

et al., 2004). This increased signal decreases again 1 to 3 s after reward presentation. The total time course for the fMRI signals lasts approximately 9 to 12 s before returning back to baseline levels. These time courses correlate well with the pH shifts seen in this study. The increased fMRI signals seem to overlap with basic pH shifts here, while a decrease in BOLD signal correlates well with the acidic pH shifts measured. Similar to this study , the start of the anticipation period has been observed to be the start activation in fMRI studies (Ernst et al., 2004).

The correlation between increased dopamine firing and metabolic signals has been established in prior work. When dopamine neurons are forced to fire, this firing is accompanied by a slightly delayed increase in oxygen level coupled to a simultaneous increase in pH (Venton et al., 2003b). The increase in oxygen is in turn correlated with an increase in local blood flow (Lowry et al., 1997). The pH change arises because extracellular pH in the brain is governed by the H_2CO_3/HCO_3^- buffering system. Because the main enzyme responsible for the formation of carbonic acid is carbonic anhydrase that catalyzes the hydration of CO_2, the local pH is critically linked to this gas. An increase in local blood flow carries CO_2 from the brain, thus raising the local pH. This process is balance by local metabolic activity that generates CO_2 and thus lowers the extracellular pH. Consistent with these concepts, long term acidic shifts following a short basic shift have been observed after neuronal activity *in vivo* (Kraig et al., 1983; Somjen, 1984). A similar time delay of alkaline pH shift has been observed after dopamine release due to administration of natural rewards (Roitman et al., 2004). Thus, like oxygen

levels, pH shifts are a measure of the balance between metabolism and cerebral blood flow.

Thus, based on this prior work, the pH changes observed here appear to reflect increased neuronal activity within the striatum. However, establishing the relationship between the observed time course of pH changes and that for the neuronal activity is not straight forward. Measurements with oxygen microelectrodes (Thompson et al., 2003) have established that an increase in neuronal activity is accompanied by an overall increase in local oxygen concentrations. Similarly, BOLD fMRI (Kim et al., 2000), that responds to levels of oxygenation levels of hemoglobin, also changes with neural activity. However, in both of these experiments there is an initial dip in response that is thought to correspond to the immediate use of oxygen because of the increased neural activity. This is followed in 2-3 s by a delayed increase in signal arising from increased blood flow. The "initial dip" is thought to be a better direct indicator for neuronal activity than the observed subsequent increases in cerebral blood flow(Ances, 2004). Some studies connect the "initial dip" with the depletion of mitochondrial oxygen buffers caused by increased neuronal activity (Aubert and Costalat, 2002). In either case, the observed pH changes reflect local neural activity in a similar manner to fMRI measurements. However, it is possible that the fast time-locked responses seen in this study might be directly linked to neural activity as is the "initial dip".

In trials where the reward probability was indicated by reward-predicting cues, two features have been observed in the pH traces beside the alkalization at the beginning of the trial and the acidification after presentation of the reward. First,

alkalization after presentation of the reward-probability predicting cue was smallest for the cue predicted the highest reward probability. After presentation of the cue associated with a low reward probability (5%) a steep basic pH shift was observed. Electrophysiological studies (Fiorillo et al., 2003) and FMRI studies (Abler et al., 2006) both have shown that neuronal activity in the striatum increased linearly with reward probability. Assuming that increased neuronal activity causes acidifications, the observations here are in agreement with this data. However, other fMRI studies also reported no activity changes with different reward probabilities(Knutson et al., 2005; Dreher et al., 2006) or even showed an increase response to negative feedback serving as measure for prediction error (Aron et al., 2004). Differences between the electrophysiological responses and the fMRI results were attributed to the fact that the differential BOLD signals respond to afferent inputs and local neural activity rather than responding to direct dopamineric neuronal activity. Similar arguments also apply to the pH measurements in this study. Even though a microenvironment is sampled, all neuronal and metabolic activities as well as local changes in blood flow in the surroundings of the electrode can influence the pH signal that is obtained, while the electrophysiological recordings only obtain firing information from one specific neuron.

A second unique feature is the delay of acidification that occurs after the reward on trials where the cue predicts a 50% probability of reward (figure 7.6). This response is in accordance with fMRI studies that report decrease in signal after a predicted reward is not delivered, but an increase is reported after delivery of an uncertain reward (Knutson et al., 2005).

In this study a close correlation between the licking behavior and the pH shifts has been observed in the trials with predicted reward. It has been shown that licking behavior differs with different reward predictions (Watanabe et al., 2001) and can serve as an indicator for the difference between “wanting” and “liking” a reward (Wilson et al., 2006). Therefore licking can serve well as a measure of the animal’s behavior during reward delivery trials. Both experimental trials presented in this study, the free reward delivery and the delivery of a predicted reward, show similar behavioral activation as can be observed on the licking patterns. For animal 1 licks increased during the anticipation period and to the reward as it has been observed previously (Hassani et al., 2001). This behavioral activation preceding the reward has been shown to accompany increased firing of striatal neurons. No significant differences between trials that involve movement and trials that do not involve movement have been seen in either the neuronal or the behavioral responses. Analogous observations have been made in this study, where the behavioral licking patterns of the free reward trial which did not involve movements are similar to the conditioned reward trial which did involve movement. Furthermore, it has been shown that the anticipatory neuronal activations were not due to differences in anticipatory licking (Hollerman et al., 1998; Hassani et al., 2001; Cromwell and Schultz, 2003). The difference in licking behavior of animal 2 during the delivery of free reward is most likely due to different training conditions between the two animals. However, licking behavior and pH shifts are identical for both animals during the predicted reward trials. During the delivery of free reward the licking pattern differ between both animals, but in 43% of the locations the pH shifts are

identical. This indicates that the pH shifts observed in this study are not directly caused by licking. The licking pattern shown here are rather an indication for behavioral activation.

Beside pH shifts it was possible to measure dopamine changes in some of the recording locations during delivery of an unpredicted reward. The burst firing of dopaminergic neurons during reward delivery (Schultz, 2002) is expected to cause phasic increases in dopamine concentrations in the terminal regions (Wightman and Robinson, 2002). When observed, the dopamine levels observed in this study are elevated for approximately one second, similar to that for naturally occurring dopamine release observed in rats (Robinson et al., 2003), but faster than dopamine release observed in rats during delivery of natural rewards (Roitman et al., 2004). The dopamine uptake rates measured in the striatum of primate brain slices exhibited a V_{max} that was twice as large as the V_{max} measured in rodents (Cragg et al., 2000, 2002). The higher dopamine uptake rate explains the shorter time course measured in this study, and may explain why it is more difficult to measure dopamine transients in primates when compared to rats. The observed dopamine release with reward delivery in low probability trials (5%) is also expected according electrophysiological responses and the theory of prediction error (Schultz and Dickinson, 2000; Fiorillo et al., 2003). Unexpected rewards show stronger neuronal firing that rewards with higher probabilities. Indeed, no dopamine release was observed to the delivery of rewards which were predicted with a higher probability.

Summary

In this study we used fast-scan voltammertric measurements at microelectrodes to measure chemical changes in striatal regions of behaving primates. During delivery of free, unpredicted reward we observed pH shifts centered around the delivery of reward that resemble data obtained with fMRI during neuronal activation. At the time of reward in a minority of the locations dopamine release could be measured directly after reward delivery. pH changes recorded during delivery of a predicted reward are similar to traces recorded during unpredicted reward. In a majority of the locations the ph traces also coded for the different probabilities. Furthermore, rewarded trails show a further pH shift after reward delivery which was absent in non-reward trials. The behavior closely mimics the pH changes. Thus, this study shows that it is possible to obtain important chemical information with fast-scan voltammetric recordings in primate brains.

REFERNECES

Abler B, Walter H, Erk S, Kammerer H, Spitzer M (2006) Prediction error as a linear function of reward probability is coded in human nucleus accumbens. Neuroimage 31:790-795.

Ances BM (2004) Coupling of changes in cerebral blood flow with neural activity: What must initially dip must come back up. Journal of Cerebral Blood Flow and Metabolism 24:1-6.

Aosaki T, Tsubokawa H, Ishida A, Watanabe K, Graybiel AM, Kimura M (1994) Responses of tonically active neurons in the primate's striatum undergo systematic changes during behavioral sensorimotor conditioning. J Neurosci FIELD Full Journal Title:The Journal of neuroscience : the official journal of the Society for Neuroscience 14:3969-3984.

Aron AR, Shohamy D, Clark J, Myers C, Gluck MA, Poldrack RA (2004) Human midbrain sensitivity to cognitive feedback and uncertainty during classification learning. Journal of Neurophysiology 92:1144-1152.

Aubert A, Costalat R (2002) A model of the coupling between brain electrical activity, metabolism, and hemodynamics: Application to the interpretation of functional neuroimaging. Neuroimage 17:1162-1181.

Berns GS, McClure SM, Pagnoni G, Montague PR (2001) Predictability modulates human brain response to reward. Journal of Neuroscience 21:2793-2798.

Cahill PS, Walker QD, Finnegan JM, Mickelson GE, Travis ER, Wightman RM (1996) Microelectrodes for the measurement of catecholamines in biological systems. Analytical Chemistry 68:3180-3186.

Cragg SJ (2003) Variable dopamine release probability and short-term plasticity between functional domains of the primate striatum. Journal of Neuroscience 23:4378-4385.

Cragg SJ, Hille CJ, Greenfield SA (2000) Dopamine release and uptake dynamics within nonhuman primate striatum in vitro. Journal of Neuroscience 20:8209-8217.

Cragg SJ, Hille CJ, Greenfield SA (2002) Functional domains in dorsal striatum of the nonhuman primate are defined by the dynamic behavior of dopamine. Journal of Neuroscience 22:5705-5712.

Cromwell HC, Schultz W (2003) Effects of expectations for different reward magnitudes on neuronal activity in primate striatum. J Neurophysiol 89:2823-2838.

Delgado MR, Nystrom LE, Fissell C, Noll DC, Fiez JA (2000) Tracking the hemodynamic responses to reward and punishment in the striatum. Journal of Neurophysiology 84:3072-3077.

Dreher JC, Kohn P, Berman KF (2006) Neural coding of distinct statistical properties of reward information in humans. Cerebral Cortex 16:561-573.

Ernst M, Nelson EE, McClure EB, Monk CS, Munson S, Eshel N, Zarahn E, Leibenluft E, Zametkin A, Towbin K, Blair J, Charney D, Pine DS (2004) Choice selection and reward anticipation: an fMRI study. Neuropsychologia 42:1585-1597.

Fiorillo CD, Tobler PN, Schultz W (2003) Discrete coding of reward probability and uncertainty by dopamine neurons. Science 299:1898-1902.

Hassani OK, Cromwell HC, Schultz W (2001) Influence of expectation of different rewards on behavior-related neuronal activity in the striatum. J Neurophysiol 85:2477-2489.

Heien MLAV, Johnson MA, Wightman RM (2004) Resolving neurotransmitters detected by fast-scan cyclic voltammetry. Analytical Chemistry 76:5697-5704.

Heien MLAV, Phillips PEM, Stuber GD, Seipel AT, Wightman RM (2003) Overoxidation of carbon-fiber microelectrodes enhances dopamine adsorption and increases sensitivity. Analyst 128:1413-1419.

Heien MLAV, Khan AS, Ariansen JL, Cheer JF, Phillips PEM, Wassum KM, Wightman RM (2005) Real-time measurement of dopamine fluctuations after cocaine in the brain of behaving rats. Proceedings of the National Academy of Sciences of the United States of America 102:10023-10028.

Hermans A, Wightman RM (2006) Conical tungsten tips as substrates for the preparation of ultramicroelectrodes. Langmuir 22:10348-10353.

Hermans A, Seipel AT, Miller CE, Wightman RM (2006) Carbon-fiber microelectrodes modified with 4-sulfobenzene have increased sensitivity and selectivity for catecholamines. Langmuir 22:1964-1969.

Hollerman JR, Tremblay L, Schultz W (1998) Influence of reward expectation on behavior-related neuronal activity in primate striatum. J Neurophysiol 80:947-963.

Hyde JS, Biswal BB, Jesmanowicz A (2001) High-resolution fMRI using multislice partial k-space GR-EPI with cubic voxels. Magn Reson Med 46:114-125.

Kawagoe KT, Zimmerman JB, Wightman RM (1993) Principles of voltammetry and microelectrode surface states. Journal of neuroscience methods 48:225-240.

Kim DS, Duong TQ, Kim SG (2000) High-resolution mapping of iso-orientation columns by fMRI. Nature Neuroscience 3:164-169.

Kim SG, Richter W, Ugurbil K (1997) Limitations of temporal resolution in functional MRI. Magn Reson Med 37:631-636.

Knutson B, Adams CM, Fong GW, Hommer D (2001a) Anticipation of increasing monetary reward selectively recruits nucleus accumbens. J Neurosci 21:RC159.

Knutson B, Fong GW, Adams CM, Varner JL, Hommer D (2001b) Dissociation of reward anticipation and outcome with event-related fMRI. Neuroreport 12:3683-3687.

Knutson B, Taylor J, Kaufman M, Peterson R, Glover G (2005) Distributed neural representation of expected value. Journal of Neuroscience 25:4806-4812.

Kraig RP, Ferreirafilho CR, Nicholson C (1983) Alkaline and Acid Transients in Cerebellar Microenvironment. Journal of Neurophysiology 49:831-850.

Lowry JP, Boutelle MG, Fillenz M (1997) Measurement of brain tissue oxygen at a carbon past electrode can serve as an index of increases in regional cerebral blood flow. J Neurosci Methods 71:177-182.

Michael D, Travis ER, Wightman RM (1998) Color images for fast-scan CV. Analytical Chemistry 70:586a-592a.

Michael DJ, Joseph JD, Kilpatrick MR, Travis ER, Wightman RM (1999) Improving data acquisition for fast scan cyclic voltammetry. Analytical Chemistry 71:3941-3947.

Ogawa S, Lee TM, Kay AR, Tank DW (1990) Brain magnetic resonance imaging with contrast dependent on blood oxygenation. Proc Natl Acad Sci U S A 87:9868-9872.

Phillips PEM, Stuber GD, Heien MLAV, Wightman RM, Carelli RM (2003) Subsecond dopamine release promotes cocaine seeking. Nature 422:614-618.

Raichle ME, Mintun MA (2006) Brain work and brain imaging. Annu Rev Neurosci 29:449-476.

Robinson DL, Venton BJ, Heien ML, Wightman RM (2003) Detecting subsecond dopamine release with fast-scan cyclic voltammetry in vivo. Clin Chem 49:1763-1773.

Roitman MF, Stuber GD, Phillips PEM, Wightman RM, Carelli RM (2004) Dopamine operates as a subsecond modulator of food seeking. Journal of Neuroscience 24:1265-1271.

Rolls ET, Cahusac PM, Feigenbaum JD, Miyashita Y (1993) Responses of single neurons in the hippocampus of the macaque related to recognition memory. Exp Brain Res FIELD Full Journal Title:Experimental brain research Experimentelle Hirnforschung Experimentation cerebrale 93:299-306.

Runnels PL, Joseph JD, Logman MJ, Wightman RM (1999) Effect of pH and Surface Functionalities on the Cyclic Voltammetric Responses of Carbon-Fiber Microelectrodes. Analytical Chemistry 71:2782-2789.

Schultz W (1998) Predictive reward signal of dopamine neurons. J Neurophysiol 80:1-27.

Schultz W (2002) Getting formal with dopamine and reward. Neuron 36:241-263.

Schultz W, Dickinson A (2000) Neuronal coding of prediction errors. Annual Review of Neuroscience 23:473-500.

Somjen GG (1984) Acidification of Interstitial Fluid in Hippocampal-Formation Caused by Seizures and by Spreading Depression. Brain Research 311:186-188.

Thompson JK, Peterson MR, Freeman RD (2003) Single-neuron activity and tissue oxygenation in the cerebral cortex. Science 299:1070-1072.

Tobler PN, Dickinson A, Schultz W (2003) Coding of predicted reward omission by dopamine neurons in a conditioned inhibition paradigm. Journal of Neuroscience 23:10402-10410.

Tobler PN, Fiorillo CD, Schultz W (2005) Adaptive coding of reward value by dopamine neurons. Science 307:1642-1645.

Venton BJ, Wightman RM (2003) Psychoanalytical electrochemistry: dopamine and behavior. Analytical Chemistry 75:414A-421A.

Venton BJ, Michael DJ, Wightman RM (2003a) Correlation of local changes in extracellular oxygen and pH that accompany dopaminergic terminal activity in the rat caudate-putamen. Journal of Neurochemistry 84:373-381.

Venton BJ, Michael DJ, Wightman RM (2003b) Correlation of local changes in extracellular oxygen and pH that accompany dopaminergic terminal activity in the rat caudate-putamen. J Neurochem 84:373-381.

Verhagen JV, Gabbott PL, Rolls ET (2003) A simple method for reconditioning epoxy-coated microelectrodes for extracellular single neuron recording. Journal of Neuroscience Methods 123:215-217.

Watanabe M, Cromwell HC, Tremblay L, Hollerman JR, Hikosaka K, Schultz W (2001) Behavioral reactions reflecting differential reward expectations in monkeys. Exp Brain Res 140:511-518.

Wightman RM, Robinson DL (2002) Transient changes in mesolimbic dopamine and their association with 'reward'. Journal of Neurochemistry 82:721-735.

Wilson DI, Laidlaw A, Butler E, Hofmann D, Bowman EM (2006) Development of a behavioral task measuring reward "wanting" and "liking" in rats. Physiol Behav 87:154-161.

Zink CF, Pagnoni G, Martin-Skurski ME, Chappelow JC, Berns GS (2004) Human striatal responses to monetary reward depend on saliency. Neuron 42:509-517.